UNIVERSITY OF BELGRADE
FACULTY OF TECHNOLOGY AND METALURGY

Nozhat Moftah El Buaishi

SINTERABILITY OF CORDIERITE POWDERS SYNTHESIZED BY DIFFERENT SOL-GEL METHODS

Doctoral Dissertation

Belgrade, 2013.

UNIVERZITET U BEOGRADU
TEHNOLOŠKO-METALURŠKI FAKULTET

Nozhat Moftah El Buaishi

PROUČAVANJE SINTERABILNOSTI KORDIJERITNIH PRAHOVA SINTETIZOVANIH RAZLIČITIM SOL-GEL POSTUPCIMA

Doktorska disertacija

Beograd, 2013.

Supervisor

dr Rada Petrović, Full Professor, Faculty of Technology and Metallurgy, University of Belgrade, Belgrade

Committee Members

1. dr Đorđe Janaćković, Full Professor, Faculty of Technology and Metallurgy, University of Belgrade, Belgrade

2. dr Snežana Grujić, Associate Professor, Faculty of Technology and Metallurgy University of Belgrade, Belgrade

3. dr Đorđe Veljović, Research Associate, Innovation center, Faculty of Technology and Metallurgy, University of Belgrade, Belgrade

Acknowledgments

I owe a tremendous amount of thanks and appreciations to so many individuals. But first, I want to thank God for giving me wisdom and strength. Without Him I could do nothing.

I would like further to express my utmost gratitude to my advisor prof. dr. Rada Petrović for the knowledge and experience that she has passed on to me, and for the patience that she has shown throughout this work. I am pleased to know her and work with her. Ivona, Bojan and Djordje deserve special thanks for helping me in the analysis, and for developing and working on this thesis.

Furthermore, I would like to thank my husband Elayadi and my children Nurelhuda and Abdulhafid. They have lost a lot, due to my research aboard. Thanks for your patience, love and devotion. Thank for my parents.

Finally, thanks go to all my friends, especially Sonja and Andjelika and everyone I know here. The greatest gratitude deserves my country Libya, since without it I could not finish my study.

Nozhat Moftah El Buaishi

Sinterability of Cordierite Powders Synthesized by Different Sol-gel Methods

Abstract

Dense cordierite-based ceramic is a promising material for technological applications due to its low thermal expansion and dielectric constant, and high chemical and thermal stability. Cordierite ceramics can be prepared by conventional methods, such as solid state reaction technique and crystallization out of glasses. However, it is difficult to sinter cordierite without sintering aids because of the narrow sintering range just before its incongruent melting point. These aids, on the other hand, increase the thermal expansion coefficient and dielectric constant. Some attempts have been made to improve the sinterability of cordierite. By wet chemical routes, cordierite powders with favorable sintering behavior can be synthesized. It is well known that the sol-gel method has the advantage of an excellent control of chemical composition and the possibility of reducing the sintering temperature.

In this dissertation, the sinterability of cordierite powders obtained by different sol-gel methods was studied. The cordierite powders were synthesized by colloidal and alkoxide sol-gel methods and starting from silicic acid and magnesium and aluminum salts. Phase transformation and shrinkage during heating of gel obtained starting from silicic acid and the kinetic parameters of cordierite crystallization from the gel, were also investigated in this dissertation. Cordierite powders for the sintering investigation were obtained by the gels calcination at a temperature where α-cordierite is formed or at a temperature where densification without crystallization of the silica-containing component occurred. The influence of synthesis method, temperature of gel calcination, duration of calcined gel grinding and temperature of sintering on microstructure and mechanical properties of sintered materials was analyzed. In order to improve sintering behavior of the cordierite powders, spark-plasma sintering was applied and results were compared to those obtained by conventional sintering.

Starting from silicic acid and magnesium and aluminum salts, a homogeneous monophasic cordierite gel was obtained, which was proved by μ-cordierite crystallization at about 900 °C. In temperature range of 800–850 °C, viscous sintering of the gel without μ-cordierite crystallization occurred. It was shown according to the DTA, XRD and FTIR results that μ- → α-cordierite transformation took place in a wide

temperature range, and α-cordierite appeared at about 1200 °C. On calcination for 2 h at 1300 °C, the transformation μ- → α-cordierite was fully completed.

The mean value of the Avrami parameter for μ-cordierite crystallization, which is close to 1, indicates interface controlled crystallization with a constant number of nuclei and one-dimensional growth or surface nucleation. Accordingly, viscous sintering occurred in the primary gel particles, which led to shrinkage, and thereafter, nucleation occurs on the surface or interface of the particles. Due to surface nucleation, the overall activation energy of μ-cordierite crystallization (382.0 kJ/mol) was lower than in cases where volume nucleation occurs.

Prolonged time of calcined gels grinding caused particle decreasing in all cases and the densification degree of the cordierite materials was improved by decreasing the mean particle size. More densified microstructures were obtained by using the powders obtained after grinding for 3 hours than for 0.5 h.

The sinterability of the powders obtained by calcination at 1300 °C, where well-crystallized α-cordierite was formed, was better in all cases than that of the powder obtained by calcination at temperatures where the most intensive shrinkage occurred before the onset of silica-containing component crystallization (850 °C for alkoxide and silicic acid gels or 950 °C for colloidal gel).

In general, powders obtained starting from silicic acid and by the colloidal sol–gel method showed better performances on sintering with respect to the alkoxide-based powders. The best mechanical properties of the conventionally sintered materials were achieved by sintering at 1400 °C of powder obtained by calcination at 1300 °C of colloidal gel and by sintering at 1430 °C of powder obtained by calcination at 1300 °C of gel obtained starting from silicic acid. Hardness of the best materials was about 7.5 to 8 GPa, while fracture toughness K_{IC} was 3.7 to 3.8 MPa $m^{1/2}$.

Despite the high sintering temperature of the alkoxide-based powders, the obtained materials were insufficiently sintered. The sinterability of the alkoxide-based powder was highly improved by spark-plasma sintering at a lower sintering temperature and during much shorter time than during conventional sintering. The density of the spark-plasma sintered materials was very close to the theoretical density of α-cordierite and the mechanical properties were better than those of materials obtained by

conventional sintering (hardness was about 8.5 GPa and fracture toughness K_{IC} was about 4,1 MPa $m^{1/2}$).

Key words:
Cordierite, Sol-gel synthesis, Grinding, Conventional sintering, Spark-plasma sintering, Microstructure, Mechanical properties

Scientific field: Chemistry and Chemical Technology
Specific scientific field: Ceramic Materials
UDC: 66.017:536.421.5

Proučavanje sinterabilnosti kordijeritnih prahova sintetizovanih različitim sol-gel postupcima

Rezime

Gusta kordijeritna keramika ima veliki značaj u nauci o materijalima i široku primenu u industriji zahvaljujući malom koeficijentu toplotnog širenja kordijerita ($2MgO{\cdot}2Al_2O_3{\cdot}5SiO_2$), maloj dielektričnoj konstanti, velikoj specifičnoj otpornosti i relativno velikoj vatrostalnosti. Kordijeritna keramika se može dobiti konvencionalnim postupcima, ali je veoma teško sinterovanjem dobiti gust materijal, zbog veoma uskog intervala sinterovanja kordijerita u blizini inkongruentne tačke topljenja. Pokušaji da se problem uskog intervala sinterovanja reši aditivima omogućili su snižavanje temperature nastajanja kordijerita i povećanje gustine gotovog proizvoda, ali su doveli do pogoršanja željenih osobina, odnosno do povećanja koeficijenta toplotnog širenja i dielektrične konstante. Zbog toga su poslednjih godina istraživanja u cilju dobijanja guste kordijeritne keramike usmerena na sintezu prahova kordijerita poboljšane sinterabilnosti. Različitim hemijskim postupcima sinteze mogu se dobiti fini prahovi velike specifične površine, velike unutrašnje energije, a time i velike sinterabilnosti. Sol-gel postupci imaju veliku primenu u sintezi prahova zahvaljujući mogućnosti precizne kontrole hemijskog sastava prahova i sniženja temperature sinterovanja.

Predmet ove doktorske disertacije je ispitivanje sinterabilnosti kordijeritnih prahova koji su sintetizovani alkoksidnim i koloidnim sol-gel postupkom, kao i sol-gel postupkom u kome je kao polazni reaktant korišćena silicijumova kiselina, dobijena iz vodenog stakla, kao jeftinog prekursora. Fazne transformacije i skupljanje tokom termičkog tretmana gela dobijenog postupkom sa silicijumovom kiselinom, kao i kinetika tih faznih transformacija su takođe proučene u ovoj doktorskoj disertaciji. Kordijeritni prahovi za ispitivanje sinterabilnosti su dobijeni kalcinacijom suvih gelova na temperaturi pri kojoj dolazi do viskoznog sinterovanja bez kristalizacije komponente koja sadrži SiO_2 i na temperaturi na kojoj nastaje α-kordijerit. Pri proučavanju sinterabilnosti kordijeritnih prahova ispitan je uticaj: vrste sinteze gela, temperature kalcinacije gelova, dužine trajanja mlevenja kalcinisanih gelova i temperature sinterovanja na mikrostrukturne i mehaničke karakteristike dobijenih materijala. U cilju

poboljšanja sinterabilnosti, primenjeno je i spark-plazma sinterovanje i rezultati su upoređeni sa rezultatima konvencionalnog sinterovanja.

Polazeći od silicijumove kiseline i soli aluminijuma i magnezijuma, dobijen je homogeni kordijeritni gel, što je potvrđeno kristalizacijom μ-kordijerita na temperaturama oko 900 °C. U temperaturnom intervalu 800–850 °C došlo je do viskoznog sinterovanja bez kristalizacije μ-kordijerita. Na osnovu rezultata DTA, XRD i FTIR analiza pokazano je da se transformacija μ- → α-kordijerit odigrava u širokom temperaturnom intervalu i da se α-kordijerit pojavljuje na oko 1200 °C. Kalcinacijom u toku 2 h na 1300 °C došlo je do potpune transformacije μ- → α-kordijerit.

Vrednost Avramijevog parametra za kristalizaciju μ-kordijerita, koja je bliska 1, ukazuje na kristalizaciju na granici faza sa konstantnim brojem nukleusa i jednodimenzioni rast ili na površinsku nukleaciju. Na osnovu toga je zaključeno da se viskozno sinterovanje odigrava u primarnim česticama gela, što dovodi do skupljanja, nakon čega se nukleacija odigrava na površini ili međupovršini čestica. Zbog površinske kristalizacije, prosečna energija aktivacije kristalizacije μ-kordijerita (382,0 kJ/mol) je niža nego u slučajevima u kojima dolazi do zapreminske nukleacije.

Produženo vreme mlevenja kalcinanih gelova u svim slučajevima je dovelo do smanjenja veličine čestica i stepen denzifikacije kordijeritnih materijala je povećan sa smanjenjem veličine čestica praha. Mnogo gušći materijali su dobijeni korišćenjem prahova koji su mleveni 3 h nego u slučaju mlevenja 0,5 h.

Sinterabilnost prahova koji su dobijeni kalcinacijom na 1300 °C, kada se formira α-kordijerit, je bolja u svim slučajevima od sinterabilnosti prahova koji su dobijeni kalcinacijom na temperaturama na kojima je dolazilo do intenzivnog skupljanja pre kristalizacije komponente koja sadrži SiO_2 (850 °C za alkoksidni gel i gel dobijen polazeći od silicijumove kiseline, 950 °C za koloidni gel dobijen polazeći od koloidnog SiO_2).

Prahovi dobijeni polazeći od silicijumove kiseline i koloidnog SiO_2 su imali bolju sinterabilnost u odnosu na prahove dobijene alkoksidnim postupkom. Najbolja mehanička svojstva materijala dobijenih konvencionalnim sinterovanjem su postignuta sinterovanjem na 1400 °C praha koji je dobijen kalcinacijom na 1300 °C koloidnog gela i sinterovanjem na 1430 °C praha dobijenog kalcinacijom na 1300 °C gela dobijenog

polazeći od silicijumove kiseline. Najbolji materijali su imali tvrdoću oko 7,5 do 8 GPa, dok je žilavost (K_{IC}) bila od 3,7 do 3,8 MPa $m^{1/2}$.

Bez obzira na visoku temperaturu sinterovanja prahova dobijenih alkoksidnim postupkom, dobijeni materijali su bili nedovoljno sinterovani. Sinterabilnost ovih prahova je bila značajno poboljšana spark-plazma sinterovanjem na nižim temperaturama i za značajno kraće vreme nego u slučaju konvencionalnog sinterovanja. Gustine spark-plazma sinterovanih materijala su bile bliske teorijskoj gustini kordijerita i mehanička svojstva su bila značajno bolja od svojstava konvencionalno dobijenih materijala (tvrdoća oko 8,5 GPa i K_{IC} oko 4,1 MPa $m^{1/2}$).

Ključne reči:

Kordijerit, Sol-gel sinteza, Mlevenje, Konvencionalno sinterovanje, Spark-plazma sinterovanje, Mikrostruktura, Mehanička svojstva

Naučna oblast: HEMIJA I HEMIJSKA TEHNOLOGIJA

Uža naučna oblast: Keramički materijali

UDK: 66.017:536.421.5

CONTENT

1. INTRODUCTION 1

2. CORDIERITE 3

2.1. MgO-Al_2O_3-SiO_2 system 4
2.2. Properties and applications of cordierite 5
2.3. Structure of polymorphic forms of cordierite 7

3. POWDERS SYNTHESIS 8

3.1. General methods for powders synthesis 9
3.2. Powder preparation by mechanical methods 11
3.2.1. Comminution 11
3.2.2. Ball mills 12
3.3. Sol-gel processing 14
3.3.1. Polymeric sol-gel processing 15
3.3.1.1. Alkoxide hydrolysis and condensation in one-component system 16
3.3.1.2. Hydrolysis and condensation in multicomponent systems 18
3.3.2. Colloidal sol-gel process 21
3.3.2.1. The properties of colloidal sols 21
3.3.2.2. Aqueous silicic acid solution and silica sols 24
3.3.3. The sol –gel transition (gelation) 26
3.3.4. Aging of gels 27
3.3.5. Drying of gels 27

4. POWDERS CONSOLIDATION 28

4.1. Dry pressing 29
4.2. Cold isostatic pressing 31

5. SINTERING 33

5.1. Driving force and basic phenomena 34
5.2. Sintering variables 36
5.3. Categories of sintering 38
5.4. Stages of sintering 39
5.5. Mechanisms of solid state sintering 42
5.6. Grain growth 44
5.7. Liquid-phase sintering 46
5.8. Spark plasma sintering 50
5.8.1. Principles of the SPS process 50
5.8.2. Basic configuration of the SPS system 51
5.8.3. Mechanism of processing SPS 51

6. SINTERING OF CORDIERITE POWDERS - A REVIEW 53

7. EXPERIMENTAL PART 58

7.1. Synthesis of gels and powders 58
7.1.1. Synthesis of cordierite gel and powders starting from silicic acid 58
7.1.2. Synthesis of cordierite gel starting from silica sol 58
7.1.3. Synthesis of cordierite gel starting from alkoxide 59
7.2. Characterization of gel and powders obtained from silicic acid 60
7.2.1. Methods 60
7.2.2. Kinetics 60
7.3. Sintering 62

8. RESULTS AND DISCUSION 65

8.1. Characterization of the gel and powders obtained starting from silicic acid 65

8.1.1. SEM and TEM of the dry gel 65

8.1.2. Phase transformations during thermal treatment of the gel 65

8.1.3. Kinetics of μ-cordierite crystallization 71

8.2. Sinterability of the cordierite powders 74

8.2.1. Sinterability of the cordierite powders obtained starting from silicic acid 74

8.2.1.1. Morphology of the powders 74

8.2.1.2. Microstructure of cordierite materials obtained by conventional sintering 76

8.2.2 Sinterability of the cordierite powders obtained starting from silica sol 79

8.2.2.1. Morphology of powders 79

8.2.2.2. Microstructure cordierite materials obtained by conventional sintering 81

8.2.3 Sinterability of the cordierite powders obtained starting from alkoxide 85

8.2.3.1 Morphology of powders 85

8.2.3.2 Microstructure cordierite materials obtained by conventional sintering 87

8.2.3.3 Microstructure of cordierite materials obtained by spark-plasma sintering 91

9. CONCLUSIONS 95

10. REFERENCES 97

1. INTRODUCTION

Cordierite ($2MgO{\cdot}2Al_2O_3{\cdot}5SiO_2$) is a technically important ceramic which is applied in a great variety of areas. Due to its low dielectric constant, high resistivity, elevated thermal and chemical stability and very low coefficient of thermal expansion, cordierite ceramic is widely used as a material in kiln furniture, honeycomb-shaped catalysts carriers in automobile exhaust systems, substrates in the microelectronic applications, and filters for liquids at high temperatures.

Cordierite ceramics used for some applications need to have high density and good mechanical properties. However, it is difficult to obtain dense cordierite ceramics because of the narrow sintering range just below its incongruent melting point. Some attempts have been made to improve the sinterability of cordierite by applying of sintering aid or by using of cordierite powders with favorable sintering behavior. Addition of sintering aid resulted in a decrease of the temperature of cordierite formation and an increase of the density of the sintered materials, but on the other hand, increases the thermal expansion coefficient and dielectric constant. Thus, the preparation of a homogeneous and fine cordierite powder that can be sintered without sintering aids is considered highly desirable.

It is well known that the sol–gel methods have the advantages of excellent control of the chemical composition and the possibility of reducing the sintering temperature. In recent years, cordierite powders and materials have been produced by the sol–gel method using alkoxides, but the starting materials are very expensive and the fabrication processes are complicated. Colloidal processing is considered an effective method for the preparation stoichiometric cordierite from starting materials that are cheaper than alkoxides and, at the same time, the sintering temperature is decreased and the density improved without the deterioration of the properties. Despite the fact that there are many studies devoted to the synthesis of cordierite powders, there have not been many systematic investigations concerning the sinterability of such powders. The sintering behavior of commercially available crystalline cordierite powders, which were sintered at temperatures near the melting point of cordierite (1460 °C), was investigated in several studies. Moreover, some researchers reported that if the densification of pure and homogeneous cordierite powder compact occurs below the crystallization

temperature, it could be possible to obtain pure and dense cordierite ceramics with relatively good properties. Therefore, these authors investigated the sinterability of amorphous powders, which were densified by viscous sintering.

In this dissertation, the sinterability of cordierite powders obtained by different sol-gel methods was studied. The cordierite powders were synthesized by previously published colloidal and alkoxide sol-gel methods and by a low-price sol–gel method, starting from silicic acid and magnesium and aluminum salts. Phase transformation and shrinkage during heating of gel obtained starting from silicic acid and the kinetic parameters of cordierite crystallization from the gel, were also investigated in this dissertation. Cordierite powders for the sintering investigation were obtained by the gels calcination at a temperature where α-cordierite is formed or at a temperature where densification without crystallization of the silica-containing component occurred. The influence of synthesis method, temperature of gel calcination, duration of calcined gel grinding and temperature of sintering on microstructure and mechanical properties of sintered materials was analyzed. In order to improve sintering behavior of the cordierite powders, spark-plasma sintering was applied and results were compared to those obtained by conventional sintering.

2. CORDIERITE

Cordierite with a composition of $2MgO\text{-}2Al_2O_3\text{-}5SiO_2$ is the most important ternary compound in the system $MgO\text{-}Al_2O_3\text{-}SiO_2$ [1]. Three forms of cordierite are known to exist [2-4]: the α form, also known as indialite; β- and μ-cordierite. Of these, indialite is the stable high-temperature form and the only one found in nature or achievable in ceramic bodies. β- and μ- cordierite can only be formed under special conditions. At 1460 °C, the indialite form undergoes an incongruent melting that converts it to a mullite phase and a liquid phase, from which forsterite can be developed. Both phases are crystalline phases with much higher coefficient of thermal expansion.

Cordierite, with a crystallo-chemical formula of $Mg_2^{[6]}Al_3^{[6]}[Si_5Al^{[4]}O_{18}]$, contains coplanar tetrahedral groups bound in the shape of hexagonal rings with five SiO_4 groups and one AlO_4 group [5, 6]. Between these tetrahedral groups are the octahedral groups MgO_6 and AlO_6, which form toward the inside of the structural unit's free cavities. A structural unit is formed by three planes of tetrahedral rings, with two cavities between them. The thermal behavior of cordierite, the anisotropy of its thermal expansion and the possibility to influence these characteristics are explained by its structure and they are very important from a theoretical and practical point of view [2, 3].

It is possible to obtain cordierite directly from oxides [7-9], as well as from other raw materials whose chemical composition equals that of cordierite [10-18]. Such materials include elementary compounds, such as hydroxides and carbonates; double compounds, such as kaolin clay, talc, steatite and sepiolite; and triple compounds, such as chlorite. Double or triple compounds, especially hydrated, are preferable. The presence of two or three oxides and the availability of the bonds resulting from the rupture of the lattice when water is released will guarantee a complete reaction and a broader vitrification range.

Besides the nature of the raw materials used, the synthesis of cordierite is also influenced by the initial structural state of the respective reactants [12-18]; by the presence or absence of impurities, which act as mineralizes; by the grain composition

and the specific surface area of the grains; and by the size of the contact area between the grains.

2.1. MgO-Al_2O_3-SiO_2 system

A ternary system MgO-Al_2O_3-SiO_2 [1], which is important in understanding the behavior of cordierite ceramic, is illustrated in Fig. 2.1. This system is composed of several binary compounds: mullite ($3Al_2O_3 \cdot 2SiO_2$), enstatite ($MgO \cdot SiO_2$), forsterite ($2MgO \cdot SiO_2$) and spinel ($MgO \cdot Al_2O_3$) together with two ternary compounds: sapphirine ($4MgO \cdot 5Al_2O_3 \cdot 2SiO_2$) and cordierite [19].

Cordierite is situated in the primary crystallization field of mullite and has a chemical composition of 13.8 wt% MgO, 34.8 wt% Al_2O_3 and 51.4 wt% SiO_2. It has an incongruent melting point, because the solid compound of cordierite does not melt to form the liquid of its own composition, but instead dissociates to form the new solid phase and the liquid. The lowest liquids temperature is at the tridymite-protoenstatite-cordierite eutectic at 1345 ^oC, but the cordierite-enstatite-forsterite eutectic at 1360 ^oC is almost as low-melting in the ternary system [20].

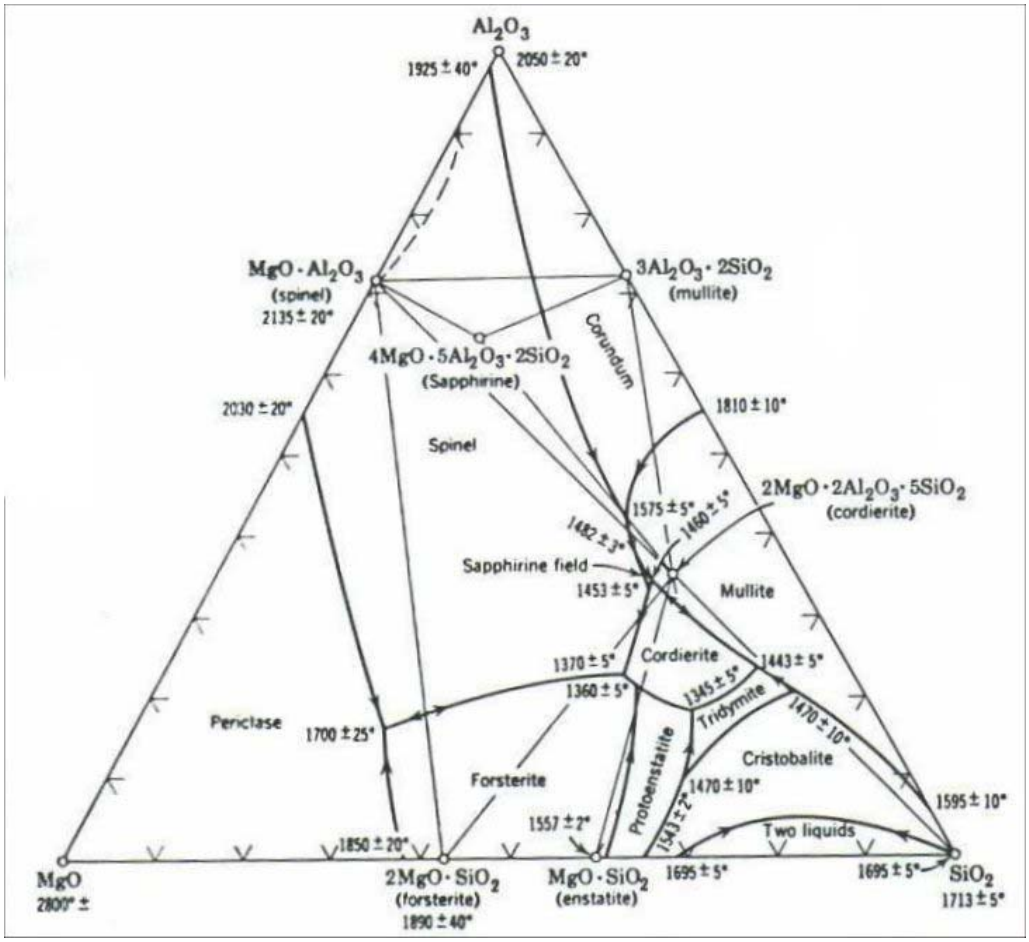

Figure 2.1. MgO-Al_2O_3-SiO_2 ternary phase diagram [1]

2.2. Properties and applications of cordierite

Cordierite, as a ceramic material, has a wide range of uses and applications in the high temperature field and electronics [10, 11, 21-27], stemming from its important properties of low coefficient of thermal expansion and dielectric constant, coupled with high chemical and thermal stability [25]. Table 2.1 shows the properties of cordierite and cordierite glass.

Table 2. 1. Properties of cordierite and cordierite glass [25]

Properties	Cordierite	Cordierite glass
Coefficient of thermal expansion, α (25 - 800 °C) (10^{-6} °C^{-1})	1.5	3.7 - 3.8
Dielectric constant, ε (25 °C, 1 MHz)	5.0	6.3
Flexural strength, σ (MPa)	245	100
Fracture toughness, K_{IC} (MPa·$m^{1/2}$)	2.3	0.9-1.2
Hardness, H (GPa)	8.2	6.6
Young's modul, E (GPa)	139	96
Poisson's ratio, ν	0.31	0.26

Cordierite electric ceramics have an important role in modern technology. So far, this material has been used in electrothermics for the production of electric heater supports. However, nowadays, due to its electrical, electromechanical, and especially thermal properties, this ceramic finds its application in electronics for the production of microelectronic components or in the machine-building industry for manufacture of internal combustion components refractory linings for application in Lost Foam process [28].

In addition, cordierite ceramics have been applied for the fabrication of the supports for catalysts for the conversion of combustion gases from engines. Recently, both cordierite ceramics and vitro ceramics have become very promising for producing substrates for high integral circuits and microchips, owing to the compatibility of their coefficients of thermal expansion with that of silicon and the possibility of co-sintering with copper.

Cordierite is used in many industrial applications, but natural cordierite is extremely rare and seldom occurs in commercial quantities. All cordierite produced are, therefore, from synthetic origin.

2.3. Structure of polymorphic forms of cordierite

There were many disagreements and controversies about the type and structure of polymorphic forms of cordierite. After numerous studies, it can be said today with certainty that cordierite exists in three polymorphic forms: hexagonal high temperature form, called α-cordierite or indianite, stable between 1450 and 1460 °C, low-temperature orthorhombic form, β-cordierite, stable at temperatures lower than 1450 °C and the metastable form μ - cordierite, which has the same structure as β - quartz [2-4, 29, 30].

μ-cordierite is obtained from cordierite glass or by crystallization from homogeneous cordierite gels at temperatures about 1000 °C. μ-cordierite transforms into α - cordierite at higher temperatures. Prolonged heating of α - cordierite gives β - cordierite.

Studies on the mechanism and kinetics of transformation of hexagonal to orthorhombic form of cordierite [31-37] have shown that the polymorphism of cordierite is associated with the process of Al/Si ordering. In both cordierite forms, Al and Si atoms are arranged in two kinds of tetrahedral sites – T_1 in chain and T_2 in ring, and Mg atoms are located in octahedral coordination. It is generally accepted that in the hexagonal form of cordierite, aluminum and silicon atoms are disorder, while the arrangement is achieved in the orthorhombic form of cordierite (Figure 2.2.).

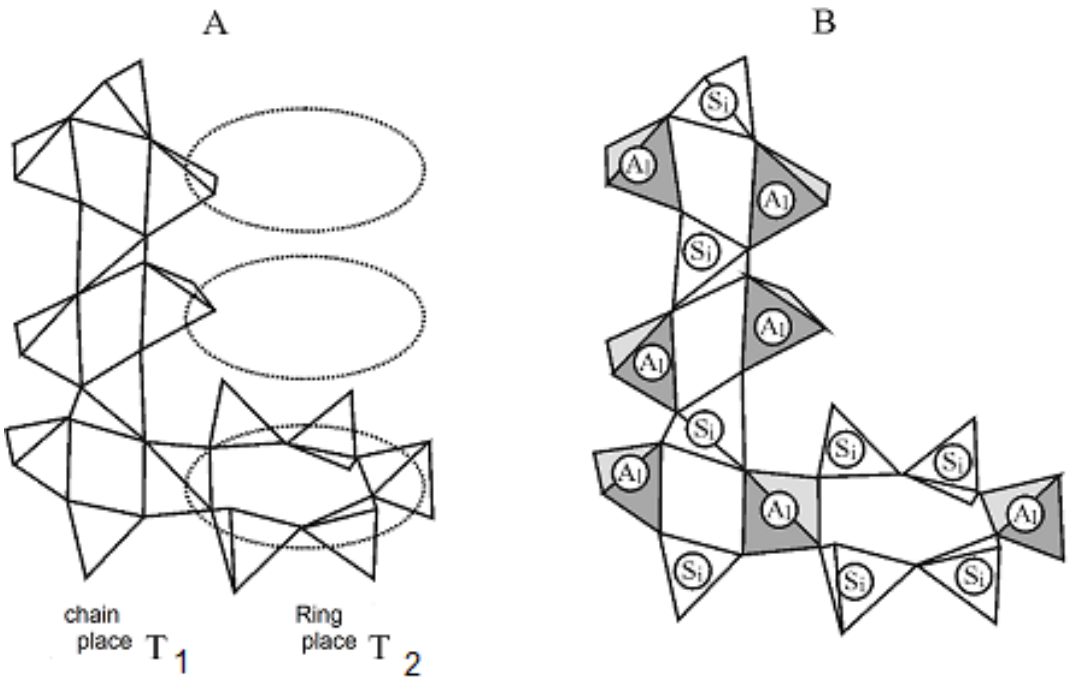

Figure 2.2. Distribution of tetrahedral in the structure of cordierite. Each tetrahedron in the ring (T_2 sites) is connected with a tetrahedron in the chain (T_1 sites) with a ring above and below the ring, so all tetradral share corners. Dashed lines show the position of similar rings of T_2 tetrahedral, forming channels along the c-axis. (B) Structure proposed for a fully ordered orthorhombic form, which shows the position of Si and Al atoms [34].

3. POWDERS SYNTHESIS

Powder synthesis is very important to the overall fabrication of ceramics. A choose of a powder preparation method will depend on the production cost and the capability of the method for achieving a certain set of desired characteristics.

Traditional ceramics generally meet less specific property requirements than advanced ceramics [38]. They can be chemically inhomogeneous and can have complex microstructure. Unlike the case of advanced ceramics, chemical reaction during firing is often a requirement. The starting materials for traditional ceramics therefore consist of

mixture of powders with a chosen reactivity. Fine particle sizes are desirable for good chemical reactivity. The powders must also be chosen to give a reasonably high packing density that serves to limit the shrinkage and distortion of the body during firing. Generally, low cost powder preparation methods are used for traditional ceramics.

Advanced ceramics must meet very specific property requirements and therefore their chemical composition and microstructure must be well controlled. Careful attention must be paid to the quality of the starting powders. The important powder characteristics are [39]: the particle size, size distribution, shape, state of agglomeration, chemical composition, and phase composition. The structure and chemistry of the surface are also important. The desirable powder characteristics for the fabrication of advanced ceramics are listed in Table 3.1.

Table 3.1. Desirable powder characteristics for advanced ceramics [39]

Powder characteristic	Desired property
Particle size	Fine (< ~ 1 μm)
Particle size distribution	Narrow or monodisperse
Particle shape	Spherical or equiaxial
State of agglomeration	No agglomeration or soft agglomeration
Chemical composition	High purity
Phase composition	Single phase

3.1. General methods for powders synthesis

Varieties of methods exist for the synthesis of ceramic powders [40]. They can be generally divided into two categories: mechanical methods and chemical methods [39].

Table 3.2 provides a summary of the common powder preparation methods for ceramics.

Table 3.2. Common powder preparation methods for ceramics [38-40]

Powder preparation method	Advantages	Disadvantages
Mechanical comminution	- inexpensive - wide applicability	- limited purity - limited homogeneity - large particle size
Mechanochemical synthesis	- fine particle size - good for nonoxides - low temperature route	- limited purity - limited homogeneity
Chemical solid-state reaction, decomposition, reaction between solids	- simple apparatus - inexpensive	- agglomerated powders - limited homogeneity for multicomponent powders
Liquid solution precipitation or coprecipitation; solvent vaporization (spray drying, spray pyrolysis, freeze drying); gel routes (sol–gel, Pechini, citrate gel, glycine nitrate)	- high purity - small particle size - composition control - chemical homogeneity	- expensive - poor for nonoxides, - powder agglomeration commonly a problem
Nonaqueous liquid reaction; Vapor-phase reaction	- high purity - small particle size	- limited to nonoxides
Gas–solid reaction	- commonly inexpensive for large particle size	- commonly low purity - expensive for fine powders
Gas–liquid reaction	- high purity - small particle size	- expensive - limited applicability
Reaction between gases	- high purity - small particle size - inexpensive for oxides	- expensive for nonoxides - agglomeration commonly a problem

Mechanical methods are generally used to prepare powders of traditional ceramics from naturally occurring raw materials. Powder preparation by mechanical

methods is a mature area of ceramic processing in which the scope for new developments is rather small. However, in recent years, the preparation of fine powders of some advanced ceramics by mechanical methods involving milling at high speeds has received a fair amount of interest.

Chemical methods are generally used to prepare powders of advanced ceramics from synthetic materials or from naturally occurring raw materials that have undergone a considerable degree of chemical refinement. Some of the methods categorized as chemical involve a mechanical milling step as part of the process. The milling step is usually necessary for the breakdown of agglomerates and for the production of the desired physical characteristics of the powder such as average particle size and particle size distribution [39, 40].

3.2. Powder preparation by mechanical methods

3.2.1. Comminution

The process in which small particles are produced by reducing the size of larger ones by mechanical forces is usually referred to as comminution. It involves operations such as crushing, grinding, and milling.

The most common way to achieve this size reduction is by milling. One or more of a variety of mills may be used, including high-compression roller mills, jet mills (also referred to as fluid energy mills), and ball mills [39, 41]. Ball mills are categorized into various types depending on the method used to impart motion to the balls (e.g., tumbling, vibration, and agitation).

In the milling process, the particles experience mechanical stresses at their contact points due to compression, impact, or shear with the mill medium or with other particles. The mechanical stresses lead to elastic and inelastic deformation and, if the stress exceeds the ultimate strength of the particle, to fracture of the particles. The mechanical energy supplied to the particle is used not only to create new surfaces but also to produce other physical changes in the particle (e.g., inelastic deformation, increase in temperature, and lattice rearrangements within the particle). Changes in the

chemical properties (especially the surface properties) can also occur, especially after prolonged milling or under very vigorous milling conditions.

Figure 3.1 summarizes the stress mechanisms and the range of particle sizes achieved with different types of mills for the production of fine powders.

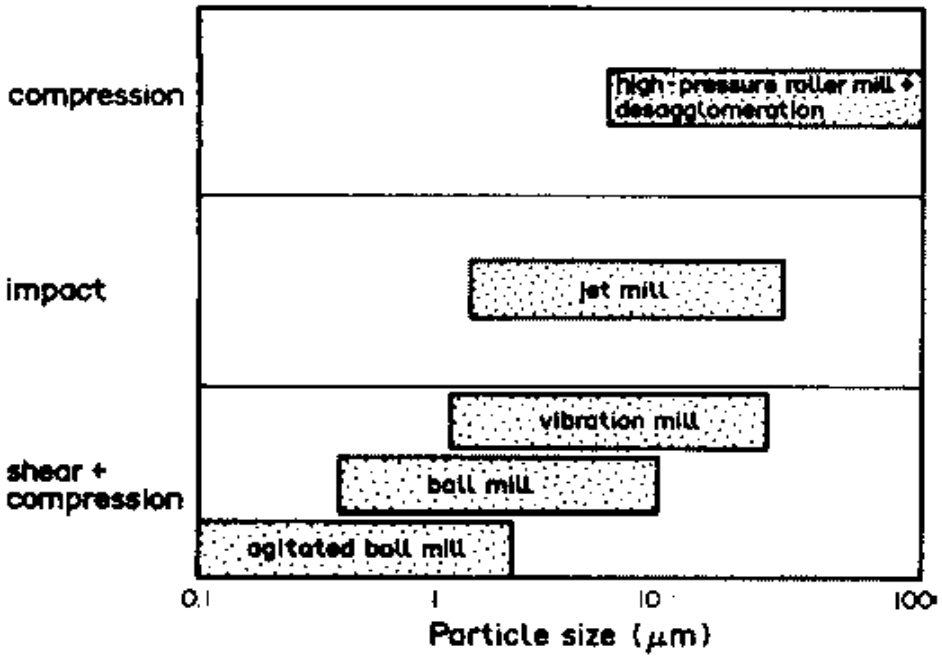

Fig 3.1. Range of particle sizes reached with different types of mills [39].

3.2.2. Ball mills

The most important mills in ceramic production are ball mills, which can produce particle sizes from ~ 10 μm to as low as a fraction of a micrometer [39, 41]. Ball milling is suitable for wet or dry milling. The rate of grinding depends on a number of factors, including the mill parameters, the properties of the grinding media, and the properties of the particles to be ground. Generally, ball mills that run at low speeds contain large balls because most of the mechanical energy supplied to the particle is in the form of potential energy. Those mills that run at high speeds contain small balls because, in this case, most of the energy supplied to the particle is in the form of kinetic energy. For a

given size of grinding medium, since the mass is proportional to the density, the grinding medium should consist of materials with as high a density as possible. In practice, the choice of the grinding medium is usually limited by cost.

The size of the grinding medium is an important consideration. Small grinding media are generally better than large ones. For a given volume, the number of balls increases inversely as the cube of the radius. Assuming that the rate of grinding depends on the number of contact points between the balls and the powder and that the number of contact points, in turn, depends on the surface area of the balls, and then the rate of grinding will increase inversely as the radius of the balls. However, the balls cannot be too small since they must impart sufficient mechanical energy to the particles to cause fracture.

The rate of grinding also depends on the particle size. The rate decreases with decreasing particle size and, as the particles become fine (e.g., about 1 μm to a few micrometers), it becomes more and more difficult to achieve further reduction in size. A practical grinding limit is approached (Fig. 3.2). The reduction of the limiting particle size may be achieved by wet milling (Fig. 3.2.) and by performing the milling in stages. For stages milling, as the particles get finer, they are transferred to another compartment of the mill or to another mill operating with smaller balls.

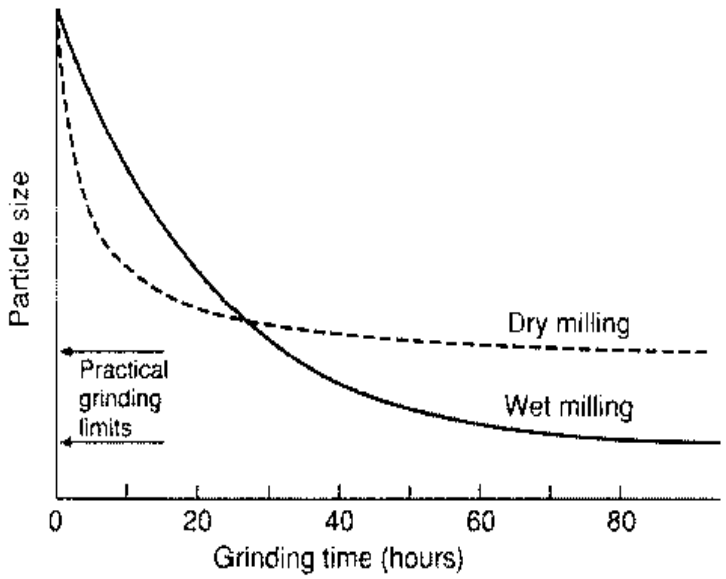

Figure 3.2 Particle size versus grinding time for ball milling [39]

A disadvantage of ball milling is that wear of the grinding medium can be high. For advanced ceramics, the presence of impurities in the powder is a serious concern. The best solution is to use balls with the same composition as the powder itself. However, this is only possible in very few cases and even for these, at great expense. Another solution is to use a grinding medium that is chemically inert at the firing temperature of the body or can be removed from the powder by washing.

3.3. Sol-gel processing

The term sol–gel is used broadly to describe the preparation of ceramic materials by a process that involves the preparation of a sol, the gelation of the sol, and the removal of the liquid [39, 41]. A sol is a suspension of colloidal particles in a liquid or a solution of polymer molecules. The term gel refers to the semi rigid mass formed when the colloidal particles are linked to form a network (Fig. 3.3.a) or when the polymer molecules are cross-linked or interlinked (Fig 3.3.b). Two different sol–gel processing routes are commonly distinguished: the particulate (or colloidal) route in which the sol consists of dense colloidal particles (1 to 1000 nm) and the polymeric route in which the sol consists of polymer chains but has no dense particles > 1 nm. In many cases, particularly when the particle size approaches the lower limit of the colloidal size range, the distinction between a particulate and a polymeric system may not be very clear.

a) b)

Fig 3.3. a) Colloidal gel, b) Polimeric gel

3.3.1. Polymeric sol-gel processing

Polymeric sol-gel route gives gels consist of a skeletal network of polymer chains that form by the entanglement and cross-linking of growing polymer chains or polymer clusters resulting from the hydrolysis, condensation and polymerization of precursors in solution [39-43]. The most common precursors used in polymeric sol–gel processing are metal alkoxides, because they react readily with water. Depending on the conditions used in the preparation, the structure of the polymer chains can vary considerably.

Metal alkoxides are a class of metal-organic compounds which have the general formula $M(OR)_z$, where M is a metal of valence z and R is an alkyl group [39, 40, 44]. They can be considered as derivatives either of an alcohol in which the hydroxylic hydrogen is replaced by the metal or of metal hydroxide in which the hydrogen is replaced by an alkyl group. Accordingly, the chemistry of the metal alkoxides involves the metal-oxygen-carbon bond system.

The method used for the preparation of a metal alkoxide depends, in general, on the electronegativity of the metal [39, 40]. The main methods may be divided into two groups: (1) reactions between metals and alcohols for the more electropositive metals (i.e., those with relatively low electronegativity values) and (2) reactions involving metal chlorides for the less electropositive metals or electronegative elements (i.e., those with relatively high electronegativity values). In addition, there are miscellaneous methods that are useful for the synthesis of some alkoxides. These include alcohol interchange or alcoholysis reactions, transesterification reactions between alkoxides and esters, and etherification reactions between oxides or hydroxides and alcohols.

Metal alkoxides are characterized by the ease with which they undergo hydrolysis. In many cases, the alkoxides are so sensitive to traces of moisture that special precautions must be taken in their handling and storage. Hydrolysis in excess water leads to the formation of insoluble hydroxides or hydrated oxides. However, when restricted amounts of water are added, metal alkoxides undergo partial hydrolysis reactions, yielding soluble species that can take part in polymerization reactions.

3.3.1.1. Alkoxide hydrolysis and condensation in one-component system

The initial steps involve a hydrolysis reaction in which alkoxide groups (OR) are replaced by hydroxyl groups (OH):

$$M(OR)_z + H_2O \rightarrow M(OH)(OR)_{z-1} + ROH \quad (3.1)$$

Subsequent condensation reactions produce polymerizable species with M—O—M bonds, plus alcohol (ROH) or water as a by-product:

$$M(OH)(OR)_{z-1} + M(OR)_z \rightarrow (RO)_{z-1}M{-}O{-}M(OR)_{z-1} + ROH \quad (3.2)$$

$$2\ M(OH)(OR)_{z-1} \rightarrow (RO)_{z-1}M{-}O{-}M(OR)_{z-1} + H_2O \quad (3.3)$$

The hydrolysis rate of metal alkoxides depends on the characteristics of the metal (electronegativity and coordination number) and those of the alkyl group (length and branchy)[39-45]. In general, silicon alkoxides are among the slowest to hydrolyze because of high electronegativity and stable coordination number, 4. In addition, silicon alkoxides are always monomeric, while other metal alkoxides may be associated. The reason for association is that the metals do not reach their full coordination number by the alkoxide groups. For example, the usual coordination number of titanium is six, but there are only four alkoxide ligands in $Ti(OR)_4$. When neat or dissolved in non-polar solvents, coordination expansion occurs by association via OR bridges. For a given metal alkoxide, the hydrolysis rate is influenced by steric factors. Any branching of the alkoxy group or increasing of the chain length lowers the hydrolysis rate.

The most common silicon alkoxide is tetraethoxysilane (TEOS). Since many alkoxy-silanes are immiscible with water, alcohols are used as solvents to homogenize the reaction mixture. However, alcohols not only serve as solvent, but are also reactants due to the reversibility of the reaction (3.1) and (3.2).

A mixture of a tetraalkoxy-silane in water and alcohol would react very slowly. Therefore, acid or base catalysis is necessary to start the hydrolysis and condensation reactions) [39-45].

In the first step of acid catalysis, it is likely that an OR group bonded to Si is rapidly protonated. Electron density is withdrawn from Si, making it more electrophilic and thus more susceptible to attack by water (hydrolysis reaction) or silanol groups, ≡Si-OH (condensation reaction):

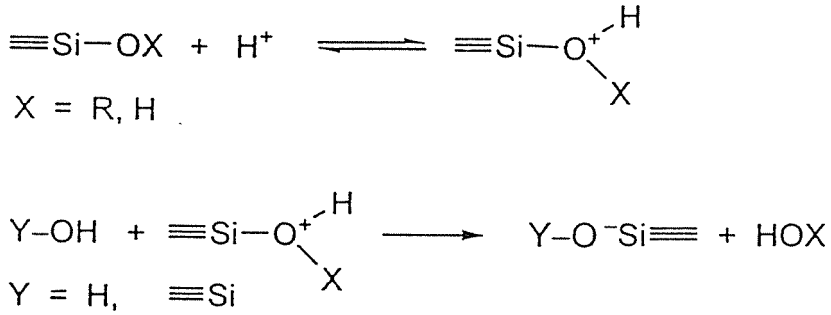

Hydrolysis reaction X = R_1 Y = H (3.4)
Condensation reaction X=R or H1 Y = Si

Under basic conditions, the reaction proceeds by attack of either an OH^- or a ≡Si-O^- ion to the silicon atom (Eq. 3.5). The entering OH^- or ≡Si-O^- are formed by dissociation of H^+ from a water molecule or a SiOH group.

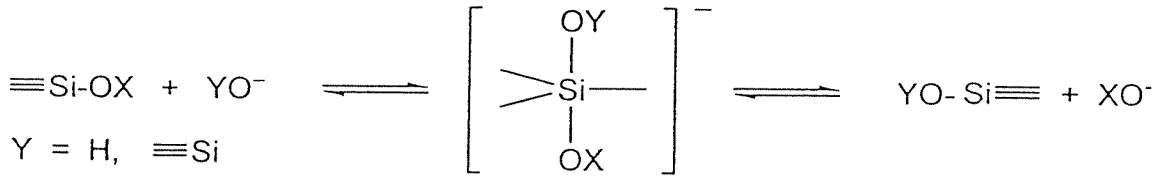

Hydrolysis reaction X = R_1 Y = H (3.5)
Condensation reaction X=R or H1 Y = Si

Obviously, the reaction mechanisms for acid or base catalysis are different. Additionally, the reaction rates for hydrolysis and condensation have a different dependence on the pH. The minimal reaction rate for hydrolysis is at pH = 7, and for condensation around pH = 4.5. Under acidic conditions (pH < 5), hydrolysis is favored, and condensation is the rate-determining step. A great number of monomers or small oligomers with reactive Si-OH groups are simultaneously formed. In contrast,

hydrolysis is the rate-determining step at pH > 5 and hydrolyzed species are immediately consumed because of the faster condensation.

Parameters which also influence hydrolysis and condensation and whose deliberate variation is used for materials design are:

- The type of precursor(s) - reaction rates are influenced by length and branching of alkoxy groups;
- The alkoxy group/H_2O ratio (R_w) - the overall reaction for sol-gel processing of silicon tetraalkoxides is:

$$Si(OR)_4 + 2H_2O \rightarrow SiO_2 + 4\ ROH \qquad (3.6)$$

Equation (3.6) implies that two equivalents of water ($R_w = 2$) are needed to convert $Si(OR)_4$ to SiO_2. Four equivalents of water ($R_w = 1$) are needed for the complete hydrolysis of $Si(OR)_4$ if no condensation would take place. Increasing the water content (i.e., lowering R_w) generally favors the formation of silanol groups over Si-O-Si groups, especially since the condensation reaction is, in principle, reversible. As a rule, $R_w >> 2$ favors the condensation reaction, and $R_w \leq 2$ favors the hydrolysis reaction. The R_w, together with the kind of catalyst, influences the properties of the silicate material very strongly.

- The solvent - the solvent is important to homogenize the reaction mixture, especially at the beginning of the reaction. The polarity, dipole moment, viscosity, protic or non-protic behavior of the solvent influences the reaction rate and thus the structure of the final sol-gel material.

3.3.1.2. Hydrolysis and condensation in multicomponent systems

The situation in multicomponent systems is much more complicated than in systems with one alkoxide. The difference in the rate of hydrolysis and condensation of different alkoxides can lead to in homogeneity of the gel. Therefore, it is necessary, in multicomponent systems, to match rates of hydrolysis and condensation of different alkoxides in order to achieve homogeneity gels.

In general, five different approaches can be used to prepare multicomponent gels [39-45]:

1. Use of double alkoxides,
2. Partial hydrolysis of the slowest reacting alkoxide,
3. Use of a mixture of alkoxides and metal salts,
4. Slow addition of small amounts of water and
5. Matching the hydrolysis rates of the individual alkoxides.

The use of double alkoxides as the starting material for sol–gel processing seeks to eliminate the problem of mismatched hydrolysis rates by forming a molecule or molecular species in which the metals are mixed in the desired ratio. The double alkoxide is hydrolyzed and polymerized in the same way described for simple alkoxides containing one metal and the gel has the same ratio of the two metals as the double alkoxide. The homogeneity of mixing therefore extends to the atomic level.

Despite the high degree of chemical homogeneity obtainable by the double alkoxide route, the method is used only for few cases because many double alkoxides are difficult to prepare or are unstable. Furthermore, for a given two-component gel, changing the chemical composition of the gel by changing the atomic ratios of the two metals becomes a tedious task because a new double alkoxide has to be synthesized in each case.

Partial hydrolysis of the slowest reacting alkoxide prior to adding the other alkoxide is based on idea that the newly added, unhydrolized alkoxide will condense with the partially hydrolyzed sites formed by the previous hydrolysis (hetero-condensation) rather than with itself (homo condensation). Unlike the method involving the use of double alkoxies where molecular-level homogeneity is predicted, the chemical homogeneity of the gel will depend on the size of the polymeric species to which the last component is added.

For some metals it is inconvenient to use alkoxides because they are not available, difficult to prepare or use, or too expensive. This is particularly the case with Group 1 and Group II elements whose alkoxides are solid, nonvolatile, and in many cases of low solubility. Metal salts are a viable alternative provided they are readily converted to the oxide by thermal or oxidative decomposition. The salt should

preferably be soluble in alcohol so that it can be mixed with alkoxide solutions without premature hydrolysis of the alkoxide. Salts of organic acids, in particular acetates, but also citrates, formates, and tartrates are potential candidates. Nitrates are possibly the only suitable inorganic salts because others, such as chlorides or sulfates, are more thermally stable and their anions are difficult to remove. However, nitrates are highly oxidizing, and care should be taken during heating of the gel to reduce the risk of explosions. A problem that is often encountered with this method is that the salt often crystallizes during the drying of the gel, leading to a loss of chemical homogeneity.

Little is known about the reaction mechanism by which the polymerizing alkoxide incorporates the ions of the metal salt into the gel structure. The normal method of preparation is first to form a solution of all components that are to be added as alkoxides, and then add one or more salts as solutions in alcohol or, if this is not possible, in the water to be used for further hydrolysis. All components are then uniformly dispersed and subsequent gelation should then incorporate the elements into a gel network.

For most metal alkoxides, hydrolysis with excess water yields insoluble oxide or hydroxide precipitates that are useless for further polymerization reactions. However, if small amounts of water are added slowly to a sufficiently dilute solution, it is possible to form polymerizable molecular species from these alkoxides.

It was noted that for a given metal M, the hydrolysis rate of the alkoxide $M(OR)_z$ depends on the length of the alkyl group R. This suggests that it may be possible to match the hydrolysis rates of the alkoxides of different metals by careful choice of the alkoxide group. For example, silicon alkoxides are among the slowest to hydrolyze, but of these, tetramethoxysilane (TMOS) has the fastest hydrolysis rate. For some binary system, e.g. SiO_2-Al_2O_3, by selecting an aluminum alkoxide with a sufficiently long alkyl group, it may be possible to match its hydrolysis rates with that of TMOS. In general, this method is rarely used because of the difficulties in matching the hydrolysis rates closely or in obtaining alkoxides with the desired hydrolysis rates. A more promising approach is using chelating agents, such as acetyl acetone, which can react with alkoxides at a molecular level, giving rise to new molecular precursors. The whole hydrolysis-condensation process can therefore be modified. For example, with

the use of chelating agents, the hydrolysis of transition metal alkoxides can be slowed so that better chemical homogeneity can be achieved in multicomponent gels.

It was shown that homogeneity of multicomponent gels prepared by methods (2), (4) and (5) did not differ significantly. The homogeneity of the glasses produced from the gels was also compared with that of a glass produced by melting a mechanically mixed gel. To produce the mixed gel, single gels were prepared separately by hydrolysis of the individual alkoxides, after which they were mixed mechanically. The three gels prepared from mixtures of alkoxides gave glasses with a homogeneity that was far better than that for the glass produced from the mechanically mixed gel.

3.3.2. Colloidal sol-gel process

Colloidal (particulate) sol-gel route gives gels, which consist of a skeletal network of essentially anhydrous particles held together by surface forces. Hydroxyl groups are present only on the surface of the particles. The pores in particulate gels are much larger than in polymeric gels, and the capillary stress developed during drying is therefore lower; thus, less shrinkage occurs [39]. The structure of the dried gel is characterized by a relatively high porosity (~ 70–80 %) and pores that are relatively large compared to the size of the particles (i.e., the average pore size is typically 1–5 times the particle size).

Particulate gels are commonly prepared by taking a stable colloidal suspension and reducing its volume by evaporating some of the liquid or reducing its stability through the addition of an electrolyte such as an acid, a base, or a metal salt [39, 40]. The attractive van der Waals forces dominate, and the particles stick on contact, forming a skeletal network.

3.3.2.1. The properties of colloidal sols

The stability and coagulation of colloidal sols is of great importance for sol-gel chemistry, since the structure of the final oxide network (gel) dependents mainly on the size and shape of aggregating species, i.e. the sol particles. The easy agglomeration of

fine particles is caused by attractive van der Waals forces and/or forces that tend to minimize the total surface or interface energy of the system. In order to prevent aggregation, repulsive forces are required. This can be done by [39, 40, 46-48]:

- Creating electrostatic repulsion between particles. This repulsion results from charges adsorbed on the particles. Electrostatic stabilization occurs when the electrostatic repulsive forces overcome the attractive van der Waals forces between particles.
- Adsorbing a tick organic layer (steric barrier). Steric stabilization can occur in the absence of an electric barrier and is particularly efficient in dispersing high concentrations of particles.

The electrostatic approach is mostly used to stabilize colloidal dispersions in aqueous systems. The repulsive electrostatic barrier results from an electric double layer: the surface of the particle is covered with ionic groups which control the potential of the surface. Counterions in solution near the particle screen the surface charges.

For hydrous oxides, the charge-determining ions are H^+ and OH^-, which create the charge at the particle surface by protonting or deprotonating M-OH groups:

$$M\text{-}OH + H^+ \rightarrow M\text{-}OH_2^+ \quad (3.7)$$

$$M\text{-}OH + OH^- \rightarrow M\text{-}O^- + H_2O \quad (3.8)$$

The pH at which the particle is electrically neutral is called the point of zero charge (PZC). At pH > PZC, particles are negatively charged, surrounded by positively charged counterions in solution (Eq. 3.8), whereas at pH < PZC the particles are positively charged (Eq.3.7). Typical values for the PZC are: MgO 12, Al_2O_3 9.0, SiO_2 2.5. It should note that acidity of the surface M-OH groups depends somewhat on the particle size and the degree of condensation. The magnitude of the surface potential depends on the difference between pH and PZC. That potential attracts the counterions present in solution.

The electric double layer is schematically shown in Figure 3.4. for a positively charged surface [39-41]. The repulsive potential drops linearly through the tightly bound layer of water and counterions (called the Stern layer). Beyond the so-called

Helmholtz plane, the linear dependence changes into a region in which the electric potential varies exponentially with the distance from the particle.

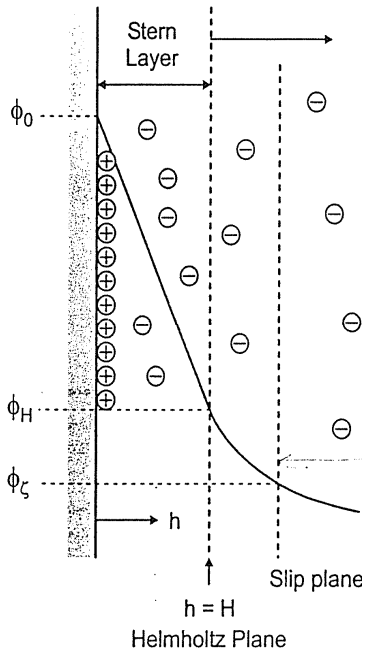

Figure 3.4. Electric double layer over a positively charged surface (ϕ_0 - potential at the particle surface, ϕ_H - potential at the Helmholtz plane, ϕ_ζ - zeta potential, h - the distance to the particle surface) [39-41]

When the particle moves, it carries along the adsorbed layer and part of the cloud of counterions, while the more distant portion of the double layer is stayed behind the particle. The "slip plane" or "shear plane" separates the region of fluid that moves with the particle from the region that flows freely. The potential at the slip plane is the zeta (ζ) potential (ϕ_ζ). The pH at which ϕ_ζ is zero is called the isoelectric point (IEP), which in general is not equal to the PZC. The stability of the colloid correlates with the magnitude of the ζ potential. The higher the ζ potential the more stable are the colloid sols.

Coagulation/gelation of sol particles results from:

- decreasing the surface potential ϕ_0 (by changing the pH) or
- increasing the electrolyte concentration in the solution. As the concentration of counterions increases, the double layer is compressed, because the number of charges required to balance the surface charge is now available in a smaller volume surrounding the particle. The colloid will eventually coagulate because the attractive force is unchanged, while the repulsive barrier is reduced.

In some cases, a coagulated colloid can be redispersed. This process is called peptization. This can be done by removing the counterions that caused coagulation (washing) or by adsorbing charge-determining ions that re-establish the double layer.

3.3.2.2. Aqueous silicic acid solution and silica sols

Sols can be obtained in various ways, either by connecting the individual ions or molecules of dissolved substances in aggregates (condensation methods), and through dispersion of relatively large particles (dispersion methods and peptization methods). For the application of colloidal sol-gel processes in the ceramics, SiO_2 sol is of the greatest interest. Silica sol can be obtained by different method, but the most common method is by using aqueous silicic acid solutions [39, 40, 50].

Silicic acid, $Si(OH)_4$, which is formed when water glass is reacted with an acid or by ion exchange of the sodium ion for H^+, is only stable in solution at pH <7. At pH > 7 deprotonated species, mainly $H_3SiO_4^-$, are found in diluted solutions (< 10^{-4} mol·1^{-1}) and mainly condensed anionic species are present in concentration anionic solution (> 0.1mol·1^{-1}).

Contrary to sol–gel processing of alkoxide precursors, there are mainly three possibilities to control the morphology and properties of the products: the concentration of the precursor, the presence of salt and pH of the solution.

Three important pH regimes have to be distinguished: pH < 2, pH 2-7 and pH > 7. At pHs lower than about 2, the silicic acid species are positively charged and according to the mechanism given in Eq. 3.4, the reaction rate of the condensation is proportional to the concentration of the H^+ ions. Between pH 2 and 7 the reaction rate of condensation is proportional to the concentration of the OH^- ions (Eq. 3.5). This means,

that the condensation rates are increasing when the pH is increased. At pHs higher than 7, the rates of solubility and for re-dissolution of particles are maximal. The solution now contains mainly anionic species which reject each other.

In all cases, in the initial stage of the sol-gel reactions, small three-dimensional oligomeric particles are formed, with Si-OH groups on their outer surface. The oligomers serve as nuclei. They may either grow or agglomerate at a certain size, depending on the experimental conditions (Figure 3.5).

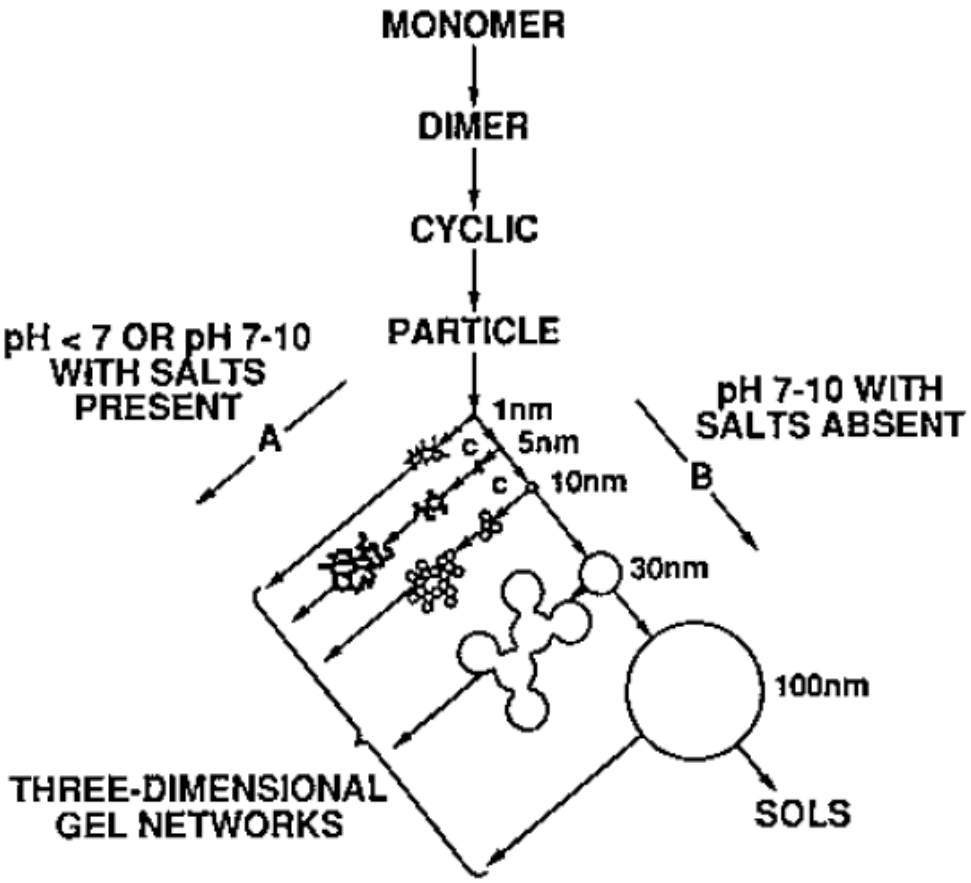

Figure 3.5. Structural development in aqueous silicic acid solution, depending on conditions [39, 40, 50].

Agglomeration of the oligomeric particles does not necessarily result in gelation; instead, larger particles with a polymeric sub-structure can be formed. Whether the

larger particles (with polymeric or dense substructure) remain suspended in solution (i. e., whether a stable sol is obtained) or agglomerate themselves to form a three-dimensional network (i.e., whether gelation occurs) again depends on the system and the experimental conditions which influence the stability of the sol.

3.3.3. The sol –gel transition (gelation)

As the sol particles aggregate and condense, the viscosity of the sol gradually increases and a gel is eventually formed (if the sol is sufficiently concentrated). The sol-gel transition (gel point) is reached when a continuous network is formed [39, 40]. From a practical point of view, the gel time (t_{gel} - time at which the gel point is reached) is determined by turning the reaction vessel upside down. Before the gel point has been reached, the sol behaves like a more or less viscous liquid, i.e., the liquid will flow out of the vessel. At the gel point, the viscosity increases sharply, and a form-stable, elastic gel body is obtained. Since all liquid is retained in the gel body, no liquid can flow out of the vessel if it turned upside down. For the same reason, the volume of the gel in this stage is the same as that of the original precursor solution.

In the case of polymeric gels, the t_{gel} is generally lowered by all parameters that increase the rate of condensation reactions. These parameters thus allow to deliberately influencing the gel times.

Colloidal gels are formed by decreasing stability of colloidal sols and thus the gel time dependence on the sol destabilization method - liquid evaporation or addition of an electrolyte [39, 40, 51]. Generally, the t_{gel} is generally lowered by increasing sol concentration and electrolyte concentration. In the case of multicomponent colloidal gels, different sols or sols and electrolyte solution are mixed. In these cases, it is necessary to take into account the mutual influence of sols or sol and electrolyte solution, especially if sols are differently charged. Therefore, in each case it is necessary to determine the optimal conditions of gelation, such as the order of mixing of sols and the electrolyte solution, the concentration of sols and the electrolyte solution and pH value in order to obtain homogeneous gels of given composition.

3.3.4. Aging of gels

The condensation reactions that cause gelation continue long after the gel point, leading to strengthening, stiffening, and shrinkage of the network. If the gel is aged in the original pore liquid, small clusters continue to diffuse and attach to the main network. As these new links form, the network becomes stiffer and stronger. Many gels exhibit the phenomenon of syneresis, shown in Fig 3.6, where the gel network shrinks and expels the liquid from the pores. Shrinkage most likely results from condensation between neighboring groups on the surface of the solid network.

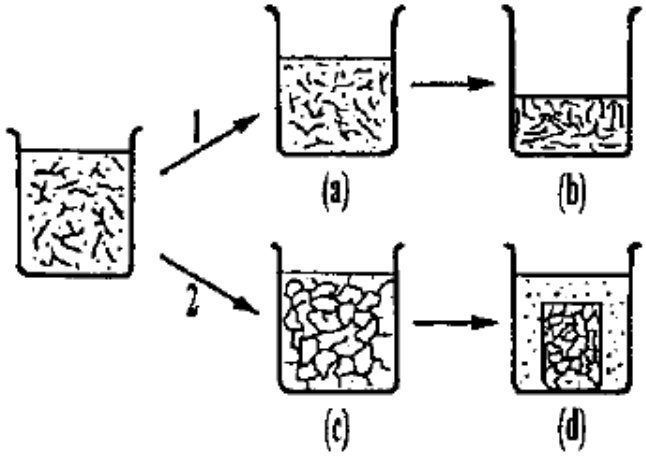

Figure 3.6. Two modes of shrinkage of a wet gel: shrinkage produced when the liquid is allowed to evaporate (route 1) and expulsion of liquid from the gel giving rise to shrinkage without evaporation (syneresis) (route 2) [39].

3.3.5. Drying of gels

The evaporation of the liquid from a wet gel by conventional methods, i.e., by temperature increase or pressure decrease, proceeds in a very complex way in which three different stages can be distinguished [39]:

1 - The gel shrinks by the volume that was previously occupied by the liquid. The liquid flows from the interior of the gel body to its surface. If the network is compliant, as it is in alkoxide-derived gels, the gel deforms. Upon shrinkage, OH groups at the inner surface approach at each other and can react with each other. For example, new

siloxane bridges are formed in SiO_2 gels. As drying proceeds, the network becomes increasingly stiffer and the surface tension in the liquid rises correspondingly because the pore radii become smaller.

2 - This stage of the drying process begins when the surface tension is no longer capable of deforming the network and the gel body becomes too stiff for further shrinkage. The tension in the gel becomes so large that the probability of cracking is highest.

3 - Here, the liquid film is ruptured. Eventually, liquid is only in isolated pockets and can leave the network only by diffusion via the gas phase.

Two processes are important for the collapse of the network. First, the slower shrinkage of the network in the interior of the gel body results in a pressure gradient, which causes cracks. Second, larger pores will empty faster than smaller pores during drying, i.e., if pores with different radii are present, the meniscus of the liquid drops faster in larger pores. The walls between pores of different size are therefore subjected to uneven stress and crack. For these reasons, xerogel powders are usually obtained when wet gel bodies are conventionally dried [39, 52]. Although strategies were developed to obtain crack-free xerogel bodies, the large shrinkage cannot be avoided. Due to the shrinkage problem, one of the most important applications of sol-gel materials is for films and coatings, where shrinkage is easier to control. Aerogels are obtained when methods are applied that allow the pore liquid of a wet gel to be replaced by air, without decisively altering the network structure or the volume of the gel body [53, 54].

4. POWDERS CONSOLIDATION

The microstructure of the green body has a significant effect on the subsequent firing stage. If severe variations in packing density occur in the green body, the fired body will contain heterogeneities that will limit the engineering properties. The homogeneous packing of particles in the green body is the desired goal of the

consolidation step. Since the packing density controls the amount of shrinkage during firing, the achievement of high packing density is also desirable [5, 39, 41].

Mechanical compaction of powders in a die is one of the most widely used forming operations in the ceramic industry. The powder may be dry pressed (i.e., without the addition of a binder) or pressed with the addition of a small amount of a suitable binder. The pressure is applied either uniaxially or isostatically. The choice of pressing method depends on the shape of the final product. We make simple shapes by applying the pressure uniaxially; more complex shapes require isostatic pressing.

4.1. Dry pressing

Dry pressing [5, 39, 41] is ideally suited to the formation of simple shapes and consists of three basic steps: filling the die, compacting the contents, and ejecting the pressed solid. Figure 4.1 shows the stages of dry-pressing process. In a double-action press both the top and bottom punches are movable. When the bottom punch is in the low position a cavity is formed in the die and this cavity is filled with free flowing powder. In dry pressing, the powder mixture will contain between 0 and 5 wt% of a binder. (So, dry does not imply that there is no binder.) Once the cavity has been filled, the powder is struck off level with the top of the die. The top punch descends and compresses the powder either to a predetermined volume or to a set pressure[24].

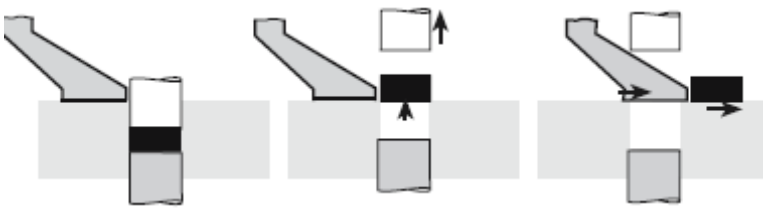

Figure 4.1. The stages of dry pressing [41].

During pressing the powder, particles must flow between the closing punches so that the space between them is uniformly filled. A particle size distribution of between 20 and 200 μm is often preferred for dry pressing: a high volume fraction of small

particles causes problems with particle flow and results in sticking of the punches. The pressures used in dry pressing may be as high as 300 MPa, depending upon material and press type, to maximize the density of the compact. After pressing, both punches move upward until the bottom punch is level with the top of the die and the top punch is clear of the powder-feeding mechanism. The compact is then ejected, the bottom punch is lowered, and the cycle is repeated.

After the completion of the die compaction process, it is important that the green body be free of macroscopic defects and that density gradients be as low as possible. Density gradients lead to the development of cracklike voids in the sintered body and can also lead to cracking and warping of the body during sintering. They also enhance the formation of defects in the compact on ejection from the die. Several factors can be controlled to reduce the extent of density gradients in the powder compact. Uniform die filling reduces the amount of internal movement of the powder during the compaction process. The use of lubricants to reduce the internal friction between the particles and die-wall friction can lead to significant improvements. Stress gradients (and hence, density gradients) due to die-wall friction are enhanced with increasing ratio of the length to diameter (L/D) of the compact. For the single-action mode of die compaction, L/D should be less than 0.5, while for the double-action mode it should be less than 1.

The common defects in compacts [5] formed by die pressing are illustrated in Fig. 4.2. They are caused by springback and by friction at the die walls. The use of a binder to increase the compact strength, reduction of the applied pressure to reduce the extent of the springback, and the use of a lubricant to reduce die wall friction can significantly reduce the tendency for defect formation.

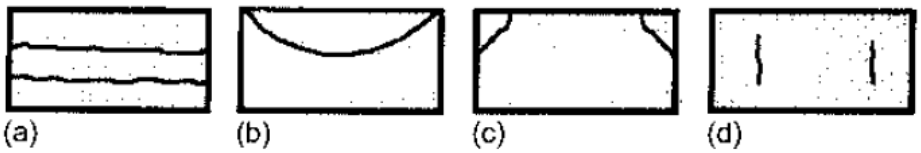

Figure 4.2. Illustrations of typical defects in die compaction of dry or semidry powders: (a) delamination, (b) capping, (c) ring capping, and (d) vertical cracks [5].

Because the dry-pressing process is so simple and involves low capital equipment costs it is the most widely used high-volume forming process for ceramics. Production

rates depend on the size and shape of the part and on the type of press used. For large components such as refractories or complex parts such as grinding wheels the production rates are 1–15 parts per minute. Simpler or smaller shapes such as seal rings and nozzles can be produced at rates up to several hundred per minute. Small flat parts such as insulators, chip carriers, or cutting tools can be produced at rates up to several thousand per minute.

4.2. Cold isostatic pressing

Isostatic pressing involves the application of a uniform hydrostatic pressure to the powder contained in a flexible rubber container. There are two modes of isostatic pressing: wet-bag pressing and dry-bag pressing [41].

Figure 4.3 illustrates the so-called wet-bag CIP process. Powder is weighed into a rubber bag and a metal mandrel is inserted that makes a seal with the mouth of the rubber bag. The sealed bag is placed inside a high-pressure chamber that is filled with a fluid (normally a soluble oil/water mixture) and is hydrostatically pressed. The pressures used can vary from about 20 MPa up to 1 GPa depending upon the press and the application. For production units the pressure is usually ≤ 400 MPa. Once pressing is complete, the pressure is released slowly, the mold is removed from the pressure chamber, and the pressed component is removed from the mold.

The advantages of the wet-bag process are:

- Wide range of shapes and sizes can be produced,
- Uniform density of the pressed product,
- Low tooling costs.

The disadvantages are:

- Poor shape and dimensional control (particularly for complex shapes),
- Products often require green machining after pressing,
- Long cycle times (typically between 5 and 60 minutes) give low production rates.

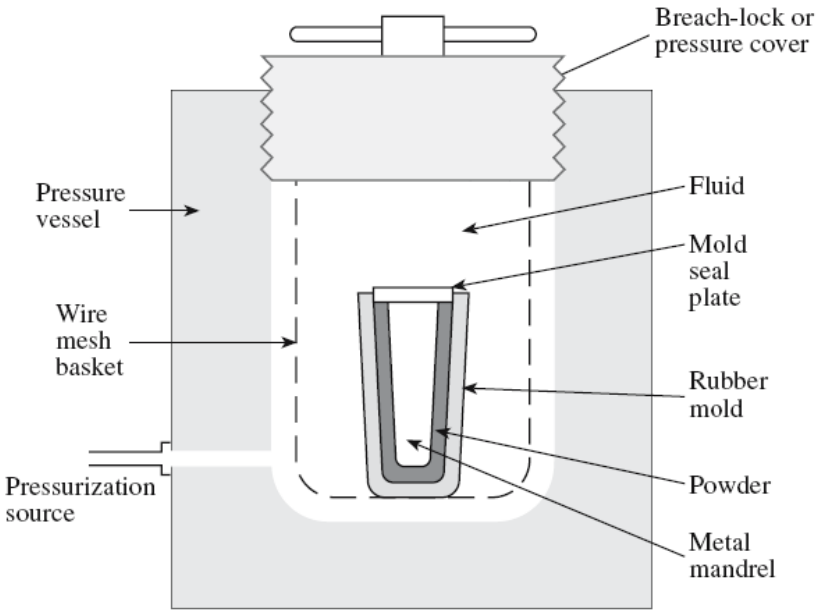

Figure 4.3. Schematic of a wet-bag isostatic pressing system [41].

A schematic diagram of a mold for the dry-bag CIP is shown in Figure 4.4. The main distinction of the dry-bag process is that the rubber mold is now an integral part of the press. The high-pressure fluid is applied through channels in the mold. After pressing, the pressed part is removed without disturbing the mold. Hence, the dry-bag press can be readily automated. Fully automated units are widely available and have been operating in the high volume production of ceramic parts for over 20 years. Production rates of up to 1 part per second are being achieved industrially.

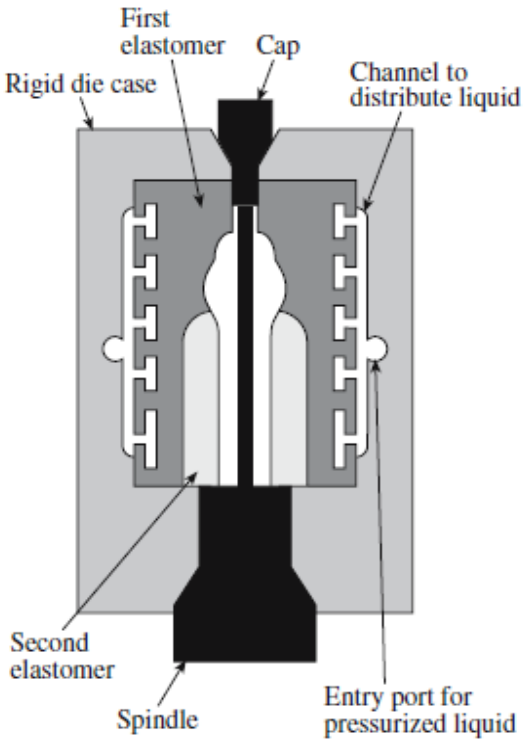

Figure 4.4. Schematic of a die for dry-bag isostatic pressing of a spark plug insulator [41].

5. SINTERING

Sintering is a processing technique used to produce density-controlled materials and components from powders by applying thermal energy. Hence, sintering is categorized in the synthesis/processing element among the four basic elements of materials science and engineering [55], as shown in Figure 5.1. As material synthesis and processing have become crucial in recent years for materials development, the importance of sintering is increasing as a material processing technology.

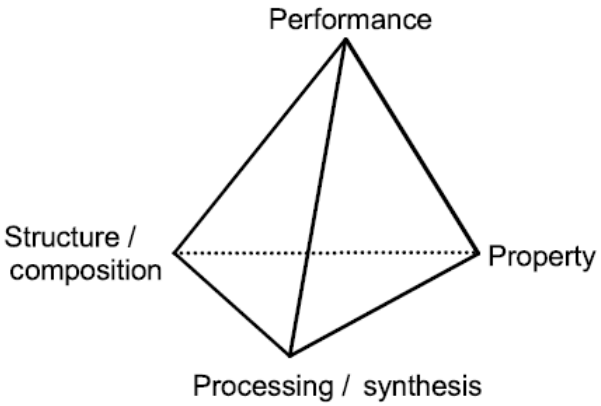

Fig 5.1. The for basic elements of material science and engineering [55]

Sintering is, in fact, one of the oldest human technologies, originating in the prehistoric era with the firing of pottery. Nevertheless, it was only after the 1940s that sintering was studied fundamentally and scientifically. Since then, remarkable developments in sintering science have been made. One of the most important and beneficial uses of sintering in the modern era is the fabrication of sintered parts of all kinds, including powder-metallurgical parts and bulk ceramic components.

Sintering aims, in general, to produce sintered parts with reproducible and, if possible, designed microstructure through control of sintering variables [5, 6, 37, 38, 55]. Microstructural control means the control of grain size, sintered density, and size and distribution of other phases including pores. In most cases, the final goal of microstructure control is to prepare a fully dense body with a fine grain structure.

5.1. Driving force and basic phenomena

Sintering is accompanied by a lowering of the free energy of the system due to the reduction of the total interfacial energy. The total interfacial energy of a powder compact is expressed as γA, where γ is the specific surface (interface) energy and A the total surface (interface) area of the compact. The reduction of the total energy can be expressed as:

$$\Delta(\gamma A) = \gamma \cdot \Delta A + A \cdot \Delta\gamma \qquad (5.1)$$

Here, the change in interfacial energy ($\Delta\gamma$) is due to densification and the change in interfacial area (ΔA) is due to grain coarsening. For solid state sintering, $\Delta\gamma$ is related to the replacement of solid/vapour interfaces (surface) by solid/solid interfaces. As schematically shown in Figure 5.2, the reduction in total interfacial energy occurs via densification and grain growth, the basic phenomena of sintering.

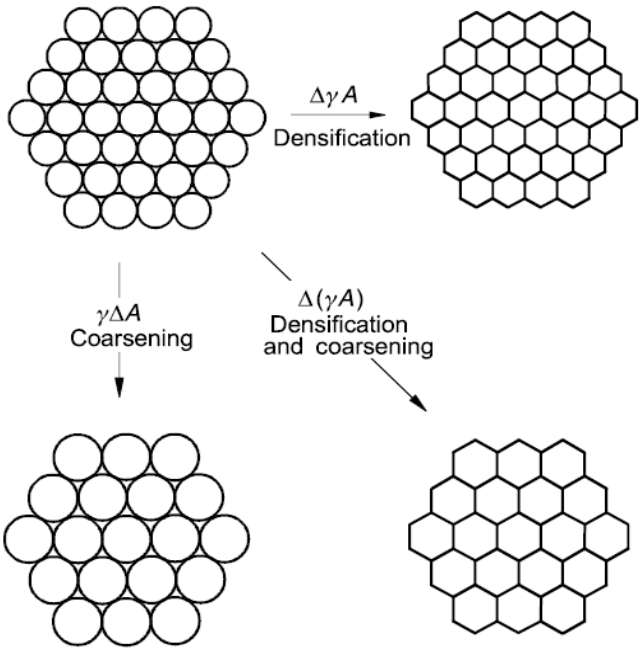

Figure 5.2. Basic phenomena occurring during sintering under the driving force for sintering, $\Delta(\gamma A)$ [55].

Hence, the thermodynamic driving force for sintering is the reduction in total interfacial energy. However, in terms of kinetics, the differences in bulk pressure, vapour pressure and vacancy concentration due to interface curvature induce material transport. Figure 5.3 shows that the pressure in region I with a positive curvature is higher than that in region II with a negative curvature. In addition, because of the pressure difference, the vapour pressure above region I is higher than that above region

II. On the other hand, for a vacancy, which can be considered as a dispersed phase of a vacuum, region I has a negative curvature and region II a positive curvature from the vacuum side. The equilibrium vacancy concentration in region II is higher than that in region I. Note that the three kinds of thermodynamic phenomena (differences in bulk pressure, vapour pressure and vacancy concentration) occur simultaneously and independently.

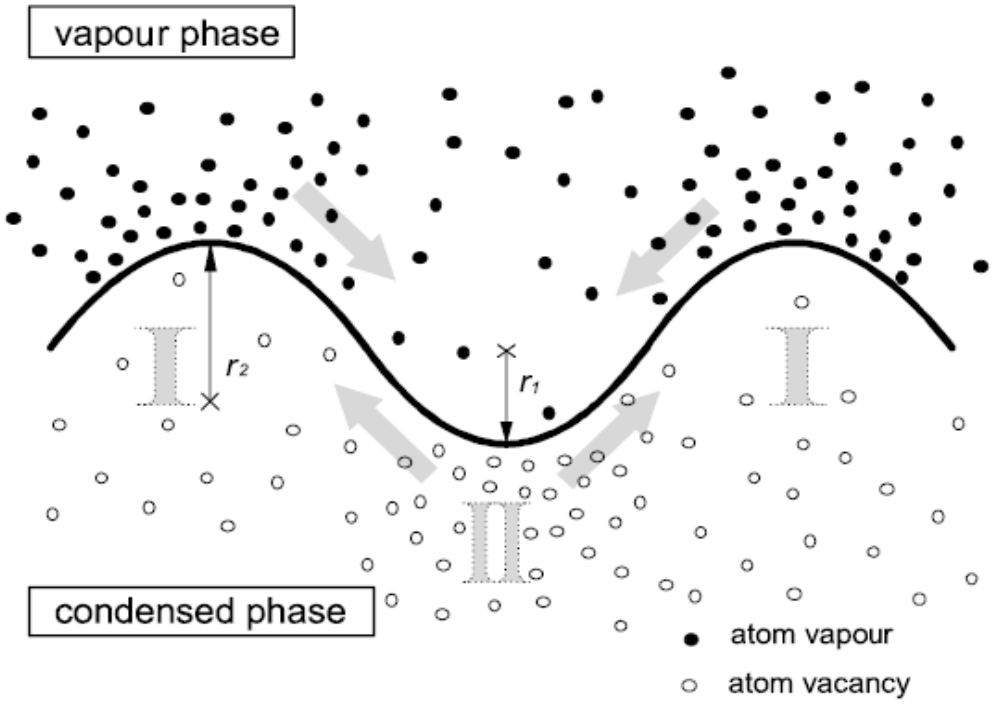

Figure 5.3. Schematic showing distributions of vacancies (o) and vapour atoms (•) near a curved interface [55].

5.2. Sintering variables

The major variables which determine sinterability and the sintered microstructure of a powder compact may be divided into two categories: material variables and process variables [5, 6, 55].

The variables related to raw materials (material variables) include chemical composition of powder, powder particle size, powder particle shape, powder particle

size distribution, degree of powder particle agglomeration, etc. These variables influence the powder compressibility and sinterability (densification and grain growth). In particular, for compacts containing more than two kinds of powders, the homogeneity of the powder mixture is of prime importance. To improve the homogeneity, not only mechanical milling but also chemical processing, such as sol-gel processes, have been investigated and utilized. The other variables involved in sintering are mostly thermodynamic variables, such as temperature, time, atmosphere, pressure, heating and cooling rate. Many previous sintering studies have examined the effects of sintering temperature and time on sinterability of powder compacts. It appears, however, that in real processing, the effects of sintering atmosphere and pressure are much more complicated and important. Unconventional processes controlling these variables have also been intensively studied and developed.

The effects of some key material and processing parameters on the densification process, e.g. on density of sintered body are shown in Fig 5.4. The rate of densification is enhanced by: higher sintering temperature, longer sintering time, smaller particles and higher green density. Densification is further enhanced by the application of an external pressure.

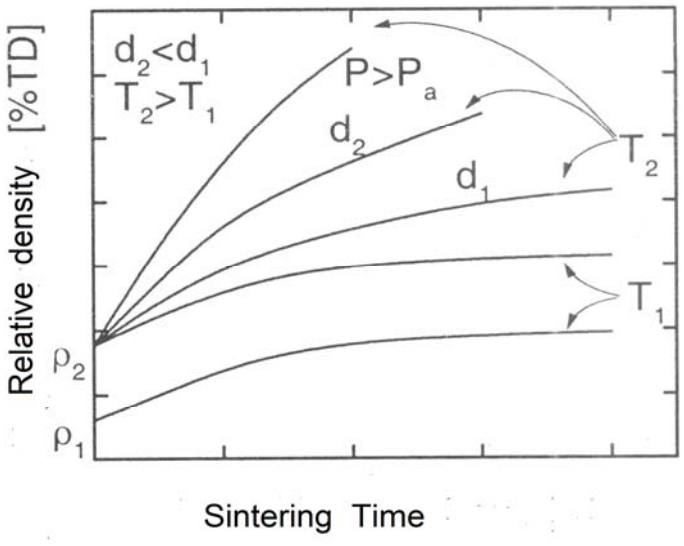

Figure 5.4. Dependence of sintered density (in percent of theoretical density, TD) on time, for various material and processing parameters (T - temperature, d - particle size, ρ - green density, P - applied pressure) [56]

A key issue that has received increasing attention in recent years is the effect of microstructural inhomogeneities present in the green body (e.g., density, grain size, and compositional variations). It is now well recognized that inhomogeneities can seriously hinder the ability to achieve high density and to adequately control the fabricated microstructure.

5.3. Categories of sintering

Sintering processes can be divided into two types: solid state sintering and liquid phase sintering [5, 6, 55-57]. Solid state sintering occurs when the powder compact is denstified wholly in a solid state at the sintering temperature, while liquid phase sintering occurs when a liquid phase is present in the powder compact during sintering. In addition to solid state and liquid phase sintering, other types of sintering, for example, transient liquid phase sintering and viscous flow sintering can be utilized. Viscous flow sintering occurs when the volume fraction of liquid is sufficiently high, so that the full densification of the compact can be achieved by a viscous flow of grain–liquid mixture without having any grain shape change during densification. Transient liquid phase sintering is a combination of liquid phase sintering and solid state sintering. In this sintering technique, a liquid phase forms in the compact at an early stage of sintering, but the liquid disappears as sintering proceeds and densification is completed in the solid state.

In general, compared with solid state sintering, liquid phase sintering allows easy control of microstructure and reduction in processing cost, but degrades some important properties, for example, mechanical properties. In contrast, many specific products utilize properties of the grain boundary phase and, hence, need to be sintered in the presence of a liquid phase. In these cases, the composition and amount of liquid phase are of prime importance in controlling the sintered microstructure and properties.

5.4. Stages of sintering

Sintering is normally thought to occur in three sequential stages referred to as (1) the initial stage, (2) the intermediate stage, and (3) the final stage [6, 39, 55-57]. A stage represents an interval of time or density over which the microstructure is considered to be reasonably well defined. For polycrystalline materials, Fig. 5.5 shows the idealized geometrical structures of the three stages [39].

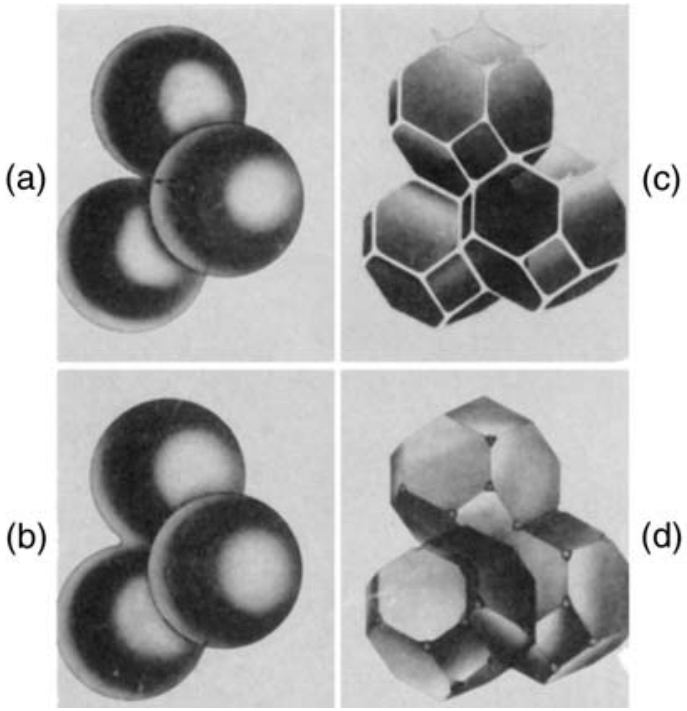

Figure 5.5. Idealized models for the three stages of sintering. (a) Initial stage: Model structure represented by spheres in tangential contact. (b) Near the end of the initial stage: spheres have begun to coalesce. The neck growth illustrated is for center-to-center shrinkage of 4%. (c) Intermediate stage: Dark grains have adopted the shape of a tetrakaidecahedron, enclosing white pore channels at the grain edges. (d) Final stage: Pores are tetrahedral inclusions at the corner where four tetrakaidecahedra meet [39].

The initial stage consists of fairly rapid interparticle neck growth by diffusion, vapor transport, plastic flow, or viscous flow. The large initial differences in surface curvature are removed in this stage, and shrinkage (or densification) accompanies neck growth for the densifying mechanisms. For a powder system consisting of spherical particles, the initial stage is represented as the transition between Figs 5.5.a and 5.5.b. It is assumed to last until the radius of the neck between the particles has reached a value of ~ 0.4–0.5 of the particle radius. For a powder system with an initial density of 0.5–0.6 of the theoretical density, this corresponds to a linear shrinkage of 3 to 5 % or an increase in density to ~ 0.65 of the theoretical when the densifying mechanisms dominate.

The intermediate stage begins when the pores have reached their equilibrium shapes as dictated by the surface and interfacial tensions. The pore phase is still continuous. In the sintering models, the structure is usually idealized in terms of a spaghetti-like array of porosity sitting along the grain edges as illustrated in Fig. 5.5.c. Densification is assumed to occur by the pores simply shrinking to reduce their cross section. Eventually, the pores become unstable and pinch off, leaving isolated pores; this constitutes the beginning of the final stage. The intermediate stage normally covers the major part of the sintering process, and it is taken to end when the density is ~0.9 of the theoretical.

The microstructure in the final stage can develop in a variety of ways. In one of the simplest descriptions, the final stage begins when the pores pinch off and become isolated at the grain corners, as shown by the idealized structure in Fig. 5.5.d. In this simple description, the pores are assumed to shrink continuously and may disappear altogether. The removal of almost all of the porosity has been achieved in the sintering of several real powder systems. Some of the main parameters associated with the three idealized stages of sintering are summarized in Table 5.1 and Figure 5.6 schematically depicts the typical densification curve of a compact through these stages over sintering time.

TABLE 5.1 Parameters associated with the stages of sintering for polycrystalline solids [39, 55]

Stage	Typical microstructural feature	Relative density (range)	Idealized model
Initial	Rapid inter-particle neck growth	Up to ~ 0.65	Two monosize spheres in contact
Intermediate	Equilibrium pore shape with continuous porosity	~ 0.65 – 0.90	Tetrakaidecahedron with cylindrical pores of the same radius along the edges
Final	Equilibrium pore shape with isolated porosity	> ~0.90	Tetrakaidecahedron with spherical monosize pores at the corners

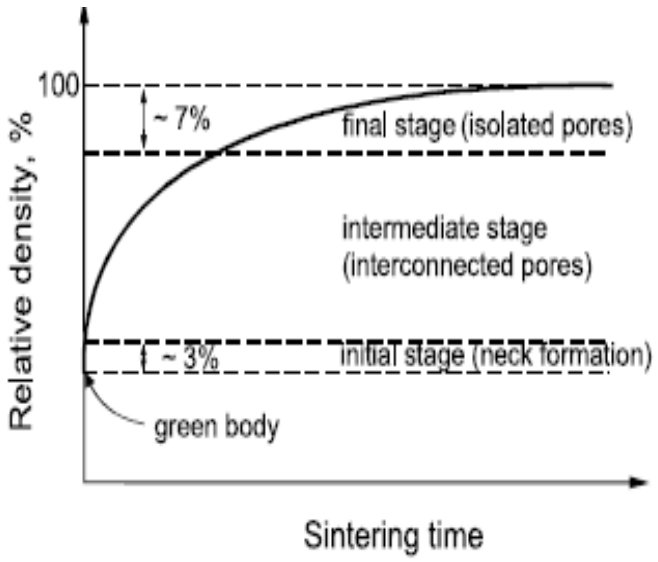

Figure 5.6. Schematic showing the densification curve of a powder compact and the three sintering stages [39, 55].

5.5. Mechanisms of solid-state sintering

Sintering of polycrystalline materials occurs by diffusional transport of matter along definite paths that define the mechanisms of sintering shown in table 5.2. Matter is transported from regions of higher chemical potential (referred to as the source of matter) to regions of lower chemical potential (referred to as the sink). There are at least six different mechanisms of sintering in polycrystalline materials, as shown schematically in Fig. 5.7. for a system of three sintering particles. They all lead to bonding and growth of necks between the particles, so the strength of the powder compact increases during sintering. Only certain mechanisms, however, lead to shrinkage or densification, and a distinction is commonly made between densifying and nondensifying mechanisms. Surface diffusion, lattice diffusion from the particle surfaces to the neck, and vapor transport (mechanisms 1, 2, and 3) lead to neck growth without densification and are referred to as nondensifying mechanisms. Grain boundary diffusion and lattice diffusion from the grain boundary to the pore (mechanisms 4 and 5) are the most important densifying mechanisms in polycrystalline ceramics. Diffusion from the grain boundary to the pore permits neck growth as well as densification. Plastic flow by dislocation motion (mechanism 6) also leads to neck growth and densification but is more common in the sintering of metal powders. The nondensifying mechanisms cannot simply be ignored because when they occur, they reduce the curvature of the neck surface (i.e., the driving force for sintering) and so reduce the rate of the densifying mechanisms. Table 5.2 summarizes the sintering mechanisms in polycrystalline solids.

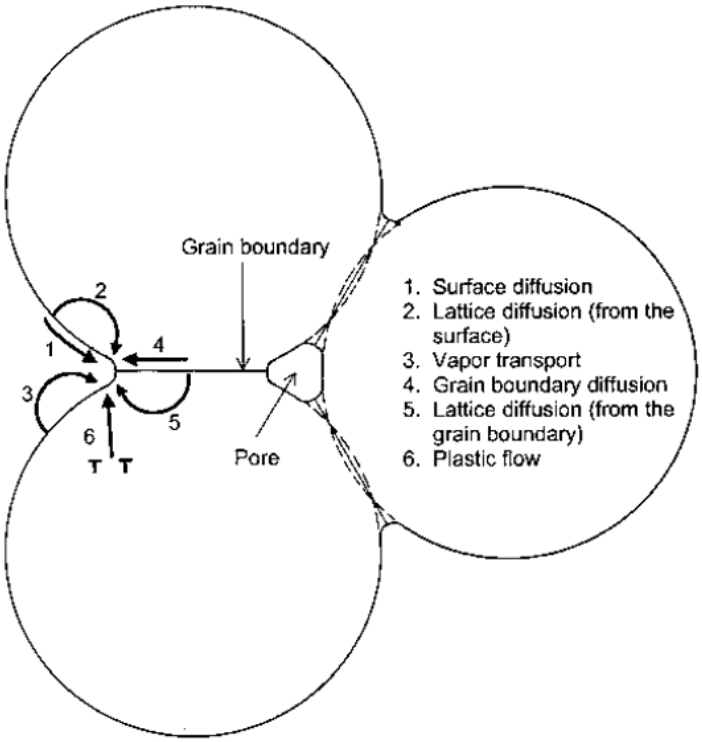

Figure 5.7 Six distinct mechanisms can contribute to the sintering of a consolidated mass of crystalline particles: (1) surface diffusion, (2) lattice diffusion from the surface, (3) vapor transport, (4) grain boundary diffusion, (5) lattice diffusion from the grain boundary, and (6) plastic flow [20]

Table 5.2. The sintering mechanisms in polycrystalline solids

Mechanism	Source of matter	Sink of matter	Densifying	Non-densifying
Surface diffusion	Surface	Neck		x
Lattice diffusion	Surface	Neck		x
Vapor transport	Surface	Neck		x
Grain boundary diffusion	Grain boundary	Neck	x	
Lattice diffusion	Grain boundary	Neck	x	
Plastic flow	Dislocations	Neck	x	

5.6. Grain growth

Grain growth is the term used to describe the increase in the grain size of a single-phase solid or in the matrix grain size of a solid containing second-phase particles. Grain growth occurs in both dense and porous polycrystalline solids at sufficiently high temperatures. For the conservation of matter, the sum of the individual grain sizes must remain constant; so an increase in the average grain size is accompanied by the disappearance of some grains, usually the smaller ones. In porous solids, both the grains and the pores commonly increase in size while decreasing in number. Frequently, the term coarsening is used to describe the process of grain growth coupled with pore growth.

The grain boundary is considered a region of disorder between two crystalline regions (the grains). Grain growth occurs as atoms (or ions) diffuse less than an interatomic distance from one side of the boundary to new positions on the other side, resulting in one grain growing at the expense of another. The atoms move from the ‘‘convex’’ surface on one side of the grain boundary to the ‘‘concave’’ surface on the other side (Fig 5.8.) more readily than in the reverse direction because the chemical potential of the atoms under the convex surface is higher than that for the atoms under the concave surface.

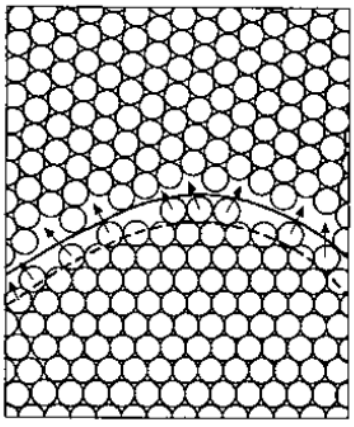

Fig. 5.8. Picture of a grain boundary. The boundary migrates downward as atoms move less than an interatomic spacing from the convex side of the boundary to the concave side [39].

The result of this net flux is that the boundary moves toward its center of curvature (Fig. 5.9).

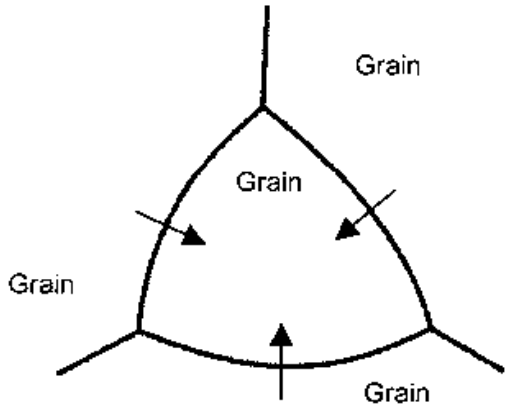

Figure 5.9. Movement of the grain boundary toward its center of curvature

The driving force for grain growth is the decrease in free energy that accompanies reduction in the total grain boundary area.

Grain growth in ceramics is generally divided into two types: (1) normal grain growth and (2) abnormal grain growth, which is sometimes referred to as exaggerated grain growth, discontinuous grain growth, or in the case of metals, secondary crystallization. In normal grain growth, the average grain size increases but the grain sizes and shapes remain within a narrow range, so the grain size distribution later is similar to that at an early time. In abnormal grain growth, a few large grains develop and grow relatively faster than the surrounding matrix of smaller grains. The grain size distribution may change significantly, giving raise to a bimodal distribution, so in this case the property of time invariance of the distribution is lost. Eventually, the large grains impinge and may revert to a normal distribution of sizes.

The control of grain growth during sintering forms one of the most important considerations in the fabrication of ceramics for two key reasons. First, grain growth increases the diffusion distance for matter transport, thereby reducing the rate of densification, so grain growth control forms an important approach for achieving the normally required high density. Second, many engineering properties of ceramics are dependent on the grain size, so grain growth control is directly related to the

achievement of the desired properties. Generally, most properties are enhanced by smaller grain size, a notable exception being the creep resistance, which increases with larger grain size. For example, the fracture strength of many ceramics is often found to increase with grain size G according to $1/G^{1/2}$. A wide range of electrical and magnetic phenomena is affected by grain size, and it is in this area that grain size control has been used most effectively to produce ceramics with properties suitable for a variety of applications.

As stated above, grain boundaries move because of many individual atomic jumps across the plane of the boundary (Fig 5.8). While this process is always necessary, it is not always the slowest or rate-limiting step. When it is, the mobility is termed intrinsic. However, rarely in ceramics is the mobility as high as intrinsic, since segregated solutes, pores and inclusions and secondary phase films can exert a drag force on the boundary. Since boundary and liquid diffusivities can be comparable in magnitude, for very thin liquid films, this mobility may approach the intrinsic limit, but it is typically lower. Even ceramics free of liquid phase films are rarely pure enough for intrinsic grain boundary migration to take place. Some form of impurity segregation nearly always occurs. Solute diffusion in the near boundary region is usually slower than the intrinsic diffusion of host atoms across the boundary plane, and become rate limiting. Pores and second-phase inclusion that intersect the boundary also present a barrier to boundary migration. The effectiveness of inclusions in limiting grain growth increases as the particle size is decreased and the volume fraction increased.

5.7. Liquid-phase sintering

In many ceramic systems, the formation of a liquid phase is commonly used to assist in the sintering and micro structural evolution. Usually the purpose of liquid-phase sintering is to enhance densification rates, achieve accelerated grain growth, or produce specific grain boundary properties. The distribution of the liquid phase and of the resulting solidified phases produced on cooling after densification is critical to achieving the required properties of the sintered material. Commonly, the amount of liquid formed during sintering is small, typically less than a few volume percent, which

can make precise control of the liquid composition difficult. Liquid-phase sintering is particularly effective for ceramics such as Si_3N_4 and SiC that has a high degree of covalent bonding and is therefore difficult to density by solid-state sintering. The process is also important when the use of solid-state sintering is too expensive or requires too high a fabrication temperature. However, the enhanced densification rates achieved by liquid-forming additives are only of interest if the properties of the fabricated ceramic remain within the required limits. A disadvantage of liquid-phase sintering is that the liquid phase used to promote sintering commonly remains as a glassy intergranular phase that may degrade high temperature mechanical properties such as creep and fatigue resistance.

A related process is activated sintering in which minor amounts of additives that segregate strongly to the grain boundaries can significantly enhance mass transport rates along the grain boundary, giving rise to accelerated densification even at temperatures well below that for liquid formation in the system. In many systems, there is no clear difference in principles between activated sintering and liquid-phase sintering, except that for the activated system, the amount of additive is small so that the presence of a liquid grain boundary film can be difficult to detect.

If sufficient liquid is present (on the order of 25–30 vol%), rearrangement of the solid phase coupled with liquid flow can lead to a fully dense material. Such large volume fractions of liquid are commonly used in traditional, clay-based ceramics such as porcelains and in cemented carbides. In the traditional ceramics, the liquid phases are molten silicates that remain as a glassy phase after cooling, giving the fabricated materials a glassy appearance. The ceramics are referred to as vitrified, and the sintering process is referred to as vitrification.

Compared to solid-state sintering, the presence of the liquid phase leads to enhanced densification through (1) enhanced rearrangement of the particulate solid and (2) enhanced matter transport through the liquid. Figure 5.10. shows a sketch of an idealized two-sphere model in which the micro structural aspects of liquid-phase sintering are compared with those of solid-state sintering. In liquid-phase sintering, if, as we assume, the liquid wets and spreads to cover the solid surfaces, the particles will be separated by a liquid bridge. The friction between the particles is significantly

reduced so that they can rearrange more easily under the action of the compressive capillary stress exerted by the liquid.

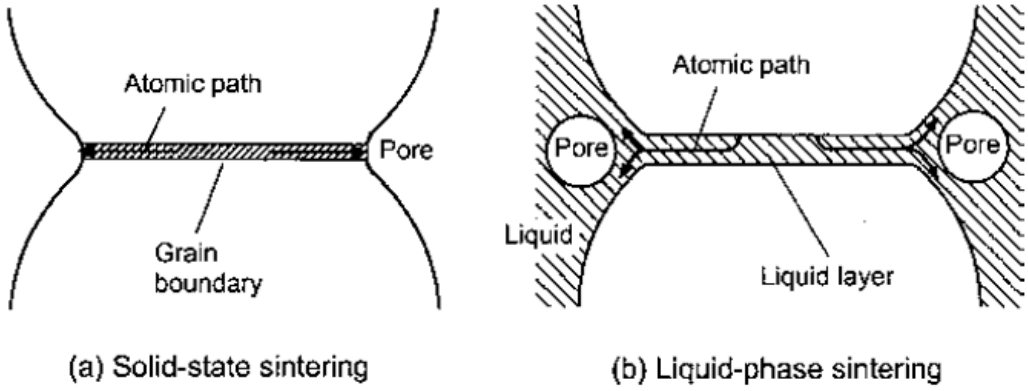

Figure 5.10. Sketch of an idealized two-sphere model comparing the micro structural aspects of (a) solid-state sintering with (b) liquid-phase sintering [39].

For liquid-phase sintering, the green body is commonly formed from a mixture of two powders: a major component and an additive phase. On heating, the additive melts or reacts with a small part of the major component to form a eutectic liquid. The formation of the liquid phase by melting of the additive is common in metallic systems, whereas in ceramic systems, the formation of a eutectic liquid is more common.

In addition to any porosity that may be present, the microstructure of the ceramic product produced by liquid-phase sintering consists of two phases: (1) the crystalline grains and (2) the grain boundary phase resulting from the liquid. Unless it is crystallizable, the grain boundary phase is commonly amorphous.

In most liquid-phase sintering systems, chemical reactions between the particulate solid and the liquid are relatively weak, so that the interfacial energies have a dominant effect on the rate of sintering. Under these conditions, as illustrated in Fig. 5.11., liquid-phase sintering is generally regarded as proceeding in a sequence of dominant stages:

1. Redistribution of the liquid and rearrangement of the particulate solid under the influence of capillary stress gradients,

2. Densification and grain shape accommodation by solution-precipitation;
3. Final-stage sintering driven by the residual porosity in the liquid.

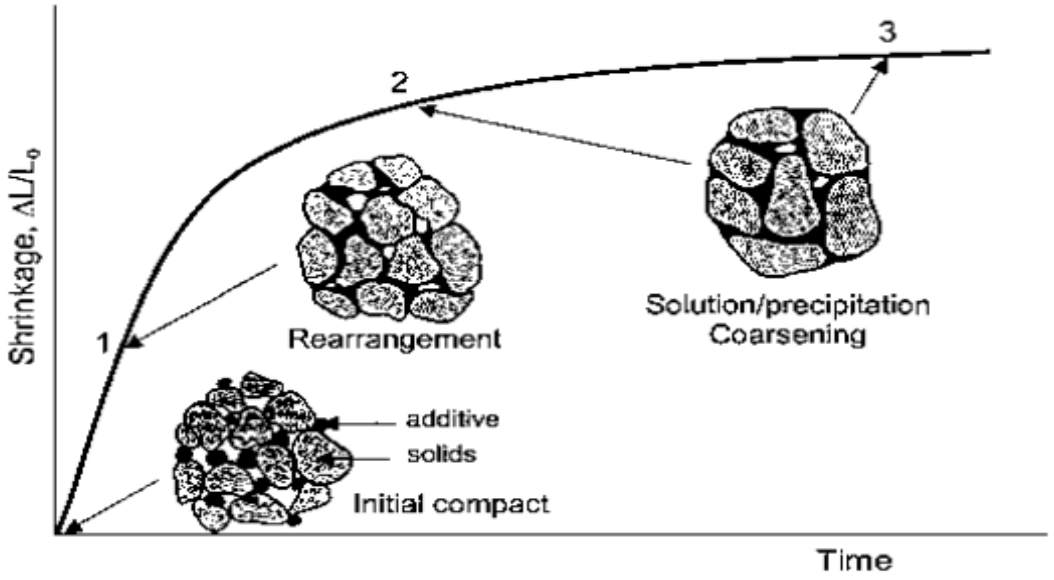

Figure 5.11. Schematic evolution of a powder compact during liquid-phase sintering. The three dominant stages overlap significantly [39].

The extent to which each stage influences densification is dependent on the volume fraction of liquid so there are many variants in conceptual picture shown in Fig. 5.11. When the volume fraction of liquid is high, complete densification can be achieved by the rearrangement process alone. On the other hand, at the low liquid contents common for many systems, the solid skeleton inhibits densification, so that solution-precipitation and final stage sintering are required to achieve further densification. During the stage of solution-precipitation, the average grain size increases via growth of large grains and dissolution of small grains in a matrix, which is referred to as Ostwald ripening.

5.8. Spark plasma sintering

Spark plasma sintering (SPS) is a newly developed process - a synthesis and processing technique - which makes possible sintering and sinter-bonding at low temperatures and short periods by charging the intervals between powder particles with electrical energy and effectively applying high temperature spark plasma generated momentarily [60-64]. It is regarded as a rapid sintering method, using self-heating action inside the powder, similar to self-propagating high temperature synthesis and microwave sintering. SPS systems offer many advantages over conventional systems using hot press sintering, hot isostatic pressing or atmospheric furnaces, including ease of operation and accurate control of sintering energy as well as high sintering speed, high reproducibility, safety and reliability. The SPS process is expected to find increased use in the fabrication of functionally graded materials, intermetallic compounds, fiber reinforced ceramics, metal matrix composites and nanocrystalline materials, which are difficult to sinter by conventional sintering methods.

5.8.1. Principles of the SPS process

The SPS process features a very high thermal efficiency because of the direct heating of the sintering graphite mold and stacked powder materials by the large spark pulse current. It can easily consolidate a homogeneous, high-quality sintered compact because of the uniform heating, surface purification and activation made possible by dispersing the spark points. SPS sintering temperatures range from low to over 2000 °C, which are 200 to 500 °C lower than in conventional sintering. Vaporization, melting and sintering are completed in short periods of approximately 5 to 20 minutes, including temperature rise and holding times.

There are some disadvantages of spark plasma sintering:

- Only simple symmetrical shapes may be prepared;
- Expensive pulsed DC generator is required.

5.8.2. Basic configuration of the SPS system

The basic configuration of a typical SPS system is shows in Figure 5.12. The system consists of a SPS sintering machine with a vertical single-axis pressurization mechanism, specially designed punch electrodes incorporating water cooler, a water-cooled vacuum chamber, a vacuum/air/argon-gas atmosphere control mechanism, a special pulsed (ON-OF) direct electric current (DC) generator, a cooling water control unit, a position measuring unit, a temperature measuring unit, an applied pressure display unit and various interlock safety units. In an SPS experiment, a weighed amount of powder is introduced in a die. The die may be built up with various materials, such as carbon, WC, refractory alloys, etc.

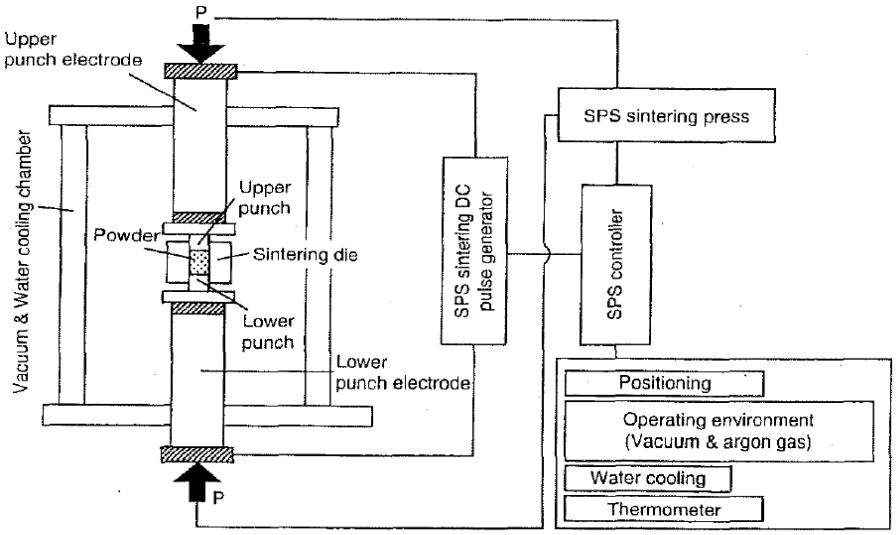

Figure 5.12. SPS system configuration [64]

5.8.3. Mechanism of processing SPS

The spark plasma sintering process proceeds through three stages [63]:

- *Plasma heating*

The electrical discharge between powder particles results in localized and momentary heating of the particles surfaces up to several thousands ºC. Since the micro-plasma discharges form uniformly throughout the sample volume the

generated heat is also uniformly distributed. The particles surfaces are purified and activated due to the high temperature causing vaporization of the impurities concentrated on the particle surface. The purified surface layers of the particles melt and fuse to each other forming “necks” between the particles.

- *Joule heating*

At this stage the pulsed DC electrical current flows from particle to particle through the necks connecting them. The Joule heat is generated by the electrical current. The Joule heat increases the diffusion of the atoms/molecules in the necks enhancing their growth. Localized character of heating (heat is concentrated primarily on the surfaces of the particles – Fig 5.13.) and its uniform distribution allow rapid temperature rise and drop, which diminish coarsening (growth) of the material grains [64].

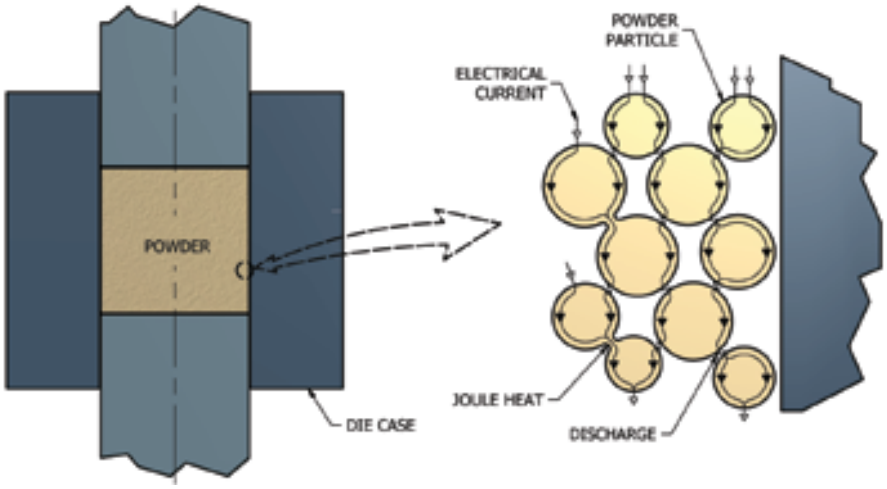

Figure 5.13. ON-OFF pulsed current path through the powder [65]

Plastic deformation

The heated material becomes softer and it exerts plastic deformation under the uniaxial force. Plastic deformation combined with diffusion result in the densification of the powder compact to over 99 % of its theoretical density.

6. SINTERING OF CORDIERITE POWDERS – A REVIEW

There are many research devoted to the synthesis of cordierite powders [66-80], but there is little literature data about sinterability of different type of cordierite powders. A review of the investigations of sinterability of cordierite powders is given in this part.

Influence of granulometric characteristics on the sintering behavior of cordierite based materials obtained from commercially available cordierite powder was studied [81]. These materials were prepared by attrition milling, uniaxial pressing and sintering at 1450 ºC. The employed cordierite powders were classified as coarse, medium and fine single granulometric fractions. Densification degree and kinetics of sintering were studied through density measurements and microstructural analysis. The characteristics of the starting powders and the particle packing were correlated to the developed microstructures and a sintering mechanism was proposed.

It was concluded that, in general, the densification degree of the materials was improved by decreasing the mean particle size of starting granulometric distributions or formulating binary granulometric mixtures with more than 50 wt. % of the smaller particles. However, the binary mixtures with the best green densities not always achieved the highest final densities by sintering. The lowest mean particle size granulometric distribution together with its more regular particle shape were assumed as the more important factors that contributed to the highest densification of this material. In addition, the most homogeneous grain size distribution (the narrowest one) with the small mean grain size was observed in sample with fine and medium particle sizes. For all materials involved, the grain sizes were smaller than the initial particle ones because the particle-particle rearrangement takes place, assuming that a liquid-phase sintering mechanism is operating. On the other hand, neither a significant grain growth with the increasing sintering time nor a change in the morphology of the grains is observed. These facts, in addition to the high viscosity and the low surface energy of siliceous liquids as the studied one, support the fact that few or no events of dissolution-reprecipitation contribute to the mechanism of densification.

In general, the more effective packing reduces the densification rate while it improves the sintered density. However, the coarse commercial material with the lowest green density exhibited the worst sintering behavior achieving the lower final density at the longest sintering times in relation to binary mixtures. The high particle size of the first material and its more irregular shape are two factors that strongly diminish its sintering rate because the rearrangement is aided by small and smooth particles.

Commercially available cordierite and mullite powders were used to obtain cordierite and composite materials by attrition milling, uniaxial pressing and sintering [82]. By formulating cordierite-mullite composites, it is possible to improve the mechanical behavior of the materials. Cordierite powders were the coarse, medium and fine granulometric fraction and the binary mixture of them. The influence of porosity, increasing mullite and glassy phase contents and grain size on the mechanical parameters were analyzed.

It was shown that as the percentage of mullite increased, the densification degree of the materials showed a no linear increment. This result indicates that mullite doesn't produce an inhibitor effect on the densification of cordierite materials. In all the studied materials, the final grain size was smaller than the initial particle size. This fact strongly support the assumption that the sintering in presence of a liquid phase occurs almost exclusively through primary and secondary (particle – particle) rearrangements. The hardness of pure cordierite and cordierite-mullite composites diminishes with the increasing porosity. For pure cordierite, the hardness changes with the porosity from 8.1 to 6.4 GPa (porosity range 2- 7.5 %) and for composite with 30 wt. % of mullite hardness changes from 9 to 7.4 GPa (porosity range 1.5 – 5 %). In respect of the variation of the fracture toughness with the porosity, a similar behavior determined for hardness was observed. It attributed to the effect of the cracks along the grain boundaries in respect of the pores as stress concentrators because of the pore and grain sizes were similar. K_{IC} decreased with the porosity increasing from 1.90 to 1.67 $MPa \cdot m^{1/2}$ for the pure cordierite and from 2.03 to 1.83 $MPa \cdot m^{1/2}$ for cordierite-30 wt % composite.

Densification behavior of powder compacts having cordierite composition prepared using metal alkoxides was studied as a function of calcination and sintering temperature and time [83, 84]. Pure and homogeneous alkoxy-derived cordierite powder

was calcinated at different temperature, ranging from 600 to 1200 °C, and time (2 and 12 h). The calcinated powders were uniaxialy pressed at 40 MPa, followed by isostatic pressing at 300 MPa. Pressed compacts were sintered for 2 h at temperatures from 900 to 1450 °C. It was showed that the specific surface area of cordierite powder gradually decreased below 800 °C, and then drastically diminished above 900 °C. Considering this fact, the cordierite powder was calcinated at a temperature below 900 °C. But, it was necessary to prolong time of calcination at 800 °C in order to remove carbon residue and adsorbed water. The investigation of the effect of the calcination temperature on the powders densification behavior showed that the calcination of the powder below 800 °C is enough to obtained dense cordierite ceramics. So, the authors calcinated cordierite powder at 800 °C for 12 h. Then, they investigated influence of sintering temperature on the bulk density and concluded that in the case of sintering below 1100 °C the bulk density of the powder compact was higher then the true density of α-cordierite, because μ-cordierite and cordierite-glass phases were the matrix phases of the sintered materials. In the case of sintering at 1200, 1300 and 1400 °C, densities were about 98 % of the true density of α-cordierite. The reduced density of the compact sintered at 1450 °C ascribed to the swelling and cracking in the compact caused by the desorption of the water in the large cavities connected to form continuous channels parallel to c-axis. Thus, it was demonstrated that the sintering of the powder compact prepared from metal alkoxides made it possible to obtain the dense cordierite ceramics without the use of any sintering aid. The fact that the densification of the powder compact occurred before crystallization and then homogeneous crystallization of cordierite occurred made it possible to prepare the dense cordierite ceramics because sintering was not halted by crystallization at an early stage.

The effect of grinding of the dry colloidal gel and calcinated gel on the synthesis and sintering of cordierite ceramics were investigated [85]. The grinding of the gel promoted the homogeneous distribution of elements in the gel, resulting in improved reactivity for the formation of cordierite. Grinding the calcined powder enhanced the homogeneity of the resulting powder and caused the accumulation of internal energy as crystal strain; consequently, the densities of the sintered bodies increased and the optimum temperature range for sintering widened. Sintered bodies without any grinding revealed a residual pore and grain growth considered to be caused by liquid - phase

generation. In this way, it was confirmed that the sintering behavior is closely related to the grinding condition of the gels and calcined powders.

There are several papers dealing primarily the synthesis of cordierite powders, but sintering of those powders were also investigated.

Thermal reactions of magnesium compounds and kaolinite were investigated to obtain dense cordierite ceramics without additives [12, 13]. Magnesium hydroxide was precipitated from aqueous solution in the form of ultrafine hexagonal tabular particles of about 0.1 mm, and heating this mixture with submicron particles of tabular kaolinite in a molar ratio of $MgO{\cdot}Al_2O_3{\cdot}2SiO_2$ resulted in the formation of an amorphous state at about 900 °C after thermal decomposition. μ-cordierite was then crystallized from the amorphous phase at about 950 °C, and gradually transformed into α-cordierite from 950 to 1200 °C. Firing the pressed specimens at 1350 °C yielded a dense α-cordierite ceramics with a relative density higher than 95 % and a negligible open porosity, and it showed a linear thermal expansion coefcient of $2.2 \cdot 10^{-6}\ K^{-1}$.

A high purity cordierite precursor was successfully synthesized by coating Mg-Al hydroxide powder with sodium silicate and magnesium chloride by a precipitation method [86]. The coated powder transformed to amorphous in the range of 500-600 °C, and then amorphous silicate crzstallized to crystobalite and an intermediate phase appeared at 850 °C. α-cordierite formation in this system is attributed to the reaction between amorphous silicate and a metastable phase of sapphirine, which resulted from the reaction between the crystalline cristobalite and an intermediate phase. The densification of green compacts was not affected by the crystallization of amorphous silicate and intermediate phase because some amorphous silicate remained in the matrix till the temperature of α-cordierite formation. A high density body with small grain sizes was obtained by sintering samples at 1280 °C for 2 h.

Synthesis and sintering of dense cordierite ceramics, prepared from magnesium and aluminium ions precipitated in dispersed silica have been reported and phase evolution at 1200 °C been studied by XRD [87] . XRD patterns of the co-precipitated mass indicated that the only crystalline phase present in the precursor powder is α-cristobalite, which came from precipitated silica. The remaining consisting of a magnesium–aluminiun hydroxide was in a finely divided amorphous state. Onset of crystallisation is quite prominent at 1200 °C with the coalescence of small pores

resulting in sporadically observed larger ones. α-cordierite and magnesium aluminate spinel were the major phases with decreasing content in the crushed pellet sintered at 1200 °C for 6 h. But, autors found that the dielectric properties of cordierite ceramics prepared by this route are good enough for substrate application.

Cordierite powder was synthesized by non-hydrolytic sol–gel route, starting from aluminum chloride, TEOS and magnesium chloride dissolved in absolute ethanol [88]. Crystallization of μ-cordierite from gel at temperatures between 900 and 1000 °C was confirmed by differential thermal analyses, X-ray and FTIR spectroscopy. The crystallization of μ-cordierite induced by heat treatment of the gel proved its homogeneity, but the appearance of spinel crystallization at the same temperature indicates certain gel inhomogeneity. Higher calcinations temperature resulted in the transformation of μ- to α-cordierite. In the temperature interval from 1200 to 1300 °C the α-cordierite was formed by the transformation of μ-cordierite, and also by the reaction of spinel and amorphous SiO_2. Cordierite powder was first uniaxially pressed at 240 MPa, then isostatically pressed at 400 MPa and sintered at 1400, 1430, 1440 and 1450 °C for 2 h. The densities of sintered cordierite materials increased with increasing sintering temperature from 86 to 90 % of theoretical density. The dielectric constant of obtained cordierite material depended on the sintering temperature and varies from 3.78 at 1400 °C to 5.18 at 1450 °C at 1 MHz. The dielectric loss and the dielectric constant of showed that this cordierite ceramic is promising for high-frequency electronic application

7. EXPERIMENTAL PART

7.1. Synthesis of gels and powders

Three types of gels and powders were synthesized by different sol-gel methods, starting from silicic acid or silica sol or alkoxides.

7.1.1. Synthesis of cordierite gel and powders starting from silicic acid

For the synthesis of cordierite gel, $Mg(NO_3)_2 \cdot 6H_2O$ and $Al(NO_3)_3$ $9H_2O$ were dissolved in an aqueous solution of silicic acid. The silicic acid was obtained by passing sodium silicate through a column filled with a cation exchanger in the H^+ form, whereby an exchange of the Na^+ ions from sodium silicate with the H^+ ions occurred. To prevent condensation, a 2% solution of silicic acid of pH ≈ 3.4 was used. The reactants were mixed in a stoichiometric ratio for cordierite and the mixture was gelled by heating and stirring with a magnetic stirrer. The obtained transparent gel (G_{acid}) was dried at 100 °C, ground and calcined at 600 °C for 2 h to remove all the thermal decomposition products. The obtained white powder was then calcined at different temperatures: 850, 900, 1000, 1100, 1200, 1300 and 1350 °C for 2 h in a programmable furnace under static air conditions.

7.1.2. Synthesis of cordierite gel starting from silica sol

Cordierite gel was synthesized starting from silica sol, boehmite sol and aqueous solution of $Mg(NO_3)_2 \cdot 6H_2O$ [72, 76].

The silica sol was prepared [89] by using an aqueous solution of sodium silicate, with a mass ratio of SiO_2:Na_2O of 3:1. The solution was diluted to give a solution containing approximately 3.5% SiO_2 and passed through a column filled with a strong acid ion-exchange resin. The effluent solution of polysilicic acid was obtained, which pH value was adjusted by NaOH to approximately 9.2. One part of this solution was

heated to boiling in order to form SiO_2 particles and then a rest of the solution was added. The obtained silica sol was characterized by the solid phase content (2.2 mass %) determined by gravimetric analysis, pH value (3.4) using a conventional glass electrode. The mean particle diameter (6 nm) was calculated from the value of the specific surface area, determined by potentiometric titration method - measuring the amount of OH^- ions adsorbed by the solid phase at pH = 4-9.

The boehmite sol (AlOOH) was prepared by peptization by HNO_3 of freshly precipitated $Al(OH)_3$, suspended in distilled water [90]. HNO_3 were added at the ratio $n(HNO_3)/n(Al(OH)_3) = 0.1$. Peptization was performed at the boiling point, under reflux during 48 h. The obtained sol was characterized by the solid phase content (2.2 wt %) determined by gravimetric analysis and pH value (3.4) using conventional glass electrode. The sol contained rod-like particles of approximately 30 nm in length and about 10 nm in width.

The boehmite and SiO_2 sols were mixed and the mixture was stirred for 2 h. Then, an aqueous solution of $Mg(NO_3)_2 \cdot 6H_2O$ was added, and the stirring continued for an additional 2 h. The obtained multicomponent colloidal dispersion was gelled by addition of ammonium carbonate, which increased the pH. The resulting gel was dried for two days at 40 ^oC and then 24 h at 110 ^oC (dried gel G_{sol}).

7.1.3. *Synthesis of cordierite gel starting from alkoxide*

Alkoxy-derived cordierite gel ($G_{aloxide}$) were synthesized [73] from tetraethylorthosilicate (TEOS, Fluka Chemic), aluminum isopropoxide ($Al(OPr^i)_3$, Fluka Chemic), and magnesium ethoxide ($Mg(OEt)_2$, Fluka Chemic). The TEOS was partially hydrolyzed for 48 h under reflux at molar ratios $H_2O/TEOS = 1.2$ in the presence of hydrochloric acid as a catalyst, HCl/TEOS = 0.1. As a solvent, commercial ethanol (96 %) was used. The water present in ethanol was used for partial hydrolysis of the TEOS [40]. $Mg(OEt)_2$ and $Al(OPr^i_3)$ were dissolved in isopropanol and the solution added to the partially hydrolyzed TEOS. The resulting mixture was refluxed for 48 h, and then enough water to complete the hydrolysis was added (at molar ratio $H_2O/TEOS$

= 20). The system was left for a week to allow aging of the gel, and then dried for 24 h at 110 °C (dried gel $G_{alkoxide}$).

7.2. Characterization of gel and powders obtained from silicic acid

7.2.1. Methods

Differential thermal and thermogravimetric analysis (DTA and TGA) of the powder obtained by gel calcination at 600 °C was performed on an SDT Q600 instrument, up to a temperature of 1380 °C. The heating rate was 20 °C/min and Al_2O_3 was used as the standard. The sample mass was 5 mg.

The phase composition of the powders obtained by the gel calcination at various temperatures was determined on an ITAL STRUCTURES APD 2000 diffractometer equipped with a back monochromator operating at a tube voltage of 40 kV and a tube current of 30 mA, using a copper cathode as the X-ray source (λ = 0.15406 nm), in the 2Θ angle range from 10° to 80°. A step size of 0.02° and a time per step of 0.5 s were used.

FTIR spectra of the dry gel and powders obtained by gel calcination were recorded on a MB BOMEM 100 HARTMANN and BRAUN spectrometer, within the wave number range from 400 to 1250 cm^{-1}. The specimens were prepared with KBr at a mass ratio of specimen to KBr of 1:100.

The morphology of the gel was studied by scanning electron microscopy (SEM), using a Jeol JSM-5800 at 20 kV, and transmission electron microscopy (TEM), using a JEOL T-100. Prior to SEM analysis, the gel was coated with gold using a splutter coater. The sample for TEM analysis was prepared by dispersing the gel in ethanol and applying a drop of very dilute suspension onto carbon-coated grids.

The relative linear shrinkage of the compact of powder obtained by the gell calcination at 600 °C was acquired using heating microscopy (E. LEITZ) up to 1430 °C, at a heating rate of 10 °C/min.

7.2.2. Kinetics

The crystallization kinetics of cordierite was studied on the gel previously calcined at 600 °C. The kinetic parameters were determined by differential thermal analysis under non-isothermal conditions at heating rates of 5, 10, 15 and 20 °C/min up to 1100 °C. The experiments were performed in the air, and Al_2O_3 was used as the reference material. The sample mass, in all cases, was 170 mg.

The Avrami parameter, n, indicating a mechanism of nucleation and growth mechanism, was determined using Ozawa method [91-93] expressed by the following relation:

$$\log(-\ln(1-\alpha) = n \log (k(T- T_0)) – n \log Q \qquad (7.1.)$$

where α is the degree of transformation, Q is the heating rate, T_0 is the initial temperature, T is the temperature recorded after time t, k is a constant and n is the Avrami parameter. The plot of $\log(-\ln(1-\alpha))$ versus $\log Q$, at the chosen temperature, results in a straight line and the value of n can be determined from its slope. The value of α was determined from a series of DTA curves obtained at various heating rates, from the following relation:

$$\alpha = S/So \qquad (7.2.)$$

where S is the partial peak area from the beginning of peak to a chosen temperature and S_0 is the total peak area [94]. Data on the early and final stages of transformations were not taken into account, due to some limitations related to these stages [95] and to application of most of the kinetic equations. Therefore, the temperatures for which the degree of transformation at all heating rates lies in the range 0.2–0.7 were selected. Values of parameter n, for different growth and nucleation conditions [96] are given in Table 7.1.

Table 7.1. Values of n for different growth and nucleation conditions [96]

Growth and nucleation conditions	Diffusion	Interface
Constant nucleation rate		
Three-dimensional growth	5/2	4
Two-dimensional	3/2	3
One-dimensional growth	1/2	2
Constant particle number		
Three-dimensional growth	3/2	3
Two-dimensional growth	2/2	2
One-dimensional growth	1/2	1
Surface nucleation	1/2	1

The overall activation energy of cordierite crystallization was calculated by the Kissinger equation [93-96]:

$$\ln \frac{Q^n}{T_p^2} = -\frac{mE_a}{RT_p} + const \qquad (7.3)$$

where Q is the heating rate, Tp is the peak temperature at a given heating rate, E_a is the overall activation energy, R is the gas constant, n is the Avrami parameter and m is a dimensionless constant dependent of the dimensionality of crystal growth. For the case where the surface nucleation is a predominant mechanism, and $n = m = 1$, Eq (7.3) is reduced to the familiar Kissinger equation.

7.3. Sintering

The cordierite powders for the sintering investigation were obtained by gel calcination at a temperature where α-cordierite was formed or at a temperature where densification without crystallization of the silica-containing component occurred.

Before calcination, all three gels (G_{acid}, G_{sol} and $G_{alkoxide}$) were ground for 0.5 h at 400 rpm in a mill with an alumina chamber using alumina balls.

It was shown previously [72, 76] that intensive shrinkage during colloidal gel heating occurred in the temperature range 800–1000 °C. X-ray analysis of the gel calcined at different temperatures showed that spinel crystallized first at about 900 °C and then crystobalite crystallized at temperatures higher than 1000 °C. α-cordierite was formed at about1300 °C by the reaction of spinel and crystobalite. According to these results, powders for sintering investigation were prepared by the gel calcination at 1300 °C, where α-cordierite is formed (powder $P_{sol}1300$), and at 950 °C, where densification without the onset of crystallization of crystobalite occurred (powder $P_{sol}950$).

Intensive shrinkage during heating of alkoxide-derived gel also occurred in the temperature range 800–1000 °C [73]. During thermal treatment of alkoxy-derived gel, μ-cordierite crystallized at 900–1000 °C and in the range from 1100 to 1300 °C transformed into α-cordierite. In order to achieve densification without μ-cordierite crystallization, the gel was calcined at 850 °C, and so obtained powder was used for sintering investigation ($P_{alkoxide}850$). The gel was also calcined at 1300 °C in order to obtain crystalline powder for sintering investigation ($P_{alkoxide}1300$).

According to results of investigation in this thesis, ground gel G_{acid} was calcined at 850 °C (powder $P_{acid}850$) and at 1300 °C (powder $P_{acid}1300$).

All powders ($P_{acid}850$, $P_{acid}1300$, $P_{sol}950$, $P_{sol}1300$, $P_{alkoxide}850$ and $P_{alkoxide}1300$) were ground for 0.5 h or for 3 h at 400 rpm in a mill with an alumina chamber using alumina balls. The obtained powders were designated as $P_{acid}850(0.5h)$, $P_{acid}850(3h)$, $P_{acid}1300(0.5h)$, $P_{acid}1300(3h)$, $P_{sol}950(0.5h)$, $P_{sol}950(3h)$, $P_{sol}1300(0.5h)$, $P_{sol}1300(3h)$, $P_{alkoxide}850(0.5h)$, $P_{alkoxide}850(3h)$, $P_{alkoxide}1300(0.5h)$ and $P_{alkoxide}1300(3h)$, indicating type of sol-gel method (acid, sol or alkoxide), temperature of calcination (850 °C, 950 °C or 1300 °C) and duration of grinding (0.5 h or 3h).

The morphology of the powders was studied by scanning electron microscopy (SEM), using a Jeol JSM-5800 at 20 kV. Prior to SEM analysis, the powders were coated with gold using a splutter coater. The particle size distribution of the powders was determined by a particle size analyzer (PSA) Mastersizer 2000 (Malvern Instruments Ltd., UK). Before determination, the powder was de-agglomerated in an ultrasonic bath (frequency of 40 kHz and power of 50 W), for 1 min.

The powders were uniaxialy pressed at 400 MPa and conventionally sintered at: 1400 °C, 1430 °C and 1450 °C for 2 h.

The powder $P_{alkoxide}$1300(3h) was also sintered by the rapid spark-plasma sintering (SPS) technique in a Dr Sinter SPS System-825C furnace, at 1400 °C for 1 min and at 1350 °C for 7 min. Approximately 3 g of powder were sintered under vacuum using a graphite mold (diameter 20 mm) with an applied pressure of 40 MPa. During sintering, the voltage was 4 V with a current of 1500 A. The required duration of sintering at the desired temperature was determined according the shrinkage of the samples, monitored with a dilatometer. The temperature of the sample during the sintering was measured by an optical pyrometer through a hole located in the graphite mold. After completion of the process, the samples were cooled for 1 h using the internal cooling system.

The densities of sintered samples were determined by the Archimedes method. The relative densities were calculated using the theoretical density (TD) of α-cordierite (2.52 g/cm^3). Microstructures of the fracture surface of the sintered materials were observed by SEM (Jeol JSM-5800). X-ray diffraction analysis of the sintered samples was done using a BRUKER D8 ADVANCE with a Vario 1 focusing primary monochromator (Cu $K_{\alpha 1,2}$ radiation, λ = 1.54059 Å). The best-sintered materials were polished and used for microhardness (H) and indentation fracture toughness (K_{IC}) determinations. The microhardness was measured with a Vicker's indenter. K_{IC} values were calculated using the formula [97]:

$$K_{IC} = 0.0824 \cdot P \cdot c^{3/2} \tag{7.4}$$

where P is the indentation load and c is the length of the induced radial crack. The average of the 20 measurements for each sample was used for the evaluation of the sample hardness and toughness.

After determination of the mechanical properties, the polished conventionally sintered samples were thermally etched at 1350 °C for 30 min, with a heating rate of 20 °C/min, and their microstructure were observed by SEM (JEOL JSM-5800). The spark plasma sintered samples were thermally etched at 1200 °C for 15 min, with a heating rate of 20 °C/min and their microstructure were observed by SEM (TESCAN Mira3 XMU) at 20 kV.

8. RESULTS AND DISCUSSION

8.1. Characterization of the gel and powders obtained starting from silicic acid

8.1.1. SEM and TEM of the dry gel

The morphology of the ground dried gel is shown in Fig (8.1.a) in which particles of irregular shapes and different sizes can be seen. On the TEM image (Fig. 8. 1.b), primary particles of the dry gel are observable. It is obvious that the dry gel is very porous, which implies that the dry gel contains high chemical energy.

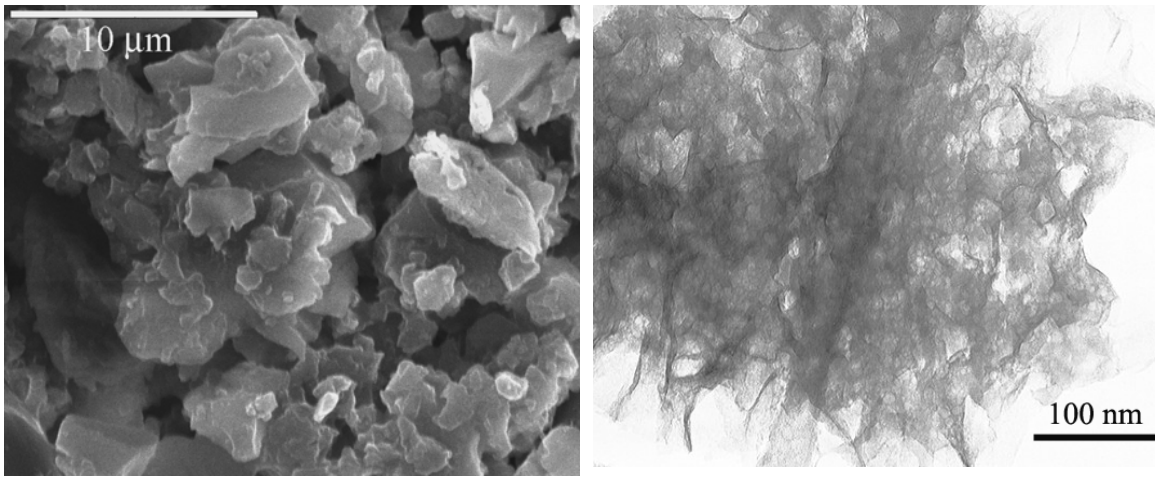

Fig 8.1. a) SEM micrograph of ground gel G_{acid}, b) TEM image of ground gel G_{acid}

8.1.2. Phase transformations during thermal treatment of the gel

The results of the DTA and TGA of the gel calcined at 600 °C for 2 h are given in Fig. 8.2. DTA and TGA were realized on calcined gel in order to eliminate all products of thermal decomposition and thus to enable a better registration of the phase transformations.

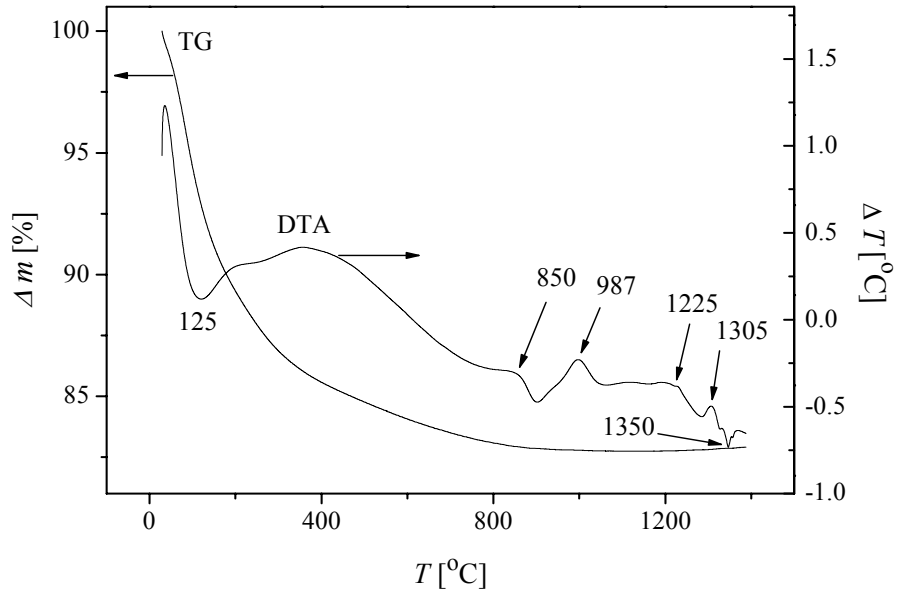

Fig. 8.2. DTA and TGA curves of the gel calcined at 600 °C for 2 h.

The endothermal peak at 125 °C on the DTA curve corresponds to desorption of physically absorbed water. This peak is accompanied by a relatively high weight loss, despite the previous calcination, which can be explained by high humidity adsorption from the air. The exothermal peak at 987 °C can be assigned to spinel and crystoballite crystallization, as in three-phase colloidal gels [67, 72, 76, 85, 98], or to μ-cordierite crystallization, as in monophase alkoxide-derived gels [66, 67, 73, 75, 100]. Thereafter, the peak at 1305 °C corresponds to α-cordierite formation by spinel and crystoballite reaction or by μ-cordierite transformation. Endothermal shifts in the DTA baseline prior to the crystallization peaks are evident on the DTA curve. The first shift (at 850 °C) corresponds to a gel → viscous liquid transition, e.g., viscous sintering of the gel. It can be seen from Fig. 8.3 that intense shrinkage of the gel occurs in the temperature range of 800–900 °C, which confirms that the first endothermal shift in the DTA baseline corresponds to viscous sintering.

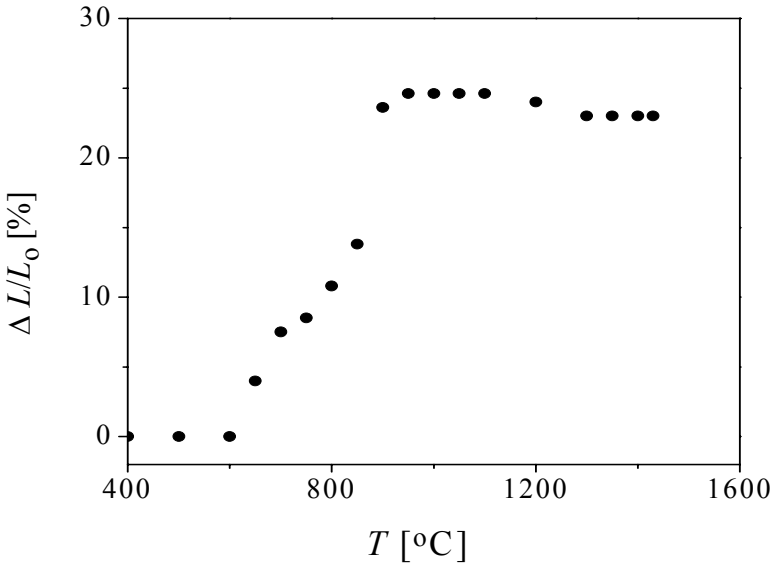

Fig 8.3. Relative linear shrinkage of the calcined gel compact.

It is assumed that the second shift (at 1225 °C) indicates some structural changes prior to α-cordierite formation, but this can be confirmed by X-ray diffraction analysis. In addition, it is assumed that the endothermal peak at 1350 °C does not corresponds to α-cordierite melting, because during the thermal-microscope analysis until 1430 °C, melting was not registered. It is possible that this peak indicates the formation of some liquid phase after α-cordierite formation, which is liquid for liquid phase sintering.

In order to determine the nature of the processes corresponding to the mentioned peaks and shifts, the phase composition of powders obtained by the gel calcination at 600, 850, 900, 1000, 1100, 1200, 1300 and 1350 °C were determined. The X-ray diffractograms of these powders are presented in Fig. 8.4

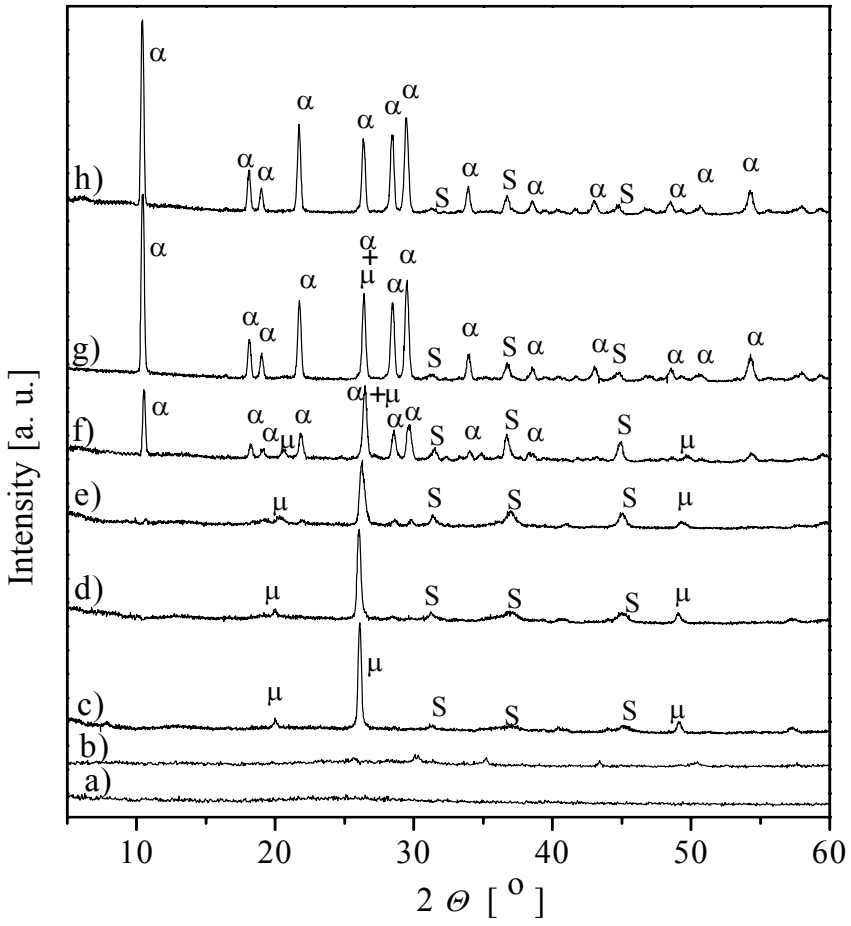

Fig 8.4 X-ray diffractograms of the powders obtained by the gel calcination at 600 °C (a), 850 °C (b), 900 °C (c), 1000 °C (d), 1100 °C (e), 1200 °C (f), 1300 °C (g) and 1350 °C (h) (S - spinel, α - α-cordierite, μ – μ-cordierite) [101].

The diffractograms of the powders obtained by the gel calcination at 600 and 850 °C revealed that the gel remained amorphous up to 900 °C. At 900 °C, crystallization of the μ-cordierite and spinel phases appeared. The diffractograms of the powders obtained by the gel calcination at 900, 1000 and 1100 °C show intense and sharp peaks corresponding to μ-cordierite and weak peaks corresponding to spinel. According to this, it may be said that the first exothermal peak on the DTA curve (at 987 °C) corresponds to μ-cordierite crystallization, because gel calcination during 2 h ensures crystallization at a lower temperature than in the DTA experiments due to

inertia in the latter case. Crystallization of μ-cordierite at about 1000 °C is proof that the gel is monophasic and homogeneous. The presence of spinel indicates either non-stoichiometry or some inhomogeneity in the gel. On increasing the temperature from 900 to 1100 °C, the intensity of the peaks corresponding to spinel increased, while the peaks corresponding to μ-cordierite become lower and wider, which indicate a decrease in crystallinity. μ-Cordierite crystallinity decrease in a wide temperature range prior to α-cordierite crystallization indicates reconstructive type of transformation (structural rearrangement) [38], meaning that bonds are broken and atoms are rearranged. Obviously, it is required for the μ-cordierite structure to partially destroy prior to commencing of α-cordierite crystallization, so the new α-phase will form out of this disordered structure. Accordingly, it can be assumed that endothermal shift at 1225 °C corresponds to transition temperature of disordered structure from which α-cordierite crystallization occurs (peak at 1305 °C).

The diffractogram of the powder obtained by gel calcination at 1200 °C shows peaks correspond to μ- and α-cordierite, indicating that the α-cordierite formation started at temperatures below 1200 °C, while the DTA results exhibited a peak corresponding to the μ- → α-cordierite transformation appeared at about 1300 °C. It is obvious that during calcination for 2 h, the transformation occurred at a lower temperature than during the DTA experiments. The slight expansion of the gel compact in the temperature interval 1100–1300 °C (Fig. 8.3) can be explained by μ- → α-cordierite transformation, because the density of α-cordierite is smaller than that of μ-cordierite. On calcination for 2 h at 1300 °C, the transformation μ- → α-cordierite was almost completed, while at 1350 °C, it was fully completed. The peaks corresponding to α-cordierite on the diffractogram of the powder obtained by calcination at 1350 °C are intense and sharp, which indicate good crystallinity of the obtained powder. This result confirmed that the endothermal peak at 1350 °C does not correspond to cordierite melting. In addition, there are no peaks corresponding to mullite, which means that incongruent melting of cordierite did not occur.

The results of FTIR spectroscopy of the dry gel and the powders obtained by the gel calcination at 600, 850, 900, 1000, 1100, 1200, 1300 and 1350 °C are illustrated in Fig. 8.5

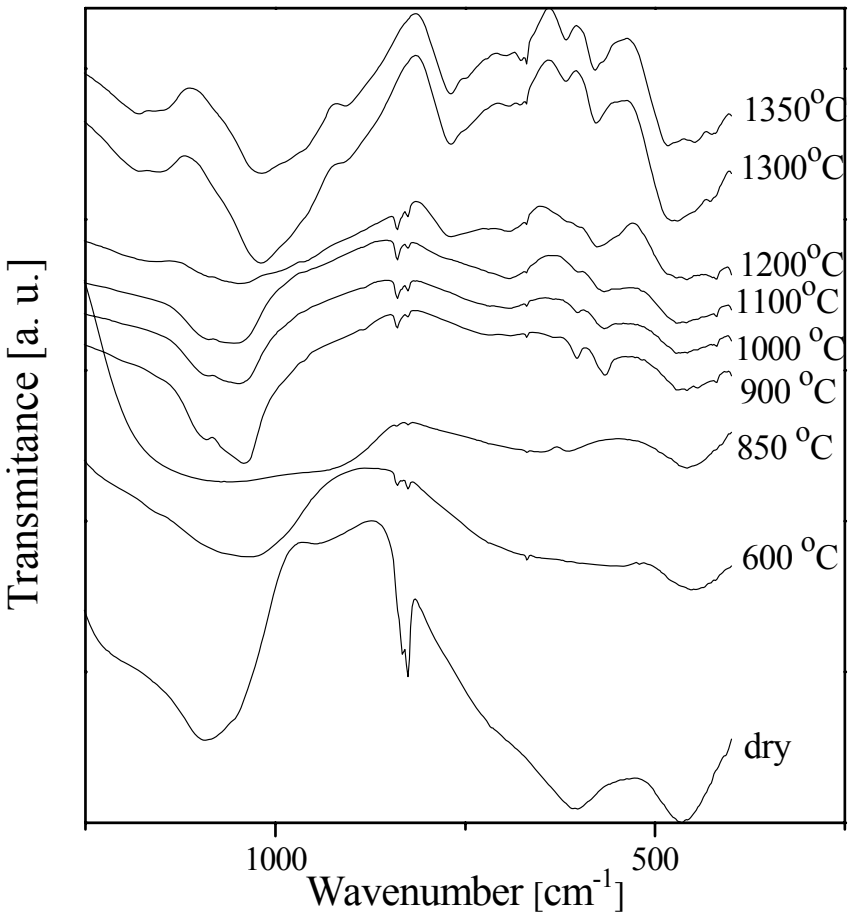

Fig 8.5. FTIR spectra of the dry gel and the powders obtained by the gel calcination at 600, 850, 900, 1000, 1100, 1200, 1300 and 1350 °C [101].

Bands corresponding to Si–O bonds are evident in the FTIR spectra of the dry gel [71-74, 76]: a broad band with a minimum at about 1090 cm^{-1}, a shoulder at about 1200 cm^{-1} and bands at 605 cm^{-1} and 465 cm^{-1}. The band at 826 cm^{-1} corresponds to nitrate ions from the $Mg(NO_3)_2$ and $Al(NO_3)_3$ used in the synthesis. The position of the band corresponding to Si–O bonds at about 1090 cm^{-1}, as in pure silica gel, indicates that bonds Si–O–M (M = Al, Mg) did not form in the dry gel. Thus, it can be supposed that Si–O–Si chains were formed during gelation and hydrated aluminum and magnesium ions remained incorporated between these chains. In the FTIR spectrum of the sample obtained by gel calcination at 600 °C, the shoulder at about 1200 cm^{-1} disappeared and

the band at about 1090 cm^{-1} shifted to lower wavenumbers (1040 cm^{-1}), indicating Si–O–M bonds (M = Al, Mg) formation. The FTIR spectrum of the sample obtained by gel calcination at 850 °C indicates transient state before μ-cordierite formation at 900 °C. The same bands are evident in the spectra of the powders obtained by gel calcination at 900, 1000 and 1100 °C, but intensities of the bands at 1090 and 1040 cm^{-1} decreased with increasing temperature. The FTIR spectrum of the powder obtained by gel calcination at 1200 °C indicates that the transformation μ→α-cordierite had commenced: a band at 770 cm^{-1} corresponding to the six-member ring in the α-cordierite structure is evident in the spectrum. In addition, there are changes in the positions and intensities of the bands at 1090 and 1040 cm^{-1}. By comparing the spectra of the powders obtained by gel calcination at 900, 1000, 1100 and 1200 °C, it seems that the transformation of μ- to α-cordierite occurred by a continuously changing structure with increasing temperature. This is in accordance with results of X-ray diffraction analysis, i.e., with decreasing intensities the μ-cordierite peaks with increasing temperature. The FTIR spectra of the powders obtained by gel calcination at 1300 and 1350 °C are typical for a well-ordered cordierite structure.

According to these results, powders for the sintering investigation were obtained by the gel calcination at 850 °C, where densification without μ-cordierite crystallization occurred (powder $P_{acid}850$) and at 1300 °C, where α-cordierite was formed ($P_{acid}1300$).

8.1.3. Kinetics of μ-cordierite crystallization

The DTA curves of the powder obtained by the gel calcination at 600 °C for 2 h, at heating rates of 5, 10, 15 and 20 °C/min, are shown in Fig. 8.6. The exothermal peak corresponding to μ-cordierite crystallization shifts towards higher temperatures as the heating rate increases.

Based on the data presented in Fig.8.6, the Avrami parameter n was determined by the method of Ozawa [91-93]. To determine this parameter, the data on the degree of crystallization (α) at different temperatures and heating rates (Q) were used and from the slope of the dependence of log ($-\ln(1-\alpha)$) on log Q for a given temperature

(Equation 7.1.), the value of n was determined. The degree of crystallization (α) at a given temperature was determined [94] according to Equation 7.2.

The values of the parameter n at temperatures 955, 959, 962, 964 and 966 °C, are presented in Table 8.1. The mean value of the Avrami parameter n for the crystallization of μ-cordierite was 0.86.

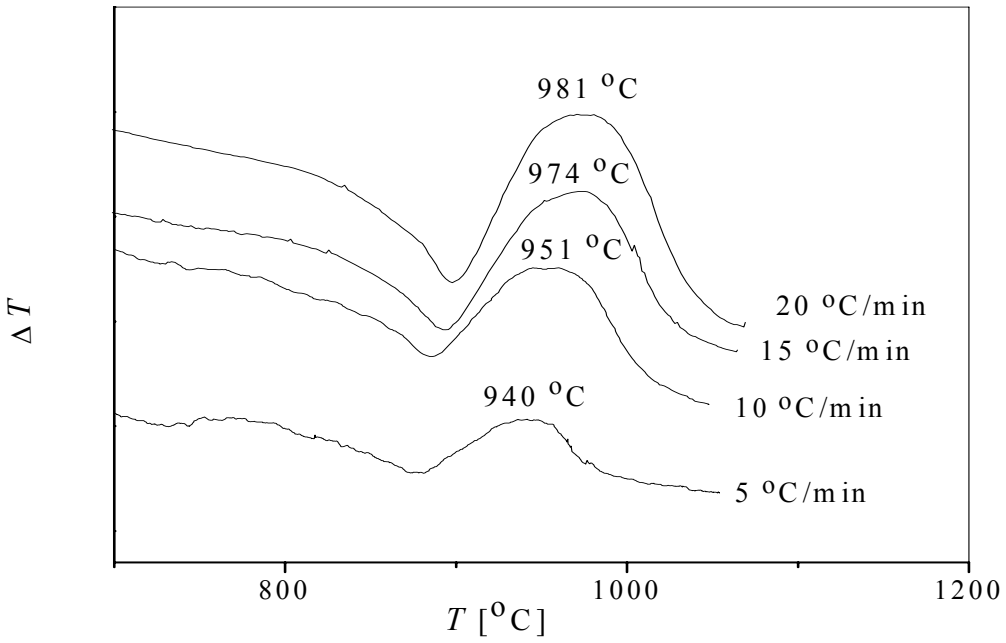

Fig 8.6. DTA curves at heating rates of 5, 10, 15 and 20 °C/min of the powder obtained by gel calcination at 600 °C for 2 h [101].

Table 8.1 Values of the Avrami parameters n at various temperatures.

T [°C]	n
955	0.88
959	0.84
962	0.91
964	0.84
966	0.83

The mean value of the Avrami parameter n, which was close to 1, indicates interface controlled crystallization of μ-cordierite with a constant nucleus number and one-dimensional growth or surface nucleation [72 – 74, 96]. This value is considerably different from the value obtained for the crystallization of μ-cordierite from alkoxy-derived cordierite gel, obtained by a hydrolytic sol–gel process [73]. In that case, μ-cordierite crystallize from homogenous monophasic gel, with constant nucleation rate and three-dimensional growth (n = 4).

On the other hand, the value of the Avrami parameter, n = 2.23, for the crystallization of μ-cordierite from a gel obtained by a non-hydrolytic sol–gel method [74] indicates the simultaneous contribution of different mechanisms: homogeneous nucleation and three-dimensional crystallite growth due to homogeneity of the gel and surface crystallization due to submicron particles of the gel. Bearing in mind the value of the Avrami parameter n obtained in this work and the results presented in Fig. 8.3, it can be said that viscous sintering occurred in the primary gel particles, which led to shrinkage (Fig. 8.3), and thereafter nucleation occurred on the surface or interface of the particles. Then, the μ-cordierite crystals grew towards the center of the particles.

The overall activation energy of μ-cordierite crystallization was calculated by the Kissinger equation [93, 95]. Fig. 8.7 presents the dependence of ln Q/T_p^2 on $1/T_p$, from which the slope, E_a/R, E_a = 382.0 kJ/mol, was obtained (Equation 7.3, for n = m = 1). This value is much lower than that determined for alkoxide sol–gel processed μ-cordierite [73, 102], probably because of the surface instead volume nucleation. However, the obtained value is higher than the value obtained for μ-cordierite crystallization from high cordierite glass (303.5 kJ/mol) [103].

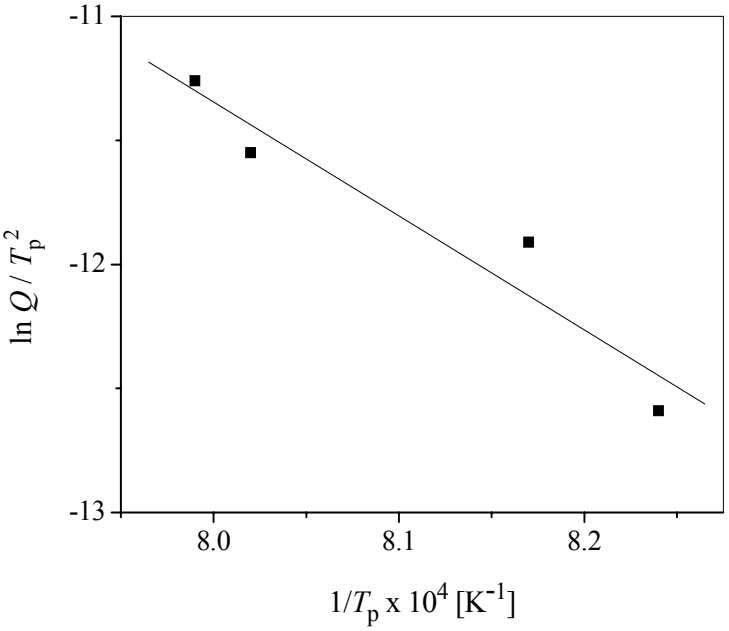

Fig. 8.7. Dependence of ln Q/T_p^2 on $1/T_p$ for the peak corresponding to μ-cordierite crystallization.

8.2. Sinterability of the cordierite powders

8.2.1. Sinterability of the cordierite powders obtained starting from silicic acid

8.2.1.1. Morphology of the powders

Morphology of powders P_{acid}850(0.5h), P_{acid}850(3h), P_{acid}1300(0.5h), P_{acid}1300(3h) are presented in figures 8.8 and 8.9.

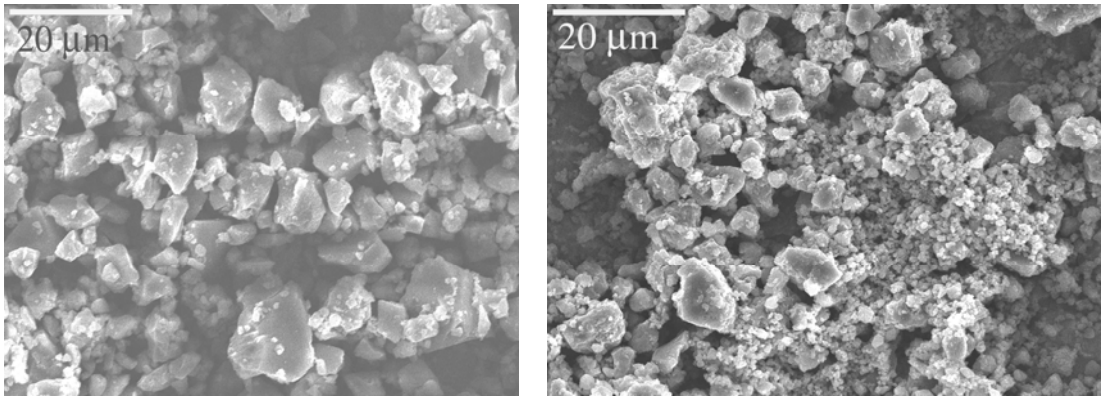

a) b)

Figure 8.8. Morphology of powders: a) P_{acid}850(0.5h) and b) P_{acid}850(3h).

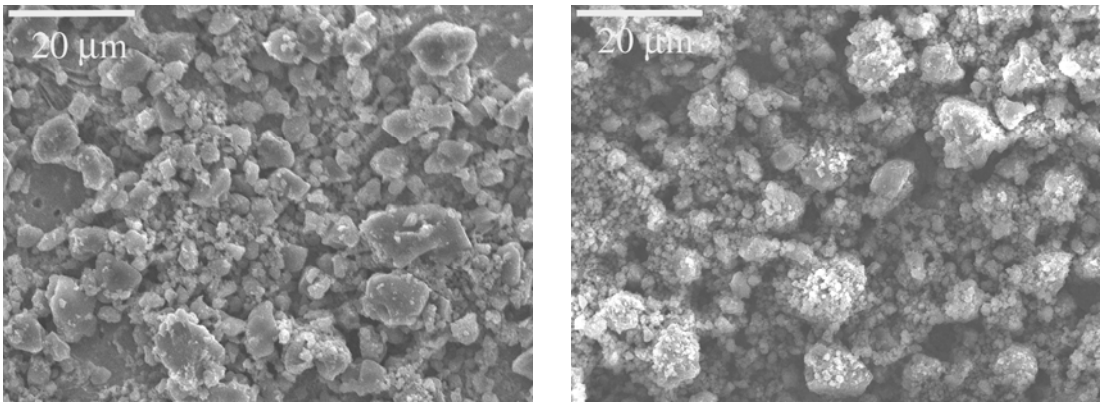

a) b

Figure 8.9. Morphology of powders: a) P_{acid}1300(0.5h) and b) P_{acid}1300(3h).

It could be seen from Fig. 8.8.a) and 8.9.a) that powders P_{acid}850(0.5h) and P_{acid}1300(0.5h) were very coarse and had particles of irregular shapes. Powder P_{acid}1300 had slightly smaller particles than powder P_{acid}850. Prolonged time of grinding caused particle decreasing in both cases. After 3 h of grinding, both powders contained nearly spherical particles, the dimensions of which were about 1 µm, but also larger particles of about 10 µm. Hence, the obtained powders had a bimodal distribution of particle sizes.

8.2.1.2. Microstructure of cordierite materials obtained by conventional sintering

Microstructures of cordierite materials obtained by conventional sintering of powders P_{acid}850(0.5h), P_{acid}850(3h), P_{acid}1300(0.5h) and P_{acid}1300(3h) are presented in figures 8.10 to 8.13.

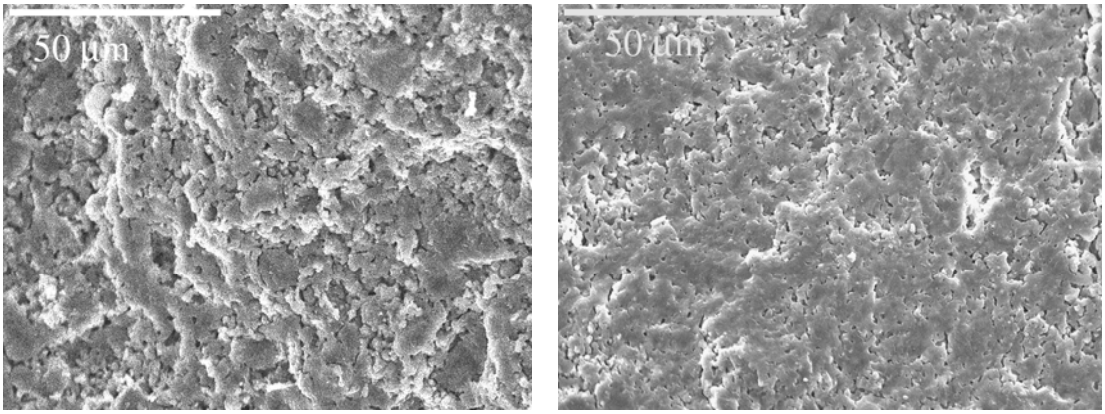

a) b)

Fig 8.10 SEM micrographs of fracture surface of cordierite materials obtained by sintering at 1400 ºC of compact of powders: a) P_{acid}850(0.5 h) and b) P_{acid}850(3 h)

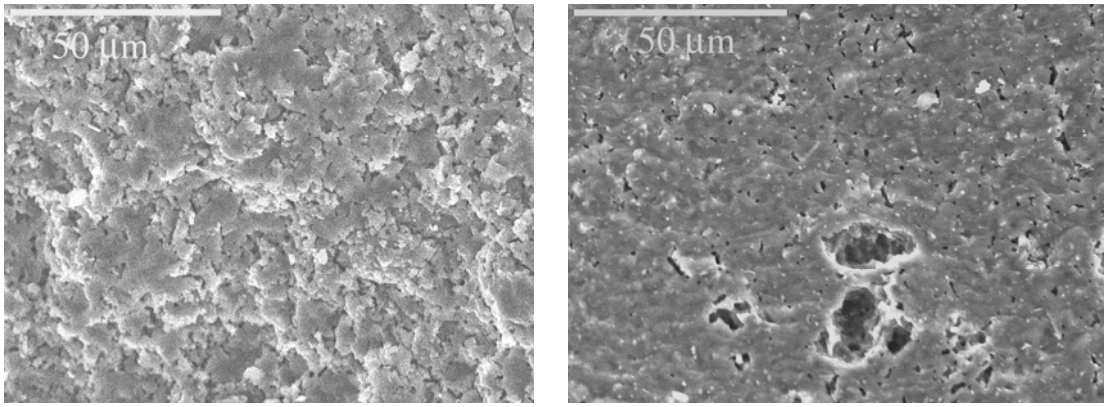

a) b)

Fig 8.11. SEM micrographs of fracture surface of cordierite materials obtained by sintering at 1430 ºC of compact of powders: a) P_{acid}850(0.5 h) and b) P_{acid}850(3 h)

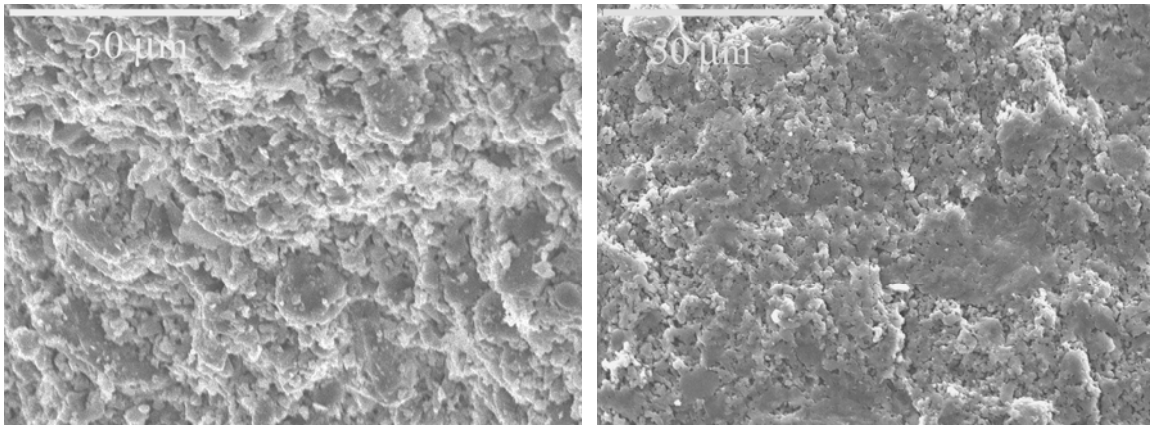

a) b)

Fig 8.12. SEM micrographs of fracture surface of cordierite materials obtained by sintering at 1400 ºC of compact of powders: a) $P_{acid}1300(0.5h)$ and b) $P_{acid}1300(3h)$

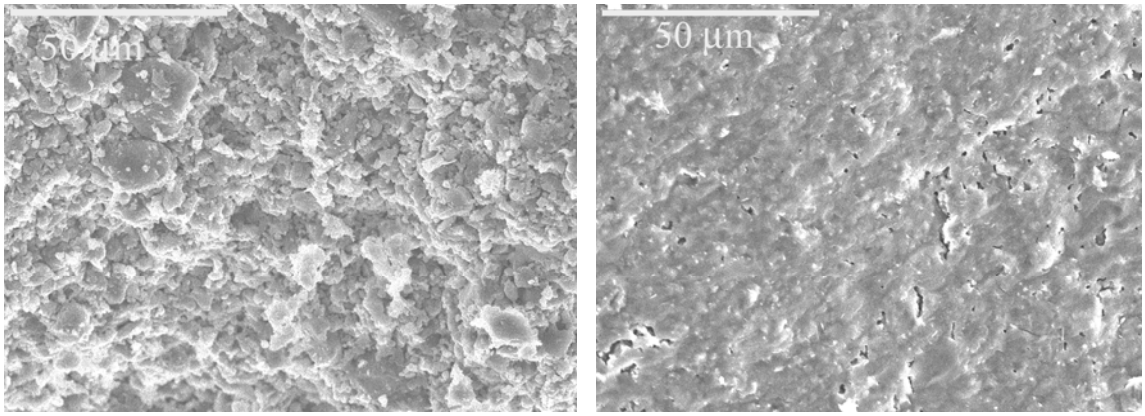

a) b)

Fig 8.13. SEM micrographs of fracture surface of cordierite materials obtained by sintering at 1430 ºC of compact of powders: a) $P_{acid}1300(0.5h)$ and b) $P_{acid}1300(3h)$

According to Figures 8.10 - 8.13 it can be seen that materials did not sinter well, but powders obtained by prolonged grinding showed better sinterability. For powders obtained after 0.5 h grinding, $P_{acid}850(0.5\ h)$ and $P_{acid}1300(0.5\ h)$, increasing of sintering temperature did not influenced sinterability, e.g., increasing of sintering temperature did not increase densification. For powders obtained by grinding for 3 h, sintering temperature increasing

improved densification of materials. But, in the case of sample $P_{acid}850(3h)$, increasing of temperature of sintering caused formation of some large pores. By comparing materials obtained starting from powders $P_{acid}850$ and $P_{acid}1300$, it can be say that better materials were obtained if gel calcinated at 1300 ºC [104].

Cordierite materials of the best microstructure were polished and thermal etched in order to determine size of grains and pores. Before thermal etching, mechanical properties of the samples were determined.

In Figure 8.14, SEM micrographs of polished and thermally etched surface of cordierite materials obtained by conventional sintering at 1430 °C of compacts of powders $P_{acid}850(3h)$ and $P_{acid}1300(3h)$, are presented.

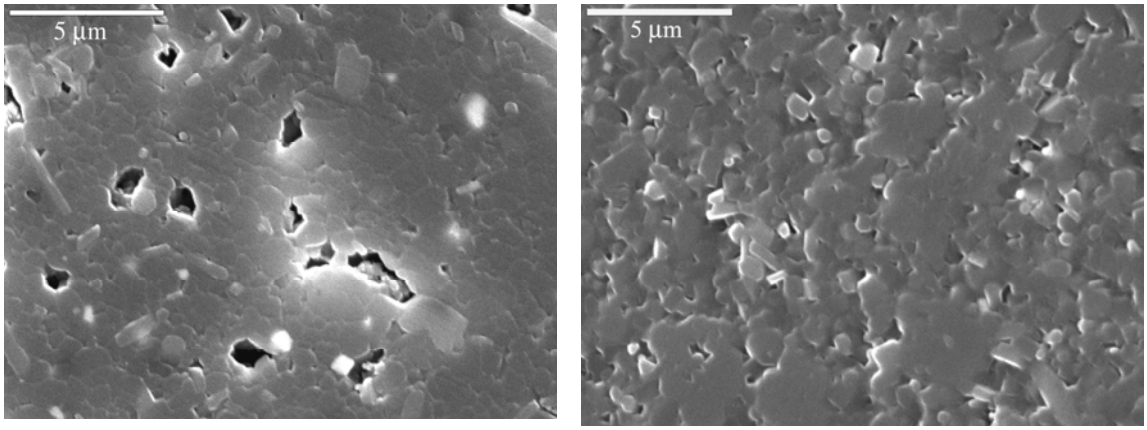

a) b)

Fig. 8.14. SEM micrographs of polished and thermally etched surface of cordierite materials obtained by conventional sintering at 1430 °C of compacts of powder: (a) $P_{acid}850(3h)$ and (b) $P_{acid}1300(3h)$ [101].

In both cases, the grain sizes are the same as the sizes of the smaller initial particles (about 1 µm) (Figures 8.8b and 8.9b). As the microstructure of the sample obtained from the powder $P_{acid}1300$ (3h) is more uniform and pore-free than the powder $P_{acid}850$ (3h), it seems that in this case, the larger particles were destroyed and more effectively packed during pressing and sintering. The presence of pores between the fully densified areas in the case of the sample obtained from the powder $P_{acid}850$ (3h) indicates that the agglomerates were not destroy during pressing and that densification during sintering occurred inside the large particles, while densification between the

agglomerates did not occur. Obviously, harder agglomerates are formed by calcination at temperatures at which viscous sintering occurs without crystallization than in the case where α-cordierite crystallize.

Mechanical properties and densities of cordierite materials obtained by conventional sintering at 1430 °C of compacts of powders $P_{acid}850(3h)$ and $P_{acid}1300(3h)$ are presented in Table 8.2

Table 8.2. Relative density (ρ/ρ_T), microhardness (H) and fracture toughness (K_{IC}) of the sintered cordierite materials

Cordierite material obtained by sintering of powder:	ρ/ρ_T (% TD)	H (GPa)	K_{IC} (MPa $m^{1/2}$)
$P_{acid}850(3h)$	94	6.84	3.62
$P_{acid}1300(3h)$	96	7.47	3.81

Material obtained from the powder $P_{acid}850$ (3h) has worse mechanical properties, probably due to lower density and presence of large pores. Also, worse mechanical properties of $P_{acid}850(3h)$ material could be explained by the presence of some microcracks, arising from the thermal mismatch between the different crystalline phases formed during sintering [83]. As stated above, powder $P_{acid}850(3h)$ is amorphous and during thermal treatment, i.e. during sintering, μ-cordierite crystallized and transformed to α-cordierite. It is known that density of μ-cordierite is lower than that of α-cordierite, and because of that, stress and microcraks are possible.

8.2.2. Sinterability of the cordierite powders obtained starting from silica sol

8.2.2.1. Morphology of powders

Morphology of powders $P_{sol}950(0.5h)$, $P_{sol}950(3h)$, $P_{sol}1300(0.5h)$, $P_{sol}1300(3h)$ are presented in figures 8.15 to 8.16.

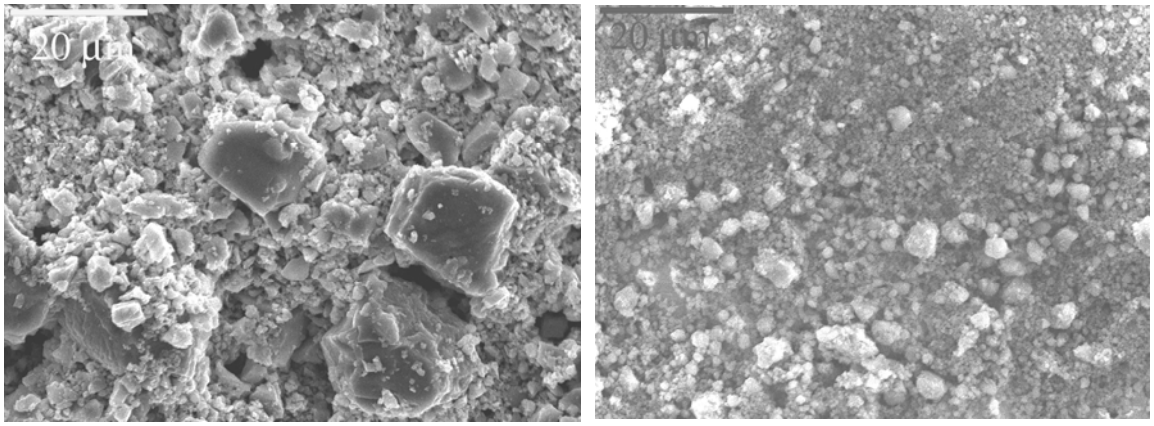

a) b)

Figure 8.15. Morphology of powders: a) $P_{sol}950(0.5h)$ and b) $P_{sol}950(3h)$

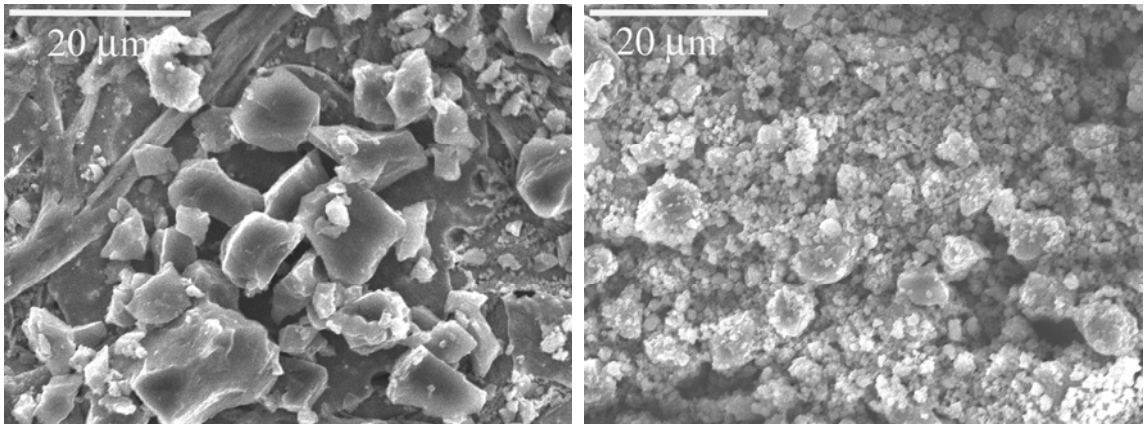

a) b)

Figure 8.16. Morphology of powders: a) $P_{sol}1300(0.5\ h)$ and b) $P_{sol}1300(3h)$.

Similar to the powders obtained starting from silicic acid, prolonged time of grinding caused finer particles of powders obtained starting from silica sol. By comparing of powders obtained by calcination at 950 and 1300 °C, it can be seen that finer powders were obtained by calcination at 950 °C.

8.2.2.2. Microstructure cordierite materials obtained by conventional sintering

Microstructure of cordierite materials obtained by conventional sintering of powders P_{sol}950(0.5h), P_{sol}950(3h), P_{sol}1300(0.5h) and P_{sol}1300(3h), are presented in figures 8.17 to 8.20 [105].

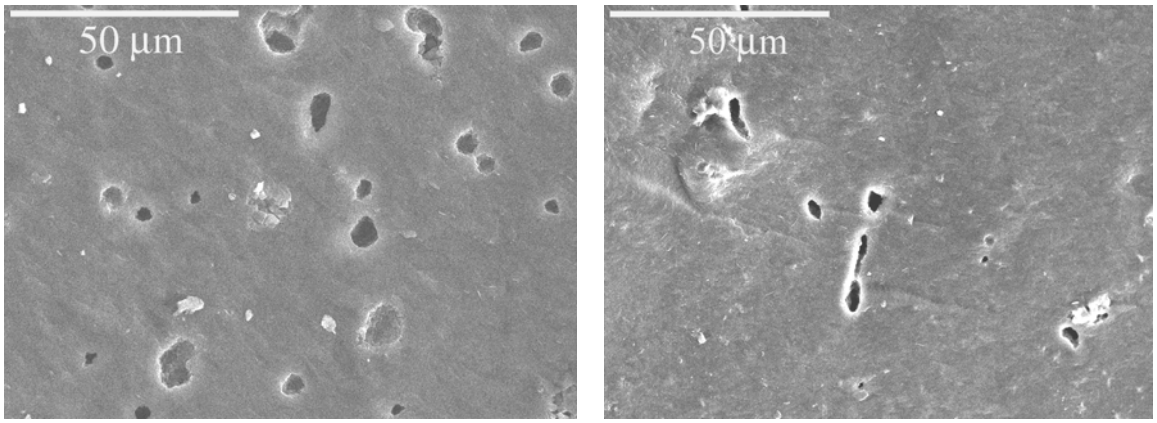

a) b)

Fig 8.17. SEM micrographs of fracture surface of cordierite materials obtained by conventional sintering at 1400 ºC of compact of powders: a) P_{sol}950(0.5h) and b) P_{sol}950(3h).

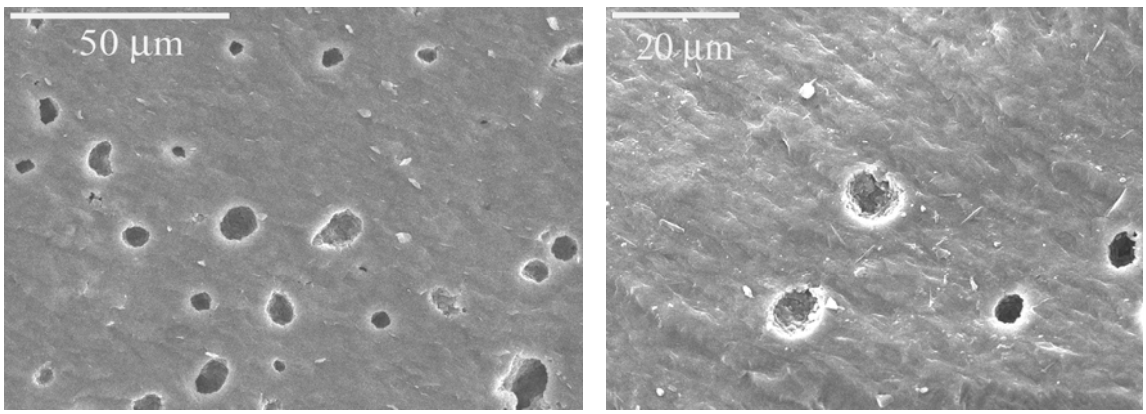

a) b)

Fig 8.18. SEM micrographs of fracture surface of cordierite materials obtained by conventional sintering at 1430 ºC of compact of powders: a) P_{sol}950(0.5h) and b) P_{sol}950(3h).

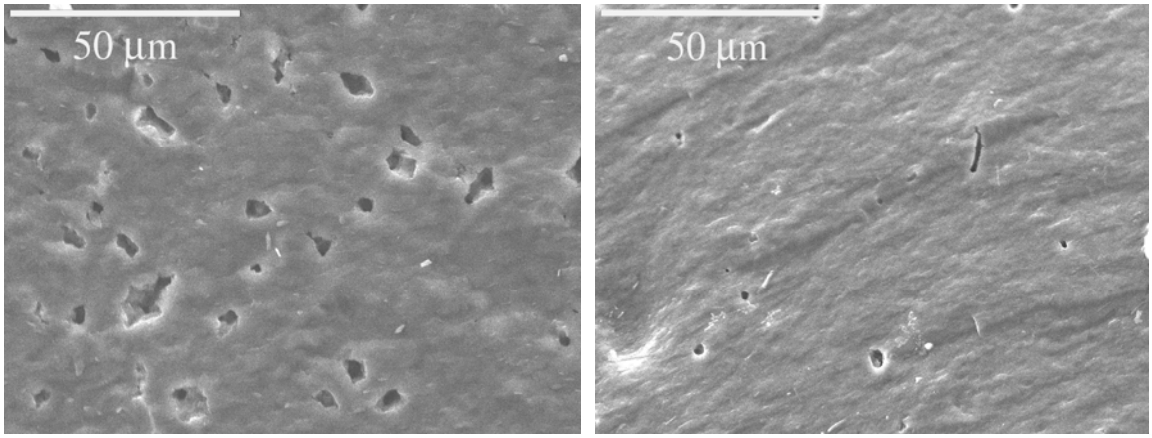

a) b)

Fig 8.19. SEM micrographs of fracture surface of cordierite materials obtained by conventional sintering at 1400 ºC of compact of powders: a) P_{sol}1300(0.5h) and b) P_{sol}1300(3 h).

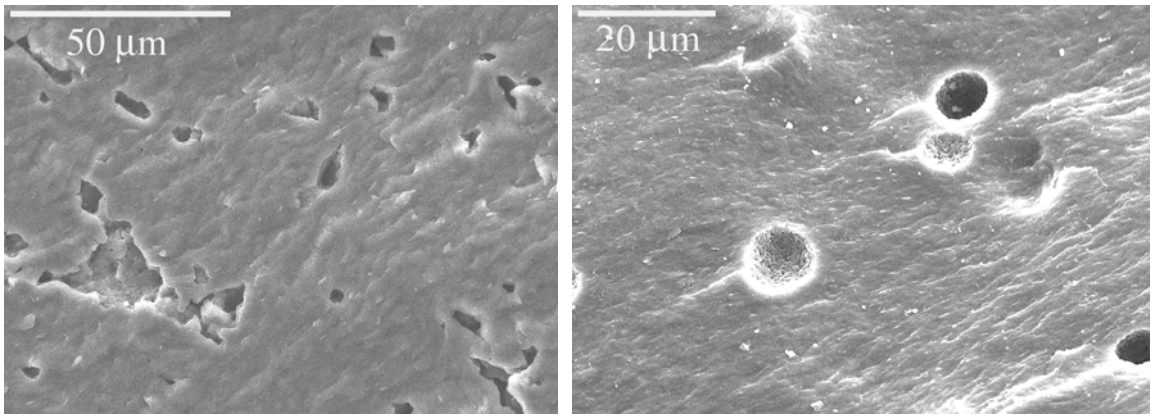

a) b)

Fig 8.20. SEM micrographs of fracture surface of cordierite materials obtained by conventional sintering at 1430 ºC of compact of powders: a) P_{sol}1300(0.5h) and b) P_{sol}1300(3h)

Sinterability of powders $P_{sol}950(0.5h)$ and $P_{sol}1300(0.5h)$ is not good, because sintered materials contained large pores as a consequence of large particles in powders. Increasing temperature of sintering did not improved microstructure of the sintered materials. Sinterability of powders $P_{sol}950(3h)$ and $P_{sol}1300(3h)$ are much better, because starting powders contained much finer particles. The materials obtained by sintering at 1400 ºC are dens, with some pores. But, with sintering temperature increasing, pore sizes increased. It can be explained by start of melting, as it was seen at samples after sintering. The reason for melting temperature decreasing (melting point for cordierite is 1460 ºC) can be presence of Na^+ ions in silica sol used for synthesis.

In figure 8.21., SEM micrographs of polished and thermally etched surface of cordierite materials obtained by conventional sintering at 1400 °C of compacts of powders $P_{sol}950(3h)$ and (b) $P_{sol}1300(3h)$, are presented.

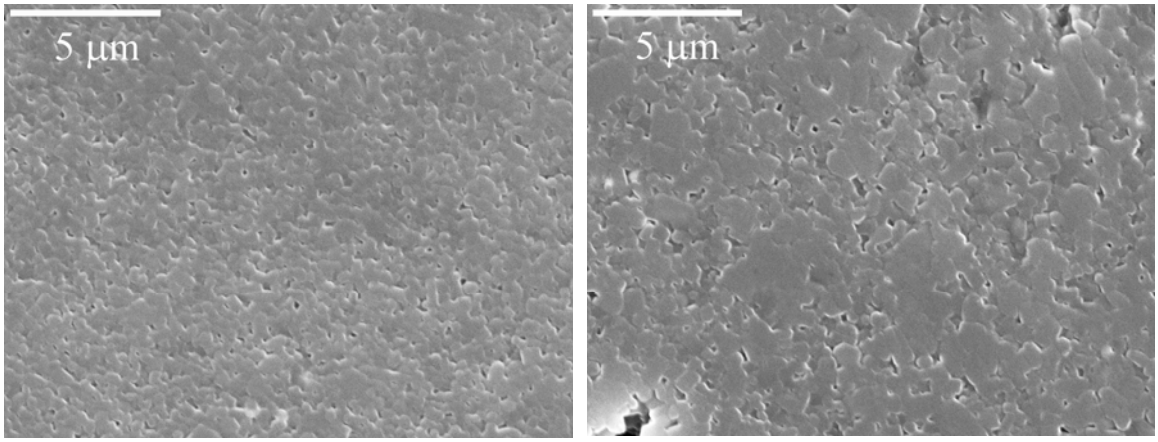

a) b)

Fig 8.21. SEM micrographs of polished and thermally etched surface of cordierite materials obtained by sintering at 1400 °C of compacts of powder: (a) $P_{sol}950(3h)$ and (b) $P_{sol}1300(3h)$ [106].

Mechanical properties of cordierite materials obtained by conventional sintering at 1400 °C of compacts of powders $P_{sol}950(3h)$ and $P_{sol}1300(3h)$ are presented in Table 8.3

Table 8.3. Relative density (ρ/ρ_T), microhardness (H) and fracture toughness (K_{IC}) of the sintered cordierite materials

Cordierite material obtained by sintering of powder:	ρ/ρ_T (% TD)	H (GPa)	K_{IC} (MPa $m^{1/2}$)
P_{sol}950(3h)	91	8.06	2.88
P_{sol}1300(3h)	96	8.05	3.67

According to the Fig. 8.21, the materials obtained by conventional sintering of P_{sol} powders at 1400 °C have dens microstructure, with a few pores. The grain size of material obtained from powder P_{sol}950(3h) seems some smaller than of material obtained from powder P_{sol}1300(3h). Therefore, a higher value of the fracture toughness of the former material could have been expected than of the latter due to its finer microstructure. However, this was not the case (Table 8.3). Generally, material fracture toughness depends on the material composition, grain size, porosity and pores size. Bearing in mind that powder P_{sol}950(3h) was amorphous and that during sintering, crystallization and solid-state reaction occurred, it was assumed that the sintered cordierite materials contained some residual amorphous, glassy phase, the fracture toughness of which is much lower than that of α-cordierite. However, X-ray diffraction analysis of the materials (Fig. 8.22) showed no presence of glassy phase in either of these two samples. Detailed analysis of the diffractograms using PeakFit software was not confirmed presence of broad peaks that would indicate the existence of glassy phase. Accordingly, lower fracture toughness of the material obtained starting from powder P_{sol}950(3h) could be explained by the presence of some microcracks, arising from the thermal mismatch between the different crystalline phases formed during sintering [83]. As stated above, powder P_{sol}950(3h) contained spinel and amorphous phase and during thermal treatment, i.e. during sintering, crystobalite crystallized and reacted with spinel, forming α-cordierite.

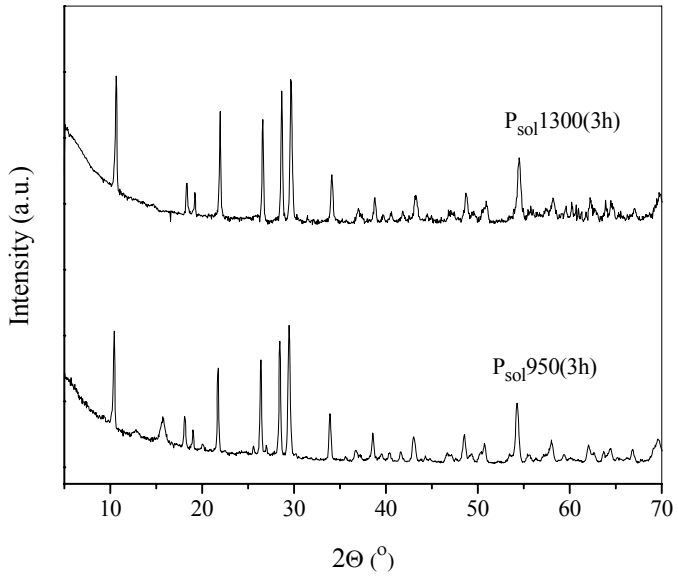

Figure 8.22. X-ray diffraction analysis of the materials obtained by sintering of powders P_{sol}950(3h) and P_{sol}1300(3h) at1400 °C.

8.2.3. Sinterability of the cordierite powders obtained starting from alkoxide

8.2.3.1. Morphology of powders

In figure 8.23 morphology of powders obtained by calcination of gel $G_{alkoxide}$ at 850 °C ($P_{alkoxide}$850) or 1300°C ($P_{alkoxide}$1300), after grinding for 3 h, are presented. Because of poor sinterability of powders P_{sol} and P_{acid} obtained by grinding for 0,5 h, powders $P_{alkoxide}$850(0.5h) and $P_{alkoxide}$1300(0.5h) were not used for sintering experiments.

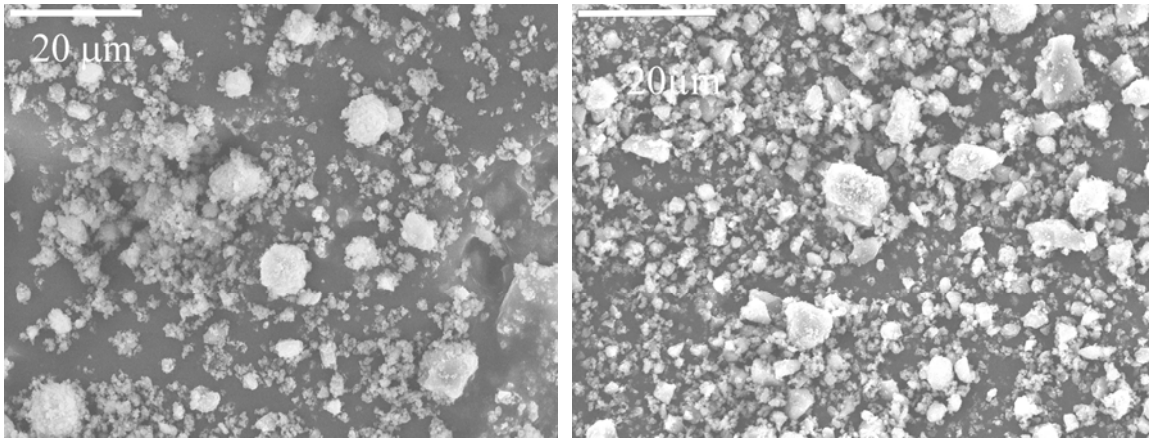

a) b)

Figure 8.23. Morphology of powders: a) $P_{alkoxide}850(3h)$ and b) $P_{alkoxide}1300(3h)$

It could be seen from Fig. 8.23 that both powders had a similar morphology: nearly spherical particles, the dimensions of which were about 0.5 – 1 µm, together with larger particles of about 5 - 10 µm, as in the case of powders $P_{sol}950(3h)$ and $P_{sol}1300(3h)$.

Particle size distributions of powders $P_{alkoxide}850(3h)$, $P_{alkoxide}1300(3h)$, $P_{sol}950(3h)$ and $P_{sol}1300(3h)$, based on the particles volume (Fig. 8.24.a), show that powders $P_{sol}950$, $P_{sol}1300$, and $P_{alxokside}850$ have a broad and bimodal distribution, with the maximums at about 2 µm and 20 µm, while the powder $P_{alkoxide}1300$ has a broad and unimodal distribution, enclosing particles in the range of 0.3–20 mm. On the other hand, particle size distributions based on the particles number (Figure 8.24.b) showed that particles of 0.5 µm are dominant in all the powders.

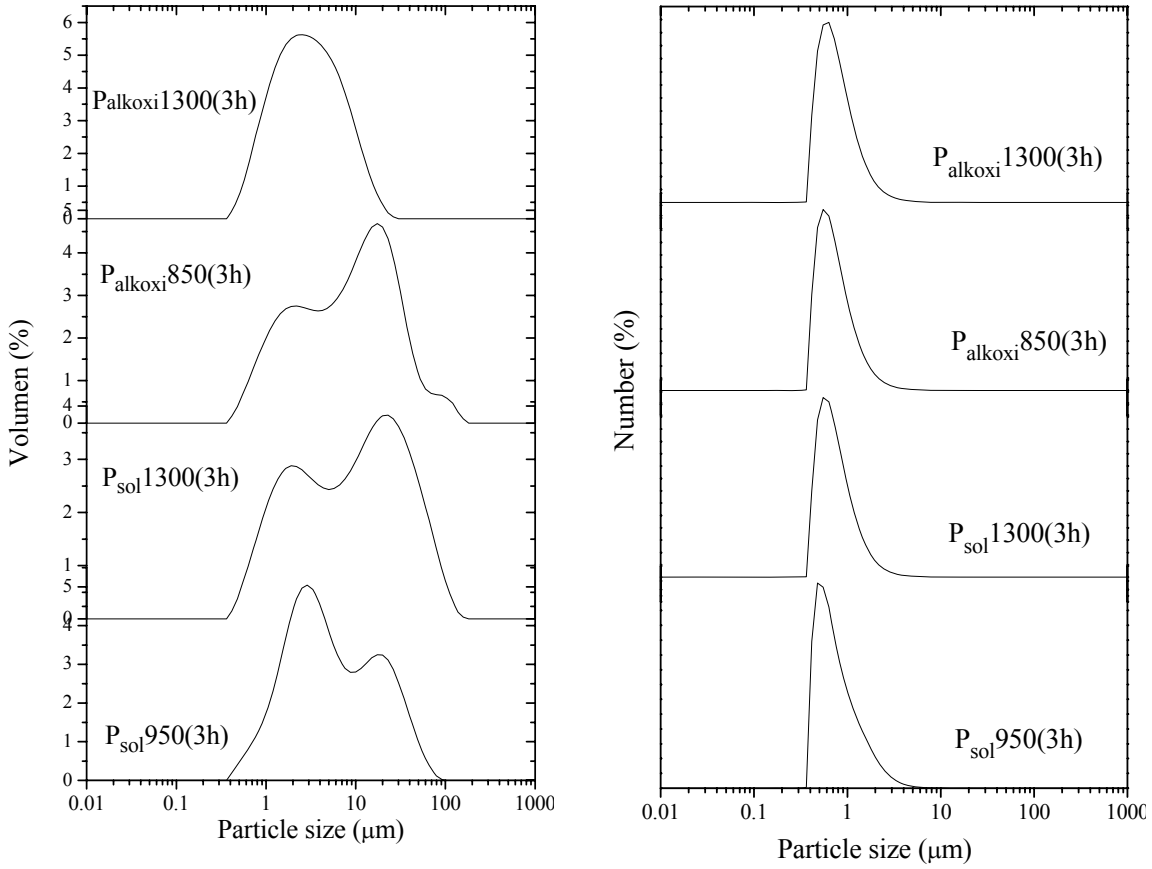

a) b)

Figure 8.24. Particle size distribution of the powders $P_{alkoxide}$850(3h), $P_{alkoxide}$1300(3h), P_{sol}950(3h) and P_{sol}1300(3h), based on the particles volume (a) and based on the particles number (b) [106].

8.2.3.2. Microstructure cordierite materials obtained by conventional sintering

Microstructures of cordierite materials obtained by conventional sintering of compact of powders $P_{alkoxide}$850(3h) and $P_{alkoxide}$1300(3h) at 1400, 1430 and 1450°C are presented in figures 8.25 to 8.27.

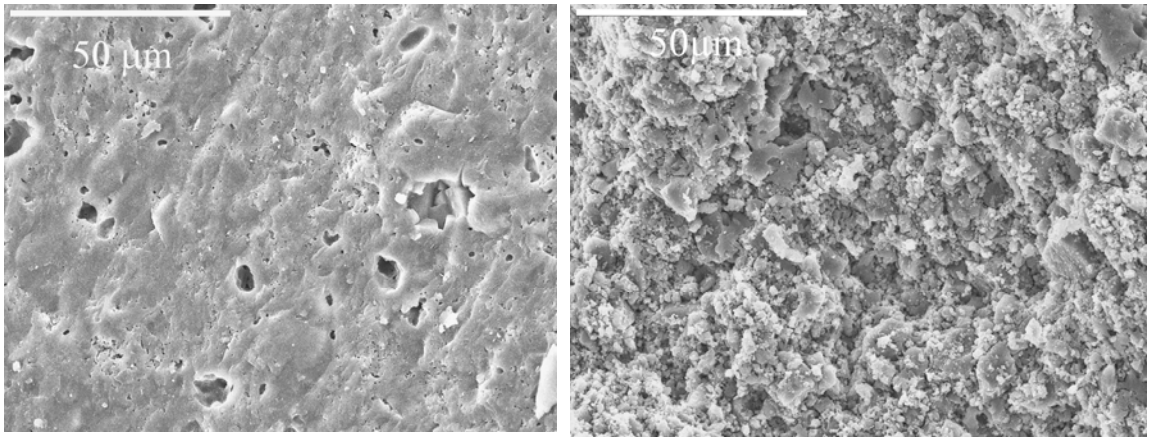

a) b)

Fig 8.25. Microstructure of the cordierite materials obtained by sintering at 1400 ºC of compacts of powder: a) $P_{alkoxide}850(3h)$ and b) $P_{alkoxide}1300(3h)$

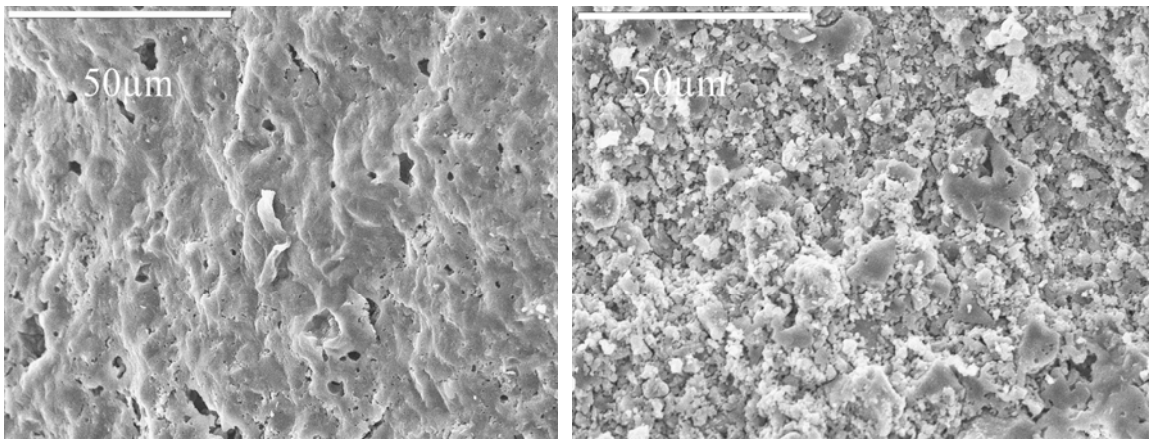

a) b)

Fig 8.26. Microstructure of cordierite materials obtained by sintering at 1430 ºC of compacts of powder: a) $P_{alkoxide}850(3h)$ and b) $P_{alkoxide}1300(3h)$.

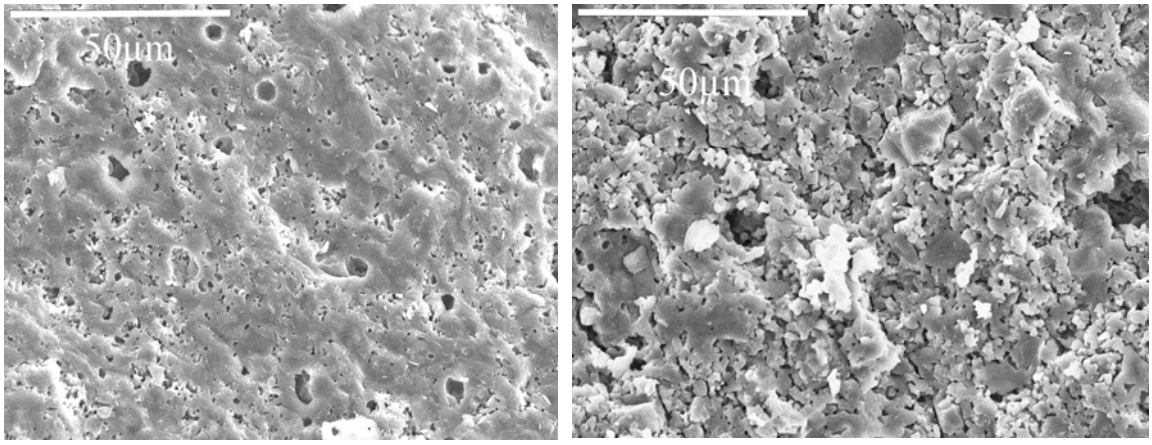

a) b)

Fig 8.27. Microstructure of cordierite materials obtained by sintering at 1450 ºC of compacts of powder: a) $P_{alkoxide}$850(3h) and b) $P_{alkoxide}$1300(3h)

According to Fig. 8.25, the materials obtained by sintering of the $P_{alkoxide}$ powders at 1400 °C were insufficiently sintered. The material obtained by sintering of compact of powder $P_{alkoxide}$850 contained densified areas, but both small pores (< 1 μm) and large pores (about 7–8 μm) were present. The dimension of the small pores was approximately equal to the dimension of the smaller particles in the powder $P_{alkoxide}$850(3h) (Fig. 8.23) and the larger pore size was approximately equal to the size of larger particles. The formation of enclosed nearly spherical pores is indicative of the end of the medium sintering stage and beginning of the final sintering stage (density of the material was about 88 % TD). Increasing of sintering temperature (Figs 8.26 and 8.27) did not cause a decrease in porosity and the material obtained by sintering at 1450 °C contained even more pores, especially small ones, than the material obtained by sintering at 1400 °C. According to some authors [83], such behavior could be explained by swelling and cracking in the compact caused by desorption of the water in the large cavities which connect to form continuous channels parallel to the c-axis. They argued that the water concentration of the alkoxy-derived powder would be very high despite powder calcination at high temperatures. The vapor pressure of the water in the cavities or pores could be high enough to expand the cavities or pores and then lead to the cracking of the compact at temperatures above1400 °C.

An insufficiently sintered sample and the formation of contact necks were the main characteristics of the sample obtained by the sintering of the compact of powder $P_{alkoxide}1300(3h)$ at 1400 °C, which means that the sample was in the initial stage of sintering. As the sintering temperature increased, the density of the sample slightly increased (from 77 % TD at 1400 °C to 84 % TD at 1450 °C) and the material obtained by sintering at 1450 °C contained more densified areas (Fig. 8.27 b) than the samples obtained by sintering at 1400 °C (Fig. 8.25.b) and 1430 °C (Fig. 8.26.b). However, it could also be the distinct appearance of some large pores, probably because the sintering occurred mainly inside larger agglomerated particles.

X-ray diffractograms of the materials obtained by sintering of compacts of powders $P_{alkoxide}850(3h)$ and $P_{alkoxide}1300(3h)$ at 1400 °C (Fig. 8.28) show in both cases presence of well-crystallized α-cordierite, without glassy phase, as in the case of materials obtained starting from P_{sol} powders.

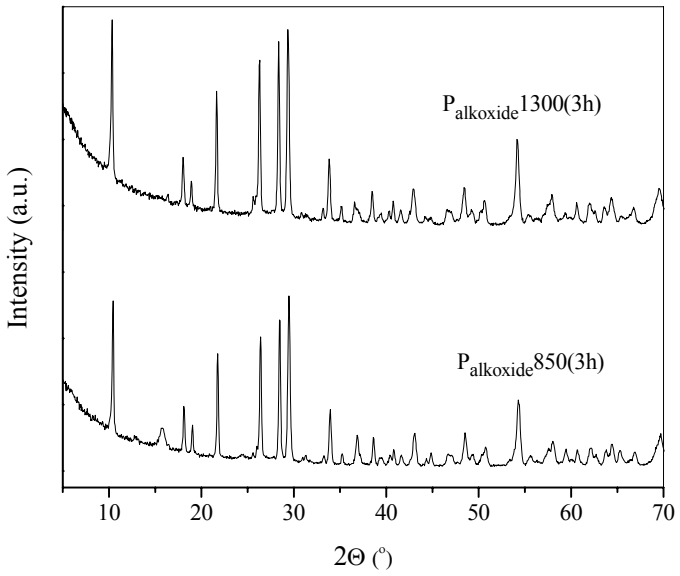

Figure 8.28. X-ray diffraction analysis of the materials obtained by sintering of powders $P_{alkoxide}850(3h)$ and $P_{alkoxide}1300(3h)$ at 1400 °C.

Obviously, despite the fact that the sintering temperatures were very close to melting temperature of cordierite, the alkoxide-derived cordierite powders showed very poor performances on sintering, especially the well-crystallized powder $P_{alkoxide}1300(3h)$. Despite the fact that powder $P_{alkoxide}1300(3h)$ had the same

composition (α-cordierite) and similar morphology and particle sizes as the powder P_{sol}1300(3h), sinterability of these powders is quite different. It could be supposed that the better performances on sintering of the P_{sol} powders were the results of the presence of Na^+ ions in the silica sol used for the synthesis, which acted as a sintering additive.

Polishing of the materials obtained from the $P_{alkoxide}$ powders was not performed and the mechanical properties were not determined due to the insufficient sintering.

8.2.3.3. Microstructure of cordierite materials obtained by spark-plasma sintering

The microstructures of the cordierite materials obtained by spark-plasma sintering of powder $P_{alkoxide}$1300(3h) at 1350 °C for 7 min and at 1400 °C for 1 min, at different magnifications, are shown in Fig. 8.29. In both cases, fully densified microstructures were obtained. Pores were rarely observed in either of the specimens. In the higher magnification Figures, no grains can be seen, which indicates that the fracture mode was mainly transgranular [107, 108].

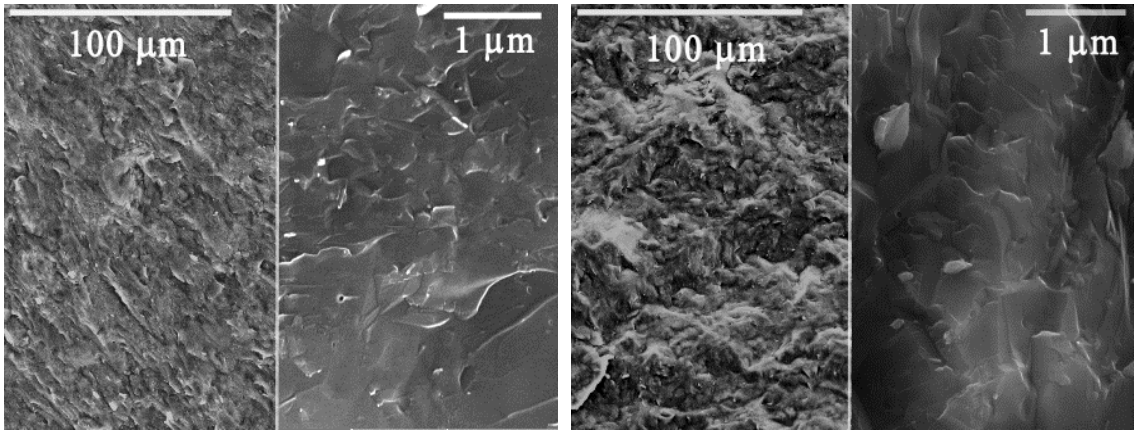

a) b)

Fig 8.29. Microstructure of cordierite materials obtained by spark plasma sintering of powder $P_{alkoxide}$1300(3h) at: a) 1350 °C (7 min), b) 1400°C (1min).

SEM micrographs of the polished and thermally etched surface of the SPS cordierite materials are shown in Fig. 8.30, while the densities and mechanical

properties of these materials are presented in Table 8.4. The densities of both materials were very similar to the theoretical value of α-cordierite and the hardness and fracture toughness were very high, higher than of those of the materials obtained by conventional sintering (Table 8.2. and 8.3).

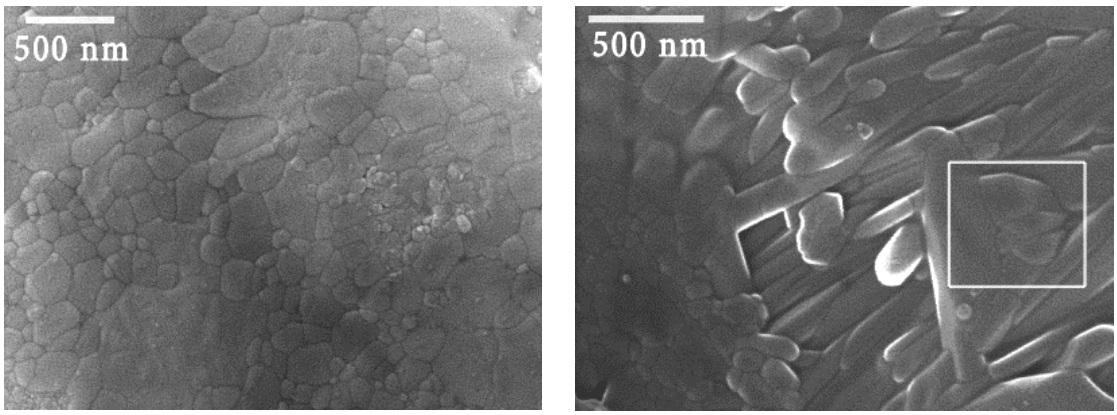

a) b)

Fig. 8.30. SEM micrographs of polished and thermally etched surface of cordierite materials obtained by spark plasma sintering at: a) 1350 °C for 7 min and (b) 1400 °C for 1 min [106].

Table 8.4. Relative density (ρ/ρ_T), microhardness (H) and fracture toughness (K_{IC}) of SPS cordierite materials

Cordierite materials obtained by spark plasma sintering of powder $P_{alkoxide}$1300(3h):	ρ/ρ_T (% TD)	H (GPa)	K_{IC} (MPa $m^{1/2}$)
at 1350 °C for 7 min	99	8.53	4.06
at 1400 °C for 1 min	99	8.63	4.02

Grains of different sizes and shapes and some occasional pores are visible in both microstructures (Fig. 8.30). In Fig. 8.30.b, two different regions can be seen: one with elongated grains and one with grains that do not look elongated. However, according to the assigned part in Fig 8.30.b, it could be supposed that both region contained elongated grains, but of different orientation. In the first case, the grains were oriented parallel to polished surface, while in the second case, the grains were oriented

perpendicular to the polished surface and a cross section of elongated grains can be seen in the SEM microphotograph. In the case of the sample sintered at 1350 °C for 7 min, elongated grains were also visible on the thermally etched fracture surface (Fig. 8.31.).

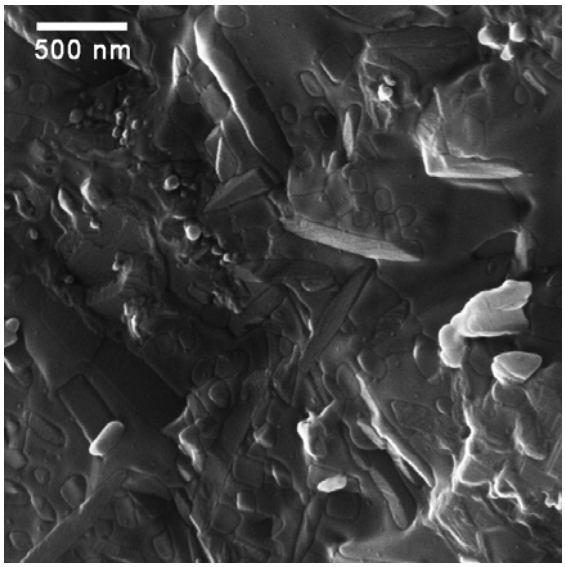

Fig 8.31. SEM micrographs of thermally etched fracture surface of cordierite material obtained by spark-plasma sintering of powder $P_{alkoxide}$1300(3h) at 1350 °C for 7 min.

During spark plasma sintering [61, 62, 107-112], as a consequence of the applied high currents, a softening or melting of the surface layers is possible, leading either to a grain rearrangement by sliding under the applied load or to an enhanced migration of species through the surface layer. The presence of a liquid phase under the applied load could be the reason for the formation of elongated grains. Such a microstructure with elongated grains provides better mechanical properties, especially higher fracture toughness. XRD analysis of SPS materials showed no presence of glassy phase (Fig. 8.32), which indicates that, even if formed, the content of liquid phase during SPS is very small.

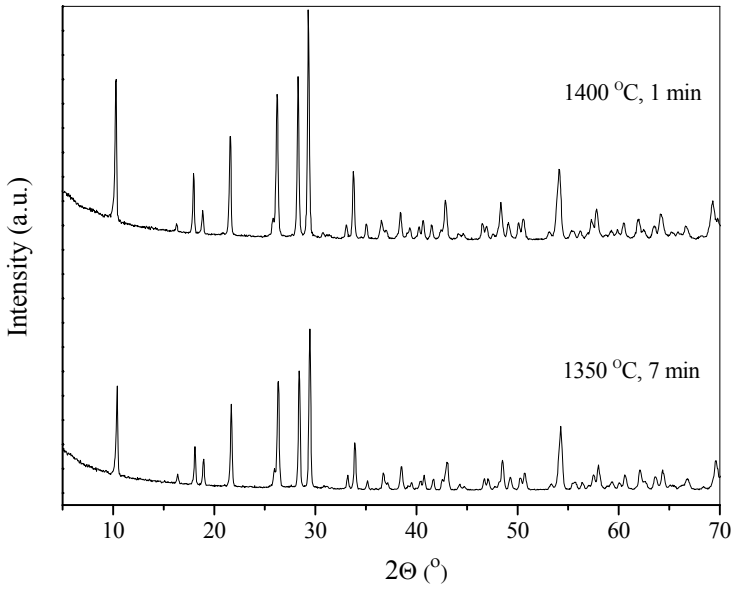

Fig. 8.32. X-ray diffraction analysis of the materials obtained by spark-plasma sintering of powders $P_{alkoxide}$1300(3h) at 1400 °C for 1 min and at 1350 °C for 7 min.

Obviously, the sinterability of the alkoxide-based powder was highly improved by spark-plasma sintering at a lower sintering temperature and during much shorter time than during conventional sintering. The density of the spark-plasma sintered materials was very close to the theoretical density of α-cordierite and the mechanical properties were better than those of materials obtained by conventional sintering.

9. CONCLUSIONS

The sintering behavior of sol–gel processed cordierite powders and the microstructure and mechanical properties of the obtained cordierite materials were investigated in dependence on the synthesis method, the temperature of gel calcination, duration of calcined gels grinding and the type and temperature of sintering. The cordierite gels were prepared by alkoxide and colloidal sol-gel methods and by a low-price aqueous sol–gel route starting from silicic acid and magnesium and aluminum salts. The phase transformations of the silicic acid-based gel during heating were also studied. The powders for the sintering investigations were obtained by calcination of the gels at a temperature where α-cordierite is formed (crystalline powders) or at a temperature where densification without crystallization of silica-containing component occurred (amorphous powders).

Starting from silicic acid and magnesium and aluminum salts, a homogeneous monophasic cordierite gel was obtained, which was proved by μ-cordierite crystallization at about 900 °C. In temperature range of 800–850 °C, viscous sintering of the gel without μ-cordierite crystallization occurred. According to the DTA, XRD and FTIR results, it was shown that μ- → α-cordierite transformation took place in a wide temperature range, and α-cordierite appeared at about 1200 °C. On calcination for 2 h at 1300 °C, the transformation μ- → α-cordierite was fully completed.

The mean value of the Avrami parameter for μ-cordierite crystallization, which is close to 1, indicates interface controlled crystallization with a constant number of nuclei and one-dimensional growth or surface nucleation. Accordingly, viscous sintering occurred in the primary gel particles, which led to shrinkage, and thereafter, nucleation occurs on the surface or interface of the particles. Due to surface nucleation, the overall activation energy of μ-cordierite crystallization (382.0kJ/mol) was lower than in the cases where volume nucleation occurs.

Prolonged time of calcined gels grinding caused particle decreasing in all cases and the densification degree of the cordierite materials was improved by decreasing the mean particle size. More densified microstructures were obtained by using the powders obtained after grinding for 3 hours than for 0.5 h.

The sinterability of the powders obtained by calcination at 1300 °C, where well-crystallized α-cordierite was formed, was better in all cases than that of the powder obtained by calcination at temperatures where the most intensive shrinkage occurred before the onset of silica-containing component crystallization (850 °C for alkoxide and silicic acid gels or 950 °C for colloidal gel).

In general, powders obtained starting from silicic acid and by the colloidal sol–gel method showed much better performances on sintering with respect to the alkoxide-based powders. The best mechanical properties of the conventionally sintered materials were achieved by sintering at 1400 °C of powder obtained by calcination at 1300 °C of colloidal gel and by sintering at 1430 °C of powder obtained by calcination at 1300 °C of gel obtained starting from silicic acid. Hardness of the best materials was about 7.5 to 8 GPa, while fracture toughness K_{IC} was 3.7 to 3.8 MPa $m^{1/2}$.

The sinterability of the alkoxide-based powder was highly improved by spark-plasma sintering at a lower sintering temperature and during much shorter time than during conventional sintering. The density of the spark-plasma sintered materials was very close to the theoretical density of α-cordierite and the mechanical properties were better than those of materials obtained by conventional sintering (hardness was about 8.5 GPa and fracture toughness K_{IC} was about 4,1 MPa $m^{1/2}$).

During spark plasma sintering, as a consequence of the applied high currents, a softening or melting of the surface layers was possible, leading either to a grain rearrangement by sliding under the applied load or to an enhanced migration of species through the surface layer. The presence of a liquid phase under the applied load could be the reason for the much better sinterability of alkoxide-based powder during spark-plasma sintering then during conventional sintering. Better performances on conventional sintering of powders obtained starting from silicic acid and silica sol compared to alkoxide-based powders were probably the results of the presence of sodium ions in the silica sol and silicic acid used for the synthesis, which acted as a sintering additive.

10. REFERENCES

1. E. M. Levin, C. R. Robbins, H. F. McMurdie, ″Phase Diagram for Ceramists″, Fig. 712. Ed. by M. K. Reser, American Ceramic Society, Columbus, OH, 1964.
2. P. Predecki, J. Haas, J. Faber Jr., J. L. Hitterman, ″Structural Aspects of the Lattice Thermal Expansion of Hexagonal Cordierite″, J. Am. Ceram. Soc. **70** (1987) 175-182.
3. D. K. Agrawal, V. S. Stubican, Y. Mehrotra, ″Germanium-Modified Cordierite Ceramics with Low Thermal Expansion″, J. Am. Ceram. Soc. **69** (1986) 847-851.
4. M. F. Hochella, Jr, G. E. Brown, Jr, ″Structural Mechanisms of Anomalous Thermal Expansion of Cordierite-Beryl and Other Framework Silicates″, J. Am. Ceram. Soc. **69** (1986) 13-18.
5. J. Hlavač, ″The Technology of Glass and Ceramics — An Introduction″, Elsevier Scientific Publishing Company, Amsterdam, Oxford, New York, 1983.
6. W. D. Kingery, H. Bowen, D. R. Uhlmann, ″Introduction to Ceramics″, John Wiley&Sons Inc., New York, 1976.
7. R. W. Dupon, R. L. McConville, D. J. Musolf, A. C. Tanous, M. S. Thompson, ″Preparation of Cordierite below 1000 °C via Bismuth Oxide Flux″, J. Am. Ceram. Soc. **73** (1990) 335-339.
8. N. Obradović , N. Đorđević, S. Filipović, N. Nikolić, D. Kosanović, M. Mitrić, S. Marković, V. Pavlović, ″Influence of mechanochemical activation on the sintering of cordierite ceramics in the presence of Bi_2O_3 as a functional additive″, Powder Technol. **218** (2012) 157–161.
9. M. K. Atanasovska-Jančetović, ″Fizičko-hemijski procesi formiranja i evolucije mikrostrukture u procesu dobijanja kordijerita″, Doktorska disertacija, Tehnološko-metalurški fakultet, Beograd, 1993.
10. M. Tecilazić-Stevanović, T. Janaćković, Lj. Kostić-Gvozdenović, R. Ćirjaković, ″Dependence of the Properties of Cordierite-Mullite Ceramics on Synthesis Conditions″, Ind. Ceram. **13** (1993) 31-34.
11. Lj. Kostić-Gvozdenović, T. Janaćković, M. Tecilazić-Stevanović, B. Todorović, ″Glazes for Cordierite Ceramics″, Ind. Ceram. **13** (1993) 11-13.

12. K. Sumi, Y. Kobayashi, E. Kato, ″Synthesis and Sintering of Cordierite from Ultrafine Particles of Magnesium Hydroxide and Kaolinite″, J. Am. Ceram. Soc. **81** (1998) 1029.
13. Y. Kobayashi, K. Sumi, E. Kato, ″Preparation of dense cordierite ceramics from magnesium compounds and kaolinite without additives″, Ceram. Int. 26 (2000) 739-743
14. V. N. Antsiferov, S. E. Porozova, S. N. Peshcherenko, ″Effect of the raw materials on the properties of cordierite ceramics″, Refract. Ind. Ceram. **38** (1997) 388-391.
15. J. R. Gonzalez-Velasco, R. Ferret, R. Lopez-Fonseca, M. A. Gutierrez-Ortiz, ″Influence of particle size distribution of precursor oxides on the synthesis of cordierite by solid-state reaction″, Powder Technol. **153** (2005) 34–42.
16. A. Yamuna, R. Johnson, Y.R. Mahajan, M. Lalithambik, ″Kaolin-based cordierite for pollution control″, J. Eur. Ceram. Soc. **24** (2004) 65–73.
17. S. Tamborenea, A. D. Mazzoni, E.F. Aglietti, ″Mechanochemical activation of minerals on the cordierite synthesis″, Thermochim. Acta **411** (2004) 219–224.
18. E. Yalamac¸ S. Akkurt, ″Additive and intensive grinding effects on the synthesis of cordierite″, Ceram. Int. **32** (2006) 825–832
19. P. Grosjean, ″Cordierite ceramics″, Interceram. **42** (1993) 11–15.
20. Y.-M. Chiang, D. Birnie III, W. D. Kingery, ″Phisical Ceramics – Principles for Ceramic Science and Engineering″, John Wiley & Sons, Inc., New York, 1997.
21. T. H. Elmer, ″Selective Leaching of Extruded Cordierite Honeycomb Structures″, Ceram. Eng. Sci. Proc. **7** (1986) 40-51.
22. K. Inoguchi, T. Nakanishi, M. Asano, ″Method for Producing a Cordierite Body″, US patent No.4.434.117, Feb. 28, 1984.
23. D. M. Ver Dow, ″High Strenght Cordierite Ceramics″, US Patent No.4.268.311, May 19, 1981.
24. J. C. Bernier, ″Sol-Gel Processing for the Synthesis of Powders for Dielectrics″, Powder Metall. Int. **18** (1986) 164-168.
25. B. H. Mussler, M.W. Shafer, ″Preparation and Properties of Mullite-Cordierite Composites″, Ceram. Bul. **63** (1984) 705-710

26. I. M. Lachman, J. L. Williams, ″Extruded monolithic catalyst supports″, Catal. Today **14** (1992) 317– 329.
27. J. B. R. Neto, R. Moreno, ″Effect of mechanical activation on the rheology and casting performance of kaolin/talc/alumina suspensions for manufacturing dense cordierite bodies″, Appl. Clay Sci. **38** (2008) 209–218.
28. Z. Aćimovic, Lj. Pavlović, Lj. Trumbulović, L. Andrić, M. Stamatović, ″Synthesis and characterization of the cordierite ceramics from nonstandard raw materials for application in foundry″, Mater. Lett. **57** (2003) 2651-2656.
29. M. F. Hochella, Jr, G. E. Brown, Jr, ″Structural Mechanisms of Anomalous Thermal Expansion of Cordierite-Beryl and Other Framework Silicates″, J. Am. Ceram. Soc. **69** (1986) 13-18.
30. D. L. Evans, G. R. Fischer, J. E. Geiger, F. W. Martin, ″Thermal Expansions and Chemical Modifications of Cordierite″, J. Am. Ceram. Soc. **63** (1980) 629-634.
31. K. Langer, W. Schreyer, ″Infrared and Powder X-ray Diffraction Studies on the Polymorphism of Cordierite, $Mg_2(Al_4Si_5O_{18})$″, Am. Mineral. **54** (1969) 5442-5459.
32. A. Putnis, ″The Distortion Index in Anhydrous Mg-Cordierite″, Contrib. Mineral. Petrol. **74** (1980) 135-141.
33. A. Putnis, D. L. Bish, ″The Mechanism and Kinetics of Al, Si Ordering in Mg-Cordierite″, Am. Mineral. **68** (1983) 60-65.
34. C. A. Fyfe, G. C. Gobbi, A. Putnis, ″Elucidation of the Mechanism and Kinetics of the Si, Al Ordering Process in Synthetic Magnesium Cordierite by ^{29}Si Magic Angle Spinning NMR Spectroscopy″, J. Am. Ceram. Soc. **108** (1986) 3218-3223.
35. B. Güttler, E. Salje, A. Putnis, ″Structural States of Mg Cordierite III: Infrared Spectroscopy and the Nature of the Hexagonal-Modulated Transition″, Phys. Chem. Minerals **16** (1989) 365-373.
36. S. A. T. Redfern, E. Salje, W. Maresch, W. Schreyer, ″X-ray Powder-Diffraction and Infrared Study of the Hexagonal to Orthorhombic Phase Transition in K-Bearing Cordierite″, Am. Mineral. **74** (1989) 1293-1299.

37. I. Gouby, P. Thomas, D. Mercurio, T. Merle-Méjean, B. Frit, ″Powder X-ray Diffraction and Infrared Study of the Structural Evolution in Highly K-Doped Cordierites″, Mater. Res. Bull. **30** (1995) 593-599.
38. H. Yanagida, K. Koumoto, M. Miyayama, ″The Chemistry of Ceramics″, John Wiley&Sons Inc., New York, 1996.
39. M. N. Rahaman, ″Ceramic Processing and Sintering″, Second Edition, Marcel Dekker Inc., New York, 2003.
40. U. Schubert, N. Hüsing, ″Synthesis of Inorganic Materials″, WILEY-VCH Verlag GmbH & Co. KGaA, Weinheim, 2005.
41. C. C. Barry, N.M. Grant, ″Ceramic Materials - Science and Engineering″, Springer, Berlin, 2007.
42. J. D. Mackenzie, ″Applications of Sol-Gel Methods for Glass and Ceramics Processing″, pp. 15-26 in ″Ultrastucture Processing of Ceramics, Glasses and Composites″. Ed. by L. L. Hench and D. R. Ulrich, John Wiley & Sons, New York, 1984.
43. D. R. Uhlmann, B. J. J. Zelinski, G. E. Wnek, ″The Ceramist as Chemist - Opportunities for New Materials″, pp. 59-70 in Better Ceramics Through Chemistry, MRS Symposia Proceedings, vol.32. Ed. by C. J. Brinker, D. E. Clark, D. R. Ulrich, North-Holland, New-York, 1984.
44. C. J. Brinker, G. W. Scherer, ″Sol-Gel Science: The Physics and Chemistry of Sol-Gel Processing″, Academic Press Inc., San Diego, 1990.
45. B. J. J. Zelinski, D. R. Uhlmann, ″Gel Technology in Ceramics″, J. Phys. Chem. Sollids **45** (1984) 1069-1090.
46. S. S. Voyuckii, ″Kurs kolloidnoi khimii″, Khimiya, Moskva, 1975.
47. C. W. Turner, ″Sol-gel Process - Principles and Applications″, Ceram. Bull. **70** (1991) 1487-1490.
48. A. C. Pierre, ″Sol-gel Processing of Ceramic Powders″, Ceram. Bull. **70** (1991) 1281-1288.
49. R. K. Ailer, ″Koloidnaya khimiya kremnezema i silikatov″, Gosstroyizdat, Moskva, 1959.

50. S. K. Milonjić, ″Surface properties of metal ions modified silicas″, Colloid. Surface. A **149** (1999) 461-466.
51. M. J. Gieselmann, M. A. Anderson, ″Effect of Ionic Strenght on Boehmite Hydrogel Formation″, J. Am. Ceram. Soc. **72** (1989) 980-985.
52. J. Zarzycki, ″Monolithic Xero- and Aerogels for Gel-Glass Processes″, pp. 27-42 in Ultrastructure Processing of Ceramics, Glasses and Composites. Ed. by L. Hench and D. Ulrich, Jonh Wiley and Sons, New York, 1984.
53. J. Zarzycki, M. Prassas, J. Phalippou, ″Synthesis of Glasses from Gels: The Problem of Monolithic Gels″, J. Mater. Sci. **17** (1982) 3371-3379.
54. J. Fricke, A. Emmerling, ″Aerogels″, J. Am. Ceram. Soc. **75** (1992) 2027-2036.
55. S.-J. L. Kang, ″Sintering–Densification, Grain Growth, and Microstructure″, Elsevier Butterworth-Heinemann, Oxford, 2005.
56. V. V. Srdić, Procesiranje novih keramičkih materijala, Tehnološki fakultet, Univerzitet u Novom Sadu, Novi Sad, 2004.
57. M. Tecilazić-Stevanović, Osnovi tehnologije keramike, Tehnološko-metalurški fakultet Univerziteta u Beogradu, Beograd, 1990.
58. Randall M. German, "Sintering theory and practice", John Wiley & Sons, Inc., New York, 1996.
59. M. F. Ashby, D. R. H. Jones, ″Engineering materials 2. An Introduction to Microstructures, Processing and Design″, Butterworth-Heinemann, Oxford, 1998.
60. R. Orrù, R. Licheri, A. M. Locci, A. Cincotti, G. Cao, ″Consolidation/synthesis of materials by electric current activated/assisted sintering″, Mat. Sci. Eng. R – Report **63** (2009) 127–287.
61. Z. A. Munir, U. Anselmi-Tamburini, M. Ohyanagy, ″The effect of electric field and pressure on the synthesis and consolidation of materials: A review of the spark plasma sintering method″, J. Mater. Sci. **41** (2006) 763–777.
62. Z. A. Munir, D. V. Quach, M. Ohyanagy, ″Electric current activation of sintering: a review of the pulsed electric current sintering process″, J. Am. Ceram. Soc. **94** (2011) 1–19.

63. http://www.substech.com/dokuwiki/doku.php?id=spark_plasma_sintering&DokuWiki=e579a03e5
64. http://www.thermaltechnology.com/pdf/SPS%20Reprint%20may08.pdf
65. http://www.mechanicalengineeringblog.com/tag/spark-plasma-sintering/
66. H. Suzuki, K. Ota, H. Saito, ″Preparation of cordierite ceramics from metal alkoxides (part 1) –preparation and characterization of the powder″, J. Ceram. Soc. Jpn. (Yogyo-Kyokai-Shi) **95** (1987) 163–169.
67. A. M. Kazakos, S. Komarneni, R. Roy, ″Sol–gel processing of cordierite: effect of seeding and optimization of heat treatment″, J. Mater. Res. **5** (1990) 1095–1103.
68. R. Ianos, I. Lazau, C. Pacurariu, ″Solution combustion synthesis of α-cordierite″, J. Alloys Compd. **480** (2009) 702–705.
69. R. Goren, H. Gocmez, C. Ozgur, ″Synthesis of cordierite powder from talc, diatomite and alumina″, Ceram. Int. **32** (2006) 407–409.
70. C. Ghitulica, E. Andronescu, O. Nicola, A. Dicea, M. Birsan, ″Preparation and characterization of cordierite powders″, J. Eur. Ceram. Soc. **27** (2007) 711–713.
71. Dj. Janaćković, V. Jokanović, Lj. Kostić-Gvozdenović, S. Zec, D. Uskoković, ″Synthesis and formation mechanism of submicrometre spherical cordierite powders by ultrasonic spray pyrolysis″, J. Mater. Sci. **32** (1997) 163–168.
72. R. Petrović, Dj. Janaćković, S. Zec, S. Drmanić, Lj. Kostić-Gvozdenović, ″Phase-transformation kinetics in triphase cordierite gel″, J. Mater. Res. **16** (2001) 451–458.
73. R. Petrović, Dj. Janaćković, S. Zec, S. Drmanić, Lj. Kostić-Gvozdenović, ″Crystallyzation behavior of alkoxide-derived cordierite gel″, J. Sol–Gel Sci. Technol. **28** (2003) 111–118.
74. I. Janković-Častvan, S. Lazarević, D. Tanasković, A. Orlović, R. Petrović, Đ. Janaćković, ″Phase transformation in cordierite gel synthesized by nonhydrolitic sol–gel route″, Ceram. Int. **33** (2007) 1263 –1268.
75. M. Okuyama, T. Fukui, C. Sakurai, ″Effects of complex precursors on alkoxide-derived cordierite powder″, J. Am. Ceram. Soc. **75** (1992) 153 –160.

76. R. Petrović, Dj. Janaćković, B. Božović, S. Zec, Lj. Kostić-Gvozdenović, ″Densification and crystallization behaviour of colloidal cordierite-type gel″, J. Serb. Chem. Soc. **66** (2001) 335 – 343.
77. M. Naskar, M. Chatterjee, ″A novel process for the synthesis of cordierite ($Mg_2Al_4Si_5O_{18}$) powders from rice husk ash and other sources of silica and their comparative study″, J. Eur. Ceram. Soc. **24** (2004) 3499 – 3508.
78. C. A. Bertran, N. T. da Silva, G. P. Thim, ″Citric acid effect on aqueous sol-gel cordierite synthesis″, J. Non-Cryst. Solids **273** (2000) 140 -144.
79. J. R. González-Velasco, R. Ferret, R. López-Fonseca, M.A. Gutiérrez-Ortiz, ″Influence of particle size distribution of precursor oxides on the synthesis of cordierite by solid-state reaction″, Powder Technol. **153** (2005) 34 – 42.
80. S.-J. Lee, W. M. Kriven, ″Crystallization and densification of nano-size amorphous cordierite powder prepared by a PVA solution- polymerization route″, J. Am. Ceram. Soc. **81** (1998) 2605 - 2612.
81. M. A. Camerucci, G. Urretavizcaya, A.L. Cavalieri, ″Sintering of cordierite based materials″, Ceram. Int. **29** (2003) 159 - 168
82. M. A Camerucci, G. Urretavizcaya, A. L. Cavalieri, ″Mechanical behavior of cordierite and cordierite–mullite materials evaluated by indentation techniques″, J. Eur. Ceram. Soc. **21** (2001) 1195 - 1204.
83. H. Suzuki, K. Ota, H. Saito, ″Preparation of cordierite ceramics from metal alkoxides (part 2) - sintering″, J. Ceram. Soc. Jpn. (Yogyo-Kyokai-Shi) **95** (1987) 170 –175.
84. H. Suzuki, K. Ota, H. Saito, Mechanical properties of alkoxy-derived cordierite ceramics, J. Mat. Sci. **23** (1988) 1534–1538.
85. M. Awano, H, Takagi, Y. Kuwahara, ″Grinding effects on synthesis and sintering of cordierite″, J. Am. Ceram. Soc. **75** (1992) 2535–2540.
86. C. Shu, X. Mingxia, Z. Cailou, T. Jiaqi, ″Fabrication of cordierite powder from magnesium–aluminum hydroxide and sodium silicate: its characteristics and sintering″, Mat. Res. Bull. **37** (2002) 1333-1340.

87. M. Majumder, S. Mukhopadhyay, O. Parkash, D. Kumar, ″Sintering and crystallisation behaviour of chemically prepared cordierite for application in electronic packaging″, Ceram. Int. **30** (2004) 1067–1070.
88. I. Janković-Častvan, S. Lazarević, B. Jordović, R. Petrović, Dj. Janaćković, ″Electrical properties of cordierite obtained by non-hydrolytic sol–gel method″, J. Eur. Ceram.Soc. **27** (2007) 3659–3661.
89. S. K. Milonjić, ″Sorpcija jona alkalnih metala na površini koloidnog SiO_2″, Doktorska disertacija, Univerzitet u Beogradu, 1981.
90. R. Petrović, S. Milonjić, V. Jokanović, Lj. Kostić-Gvozdenović, I. Petrović-Prelević, Đ. Janaćković, ″Influences of synthesis parameters on the structure of boehmite sol particles″, Powder Technol. **133** (2003) 185-189.
91. T. Ozava, ″Kinetics of non-isothermal crystallization″, Polymer **12** (1971) 150–158.
92. J. A. Augis, J. E. Bennett, ″Calculation of the Avrami parameters for heterogeneous solid state reactions using a modification of the Kissinger method″, J. Therm. Anal. **13** (1978) 283–292.
93. H. Yinnon, D.R. Uhlmann, ″Applications of thermoanalytical technicues to the study of crystallization kinetics in glass-forming liquids, Part I: theory″, J. Non-Cryst. Solids **54** (1983) 253–275.
94. K.Matusita, S.Sakka, ″Kinetic study of crystallization of glass by differential scanning calorimetry″, Phys. Chem. Glasses, **20** (1979) 81-84.
95. I. W. Donald, ″The crystallization kinetics of a glass based on the cordierite composition studied by DTA and DSC″, J. Mat. Sci. **30** (1995) 904–915.
96. D. R. Mc Farlane, M. Fragoulis, ″Theory of diversification in multicomponent glass forming systems under diffusion control″, Phys. Chem. Glasses **27** (1986) 228–234.
97. A. G. Evans, E. A. Charles, ″Fracture toughness determinations by indentation″, J. Am. Ceram. Soc. **59** (1976) 371–372.
98. M. G. M. U. Ismail, H. Tsunatori, Z. Nakai, ″Preparation of Mullite-Cordierite Composite Powders by the Sol-Gel Method: Its Characterizatics and Sintering″, J. Am. Ceram. Soc. **73** (1990) 537-543.

99. M. Awano, H. Takagi, ″Synthesis of cordierite and cordierite–$ZrSiO_4$ composite by colloidal processing″, J. Mater. Sci. **29** (1994) 412–418.
100. R. Salmon, E. Matijević, ″Preparation of colloidal magnesium–aluminum–silicates by hydrolysis of a mixed alkoxide″, Ceram. Int. **16** (1990) 157–163.
101. N. M. El-Buaishi, I. Janković-Častvan, B. Jokić, Dj. Veljović, Dj. Janaćković, R. Petrović, ″Crystallization behavior and sintering of cordierite synthesized by an aqueous sol–gel route″, Ceram. Int. **38** (2012) 1835–1841.
102. B. C. Lim, H. M. Jang, ″Crystallization kinetics and phase transformation characteristics in seeded monophasic cordierite gel″, J. Mater. Res. **6** (1991) 2427–2433.
103. K. Watanabe, E. A. Giess, ″Crystallization kinetics of high-cordierite glass″, J. Non-Cryst. Solids **169** (1994) 306–310.
104. N. M. El-Buaishi, I. Janković-Častvan, B. Jokić, Dj. Veljović, Dj. Janaćković, R. Petrović, ″Sinterability of Cordierite Powders Synthesized by Sol-gel Methods″, Proceedings of the EUROMAT 2011, Montpellier, France, 2011., p.65.
105. N. M. El-Buaishi, V. Arsovski, Đ.Veljović, J. Kovrlija, Đ. Janaćković, R. Petrović: ″Sinterabilnost kordijeritnih prahova sintetizovanih koloidnim sol-gel postupkom″, Zbornik radova 49. Savetovanja SHD, Kragujevac, 2011, str. 193 – 197.
106. N. M. El-Buaishi, Dj.Veljović, B. Jokic, Ž. Radovanović, I. Steins, Dj. Janaćković, R. Petrović, ″Conventional and spark-plasma sintering of cordierite powders synthesized by sol–gel methods″, Ceram. Int. **39** (2013) 5845-5854.
107. N. Tamari, T. Tanaka, K. Tanaka, M. Kawahara, M. Tokita, ″Effect of spark plasma sintering on densification and mechanical properties of silicon carbide″, J. Ceram. Soc. Jpn. (Yogyo-Kyokai-Shi) **103** (1995) 740-742.
108. L. An, A. Ito, T. Goto, ″Transparent yttria produced by spark plasma sintering at moderate temperature and pressure profiles″, J. Eur. Ceram. Soc. **32** (2012) 1035 – 1040.
109. F. C. Sahin, H. E. Kanbur, B. Apak, ″Preparation of AlON ceramics via reactive spark plasma sintering″, J. Eur. Ceram. Soc. **32** (2012) 925–929.

110. M. Demuynck, J.-P. Erauw, O.Van der Biest, F. Delannay, F. Cambier, ″Densification of alumina by SPS and HP: A comparative study″, J. Eur. Ceram. Soc. **32** (2012) 1957 – 1964.
111. O. Eser, S. Kurama, ″A comparison of sintering techniques using different particle sized β-SiAlON powders″, J. Eur. Ceram. Soc. **32** (2012) 1343–1347.
112. L. An, A. Ito, T. Goto, ″Effect of sintering temperature on the transparency and mechanical properties of lutetium aluminum garnet fabricated by spark plasma sintering″, J. Eur. Ceram. Soc. **32** (2012) 3097–3102

Biografija autora

Mr Nozhat Moftah El Buaishi je rođena 26. 12. 1966. godine u Tripoliju u Libiji. Diplomirala je 1991. godine na Univerzitetu Al-Fateh (University of Al-Fateh) u Tripoliju, na Fakultetu za umetnost i medije (Faculty of Arts & Inform), na Katedri za keramiku i staklo. Na istom fakultetu je držala vežbe iz predmeta „Hemija keramike“ i „Svojstva keramike i sirovine“ u periodu od 1992. do 2000. godine. U srednjoj školi u Tripoliu je predavala „Opštu hemiju“ od 1992. do 1999. godine. Magistarsku tezu na temu „Uticaj veličine čestica na svojstva staklo-keramičkih pločica“ je odbranila 2005. godine na Univerzitetu kulture u Istanbulu (Istanbul Cultur University – Institute of Science and Engineering). Diploma koju je Nozhat Moftah El Buaishi stekla završetkom ovih magistarskih studija priznata je Odlukom Univerziteta u Beogradu od 26. 05. 2010. godine kao diploma magistarskih studija sa zvanjem magistar tehničkih nauka iz oblasti građevinarstva. Nakon magistriranja, u periodu od 2005. do 2009. godine, radila je kao asistent na Univerzitetu Al-Fateh, na Fakultetu za umetnost i medije, na Katedri za staklo i keramiku. U toku izrade doktorske disertacije na Katedri za neorgansku hemijsku tehnologiju Tehnološko-metalurškog fakulteta Univerziteta u Beogradu objavila je dva rada u vrhunskom časopisu međunarodnog značaja (M21), jedan rad je saopšten na naučnom skupu međunarodnog značaja koji je štampan u izvodu (M34) i jedan rad je saopšten na skupu nacionalnog značaja i štampan u celini (M63).

Prilog 1.

Izjava o autorstvu

Potpisana Nozhat Moftah El Buaishi

broj indeksa _____

Izjavljujem

da je doktorska disertacija pod naslovom

Sinterability of Cordierite Powders Synthesized by Different Sol-gel Methods (Proučavanje sinterabilnosti kordijeritnih prahova sintetizovanih različitim sol-gel postupcima)

- rezultat sopstvenog istraživačkog rada
- da predložena disertacija u celini ni u delovima nije bila predložena za dobijanje bilo koje diplome prema studijskim programima drugih visokoškolskih ustanova,
- da su rezultati korektno navedeni i
- da nisam kršila autorska prava i koristila intelektualnu svojinu drugih lica.

Potpis doktoranta

U Beogradu, _____

_____

Prilog 2.

Izjava o istovetnosti štampane i elektronske verzije doktorskog rada

Ime i prezime autora Nozhat Moftah El Buaishi
Broj indeksa _____
Studijski program _____

Naslov rada Sinterability of Cordierite Powders Synthesized by Different Sol-gel Methods (Proučavanje sinterabilnosti kordijeritnih prahova sintetizovanih različitim sol-gel postupcima)

Mentor dr Rada Petrović, redovni profesor

Potpisana _____

Izjavljujem da je štampana verzija mog doktorskog rada istovetna elektronskoj verziji koju sam predala za objavljivanje na portalu **Digitalnog repozitorijuma Univerziteta u Beogradu.**
Dozvoljavam da se objave moji lični podaci vezani za dobijanje akademskog zvanja doktora nauka, kao što su ime i prezime, godina i mesto rođenja i datum odbrane rada.
Ovi lični podaci mogu se objaviti na mrežnim stranicama digitalne biblioteke, u elektronskom katalogu i u publikacijama Univerziteta u Beogradu.

Potpis doktoranta

U Beogradu, _____

_____

Prilog 3.

Izjava o korišćenju

Ovlašćujem Univerzitetsku biblioteku "Svetozar Marković" da u Digitalni repozitorijum Univerziteta u Beogradu unese moju doktorsku disertaciju pod naslovom:

Sinterability of Cordierite Powders Synthesized by Different Sol-gel Methods (Proučavanje sinterabilnosti kordijeritnih prahova sintetizovanih različitim sol-gel postupcima)

koja je moje autorsko delo.

Disertaciju sa svim prilozima predala sam u elektronskom formatu pogodnom za trajno arhiviranje.

Moju doktorsku disertaciju pohranjenu u Digitalni repozitorijum Univerziteta u Beogradu mogu da koriste svi koji poštuju odredbe sadržane u odabranom tipu licence Kreativne zajednice (Creative Commons) za koju sam se odlučila.

1. Autorstvo
2. Autorstvo – nekomercijalno
3. Autorstvo – nekomercijalno – bez prerade
4. Autorstvo – nekomercijalno – deliti pod istim uslovima
5. Autorstvo – bez prerade
6. Autorstvo – deliti pod istim uslovima

(Molimo da zaokružite samo jednu od šest ponuđenih licenci, kratak opis licenci dat je na poleđini lista).

Potpis doktoranta

U Beogradu, _____

_____

1. Autorstvo – Dozvoljavate umnožavanje, distribuciju i javno saopštavanje dela, i prerade, ako se navede ime autora na način određen od strane autora ili davaoca licence, čak i u komercijalne svrhe. Ovo je najslobodnija od svih licenci.
2. Autorsko – nekomercijalno. Dozvoljavate umnožavanje, distribuciju i javno saopštavanje dela, i prerade, ako se navede ime autora na način određen od strane autora ili davaoca licence. Ova licenca ne dozvoljava komercijalnu upotrebu dela.
3. Autorsko – nekomercijalno – bez prerade. Dozvoljavate umnožavanje, distribuciju i javno saopštavanje dela, bez promena, preoblikovanja ili upotrebe dela u svom delu, ako se navede ime autora na način određen od strane autora ili davaoca licence. Ova licenca ne dozvoljava komercijalnu upotrebu dela. U odnosu na sve ostale licence, ovom licencom se ograničava najveći obim prava korišćenja dela.
4. Autorstvo – nekomercijalno – deliti pod istim uslovima. Dozvoljavate umnožavanje, distribuciju i javno saopštavanje dela, i prerade, ako se navede ime autora na način određen od strane autora ili davaoca licence i ako se prerada distribuira pod istom ili sličnom licencom. Ova licenca ne dozvoljava komercijalnu upotrebu dela i prerada.
5. Autorsko – bez prerade. Dozvoljavate umnožavanje, distribuciju i javno saopštavanje dela, bez promena, preoblikovanja ili upotrebe dela u svom delu, ako se navede ime autora na način određen od strane autora ili davaoca licence. Ova licenca dozvoljava komercijalnu upotrebu dela.
6. Autorstvo – deliti pod istim uslovima. Dozvoljavate umnožavanje, distribuciju i javno saopštavanje dela, i prerade, ako se navede ime autora na način određen od strane autora ili davaoca licence i ako se prerada distribuira pod istom ili sličnom licencom. Ova licenca ne dozvoljava komercijalnu upotrebu dela i prerada. Slična je softverskim licencama, odnosno licencama otvorenog koda.